

POLITECNICO DI TORINO

Master degree in Energy and Nuclear Engineering

POLY²NUC Program

Master Thesis

Preliminary reactor design for nuclear thermal propulsion



Supervisor:

Prof. Sandra Dulla

Candidate:

Samuele Meschini

Co-Supervisors:

Prof. Antonio Cammi

Prof. Piero Ravetto

July 2019

Abstract

In the last years, new interest in nuclear space propulsion has been shown by space agencies. NASA defines Nuclear Thermal Propulsion (NTP) as a key technology for long-range spaceflight. Many HEU (High-Enriched Uranium), fast reactors design for space applications were proposed during and after NERVA and ROVER projects. HEU reactors have many advantages: they are usually more compact than LEU (Low-Enriched Uranium) reactors, they show a longer operating lifetime and safety in accidental scenarios can be easily ensured. Their main drawback is the high content of fissile materials, which is a primary security concern. The present work investigates the possibility of a LEU reactor design with CERMET (Ceramic Metallic) fuel and its optimization. Due to the lower U-235 content, LEU reactors are preferable from the nuclear proliferation viewpoint, while CERMET fuel may provide better performances than NERVA derived fuels, such as $(U, Zr)C$. Neutronics, burnup, safety and thermal-hydraulics simulations were performed by Serpent and MATLAB: the model was first tested against an available case in literature, then applied to the reactor of interest. Criticality eigenvalue in both operating and fault conditions, peaking factors, reactor mass, burnup time, coolant average temperature and fuel maximum temperature were chosen as figures of merit to lead the design. It is found that safety is much harder to ensure in a LEU reactor than in a HEU reactor, leading to the necessity of exploring a large number of configurations: for this reason, a Python code was developed; the code can handle the whole process, from pre-processing to post-processing, including the integration between Serpent and MATLAB. Thus, the following procedure was implemented: a group of new reactor configurations were built and tested; checking the figures of merit, only the most promising configurations are selected for the optimization and for a safety analysis that simulates reactor behaviour in four accidental scenarios; finally, the cores that satisfy safety requirements undergo a thermal-hydraulic analysis, which verifies that thermal limits are not exceeded and evaluates rocket performances. In that way it was possible to simulate about 1000 configurations, which differ in core materials, core geometry, fuel element enrichment and enrichment zones. Results show that radial reflector thickness heavily affects neutronics and safety, while coolant mass flow rate needs a precise tuning to lower fuel temperature and to ensure competitive rocket performances, making orificing a desirable optimization. In addition, spectral shift absorbers look not as effective as in fast reactors, owing to their massive absorption of thermal neutrons during normal operations. Therefore, an advanced control drums system is proposed to ensure subcriticality even in the worst accidental scenario. It is found that few configurations fulfil both safety requirements and NASA requirements for rocket thrust, specific impulse and mission time. Thus, a LEU, CERMET fuelled reactor design is challenging but feasible, and both the developed code and the optimization procedure may be applied successfully to find the best configuration.

Contents

- 1. Introduction1**
 - 1.1 Propulsion technologies review2
 - 1.1.1 Rocket science background.....2
 - 1.1.2 Nuclear Electrical Propulsion5
 - 1.1.3 Nuclear Thermal Propulsion6
 - 1.2 Reactor configuration.....8
 - 1.2.1 Fuel elements.....11
 - 1.2.2 Moderator elements13
 - 1.2.3 Reflector and control drums15
 - 1.3 Methodology and goals16

- 2. Neutronic Analysis18**
 - 2.1 Base case: NERVA derived reactor21
 - 2.1.1 Control Drums reactivity worth.....26
 - 2.1.2 Reactor mass.....27
 - 2.1.3 Reflector thickness and power distribution29
 - 2.1.4 Burnup analysis33
 - 2.1.5 Results comparison and conclusions36
 - 2.2 CERMET reactor37
 - 2.2.1 Optimization.....43
 - 2.2.3 Conclusions48

- 3. Accidental scenarios analysis49**
 - 3.1 Accidental scenarios50
 - 3.2 Spectral shift absorbers52
 - 3.3 Control rods54
 - 3.4 Advanced control drums system.....55
 - 3.5 Conclusions58

- 4. Thermal-hydraulics analysis60**
 - 4.1 Fuel element model61
 - 4.2 0-D analysis64
 - 4.3 Hot channel analysis.....66
 - 4.4 Rocket performances74
 - 4.5 Conclusions77

- 5. Conclusions79**

Bibliography	81
List of figures	84
List of tables	86
Acknowledgments	87

1. Introduction

Explore the unknown is a deep desire of mankind. Having explored the whole planet, man's interest moved toward the space: Moon landing was the first big step. There is no doubt that the next, extremely important step will be bringing a man to Mars. But it is not only a matter of exploration desire: setting the goal of a manned mission to Mars encourages the development of new, useful technologies, with a widespread impact on everyday life. It has already been the case for LEDs, scratch-resistant lenses, computer mouse and other common technologies [1]. Furthermore, the search for extra-terrestrial life is unavoidably related to Mars and to our ability to bring men on this planet. Finally, it will set the bases for a possible future colonization of the Red Planet, increasing the mankind capability to survive on a long-time scale. This process will require many decades, both for the intrinsic difficulty and for the time required to unlock key technologies: hopefully, this path will lead to a deeper awareness of our planet and to a stronger collaboration among people.

At the present time, many countries can place their objects into stable orbits, thanks to their launch systems; alongside, private companies' interest in space led to the development of similar technologies, culminating in the construction of vehicles which may be reused. Nevertheless, a long journey such as a mission to Mars poses many challenges that are still not completely overcome: the travel duration implies a large radiation dose to the crew, especially for chemical propulsion based systems; energy must be provided to the spacecraft; reliability and safety must be assured for the whole mission time; finally, cost should be kept below reasonable values. The most promising technology able to fulfil these requirements on a short-time term is Nuclear Propulsion.

The present work focuses on the neutronic and thermal-hydraulics design of a reactor for nuclear thermal propulsion, exploring different configurations and possible solutions to the main issues that affect this class of reactors.

1.1 Propulsion technologies review

Before starting with the system description, it may be useful to illustrate the main technologies involving nuclear space propulsion: nuclear electrical propulsion (NEP), nuclear thermal propulsion (NTP) and bimodal propulsion, which is nothing but the combination of the previous two concepts.

1.1.1 Rocket science background

For the reader that is not familiar with rocket science, it may be worth to briefly introduce some key parameter for the comparison among different propulsion systems [2].

The thrust F is nothing but the force that a propulsion system is able to produce. In chemical or nuclear thermal propulsion rockets, the thrust is generated by the ejection of mass, specifically the hot propellant: once the propellant reaches extremely high temperatures, it is accelerated through a nozzle and finally ejected.

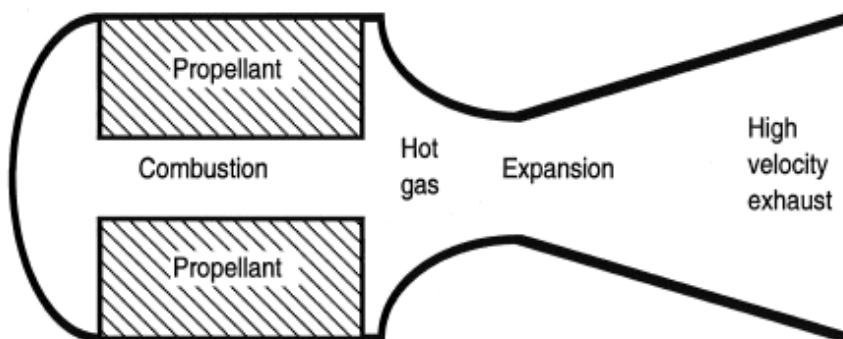


Fig. 1.1 - A common solid-core rocket engine [2].

Thrust can be easily evaluated according to Newton's third law of motion as:

$$F = \dot{m} \cdot u_{eff} \quad (1.1)$$

Where \dot{m} is the propellant mass flow rate and u_{eff} is the effective propellant velocity, which depends on the pressure at the nozzle exit p_e , outer (ambient) pressure p_o and nozzle flow area A_0 at the exit.

$$u_{eff} = u_{exit} + \frac{(p_e - p_o)A_o}{\dot{m}} \quad (1.2)$$

Even if it may not look obvious at first glance, u_{eff} can be maximized letting p_e approach the ambient pressure. To understand it qualitatively, one should recall that both the force accelerating the exhaust and the retarding force depend on the integral over the entire area (chamber and nozzle): increasing the nozzle length will increase the total area over which the integral is evaluated. If the internal pressure is greater than the ambient pressure, the net force resulting from length increase will add to the thrust. Clearly, the pressure drop inside the nozzle is directly related to nozzle length, thus the maximum length is reached when $p_e = p_o$. From an engineering viewpoint, there is a threshold value above which the nozzle mass increase overcomes the benefit of the surface increase, implying an exit pressure higher than the ambient one. In the following analysis it is assumed that $p_e = p_o$ for sake of simplicity. Coming back to the expression for u_{eff} , the exit velocity can be derived from basic thermodynamics as:

$$u_{exit} = \sqrt{\frac{T_c \cdot R}{MM} \cdot \frac{2\gamma}{\gamma-1} \left(1 - \left(\frac{p_e}{p_c} \right)^{\frac{\gamma-1}{\gamma}} \right)} \quad (1.3)$$

Where T_c is the combustion chamber gas temperature (or, in case of a reactor, the core outlet temperature), R is the universal gas constant, MM is the molecular mass of the gas, γ is the isentropic coefficient and p_c is the chamber pressure (or, for a reactor, the outlet coolant pressure). Thus, for a perfect nozzle in vacuum ($p_e = 0$), the above expression reduces to:

$$u_{exit,vac} = \sqrt{\frac{T_c \cdot R}{MM} \cdot \left(\frac{2\gamma}{1-\gamma} \right)} \quad (1.4)$$

meaning that a rocket performs better in vacuum. Exit velocity depends on chamber temperature, which is reasonable since a higher propellant temperature translates in higher internal energy, thus larger kinetic energy at nozzle exit. The dependence on the propellant

molecular mass plays an important role in rocket optimization and propellant choice: when possible, hydrogen is obviously the best choice.

Concerning electrical propulsion, its working principle is slightly different: ions are accelerated by means of an electromagnetic field and then ejected; however, since it is not the topic of this work, the mathematical background for this technology is not presented.

The second relevant rocket parameter is the specific impulse i_{sp} : it is a measure of the momentum variation per unit propellant mass; it can be therefore considered a quantity related to rocket propellant efficiency.

$$I_{sp} = \frac{F}{\dot{m}g} \propto \sqrt{\frac{T_c}{MM}} \quad (1.5)$$

where F is the thrust and g is the Earth gravity acceleration.

Finally, the thrust-to-weight ratio is a dimensionless parameter that measure the ratio between the thrust generated and the rocket or engine weight:

$$TWR = \frac{F}{Mg} \quad (1.6)$$

The TWR plays an important role when comparing different engines and rockets, or when an optimization is carried out. Indeed, an increase in thrust may not be advantageous if the consequent mass increase overcomes possible benefits.

At the present time, the main, available technologies for space propulsion rely on chemical or nuclear fuel. Chemical propulsion has been used since the first launch: nowadays, it is a well-known and established concept all over the world. It provides high thrust, reasonable thrust to weight ratio, and specific impulse of the order of 400s. However, nuclear propulsion may constitute a valid alternative to chemical propulsion, as illustrated in the following sections.

1.1.2 Nuclear Electrical Propulsion

In this concept a solid core operating at low thermal power is coupled with a power conversion system that provide electric power to ion thrusters. Thermal power from the core is extracted passively by thermoionic or thermoelectric converters, actively by a closed thermodynamic loop: in any case there is not high-temperature propellant ejection.

Thermoionic [3] and thermoelectric [4] systems are characterized by no moving parts and no vibrations related to power conversion components (turbines, pumps), low maintenance requirements, high power density and efficiency independent of size.

Standard thermodynamic conversion relies on well know concepts (e.g. Brayton cycle) and components, making NEP a mature technology on a wide power range. However, the lower cycle temperature constitutes a relevant issue: if it is too low, the radiator cannot radiate enough waste power; if it is too high, the cycle efficiency drops. Specific impulse of NEP is quite large ($i_{sp} = 2000 \div 5000 \text{ s}$) [5] if compared to NTP, but its TWR is dramatically lower: the required components for NEP add much weight to the spacecraft, leading to TWR tens or hundreds lower than NTP. For these reasons, NEP is suitable for manoeuvres far from high gravity fields; in addition, it may provide electric power for payload and crew for the whole mission time.

1.1.3 Nuclear Thermal Propulsion

The working principle of NTP [2] is quite different from chemical rockets: the propellant, liquid H_2 , provides also reactor cooling, keeping the temperatures at an acceptable level. The core works as the heating source, while a turbine in the turbopump assembly generates power for auxiliary systems, such as pumps or propellant tank cooling system. The hydrogen is heated by flowing through the core and finally ejected through the nozzle to generate thrust.

Specifically, from the propellant tank, hydrogen in cryogenic conditions is pumped into the main circuit: this is usually done by two stages pump, where the first stage is an impeller that raises the pressure up to 20 bar and the second stage is an high-pressure pump that increases the pressure to its maximum value. Then, the propellant is sent to moderator channels (except for a fraction which is sent to the nozzle), it flows from top to bottom and to the top again, where it mixes in an upper plenum. The hydrogen that is sent to the nozzle flows inside channels that wrap around this component and carry out a critical function, because the propellant must cool down the nozzle itself to avoid damages and localized melting due to the high temperature exhausts. These two different propellant flows finally mix in the upper plenum and enter the fuel channels, raising the hydrogen temperature up to 2500 – 3000 K. A lower plenum collects the propellant coming from the channels and sends it to the nozzle. In addition to these systems, a radiation shield is mandatory, in order to protect the crew from possible radiations coming from the reactor; since neutrons shields are often made of high-density materials, they add a non-negligible mass to the whole system.

Waste heat is another issue to deal with: even the dissipation of a small power fraction may be challenging in space and requires large radiators. The reactor will not work at full power for the whole mission time, thus the decay heat must be handled carefully; as an example, a 500 MW_{th} reactor in idling mode would produce 5 MW_{th} (assuming decay heat as 1% of nominal power) for a long time, which may need a small fraction of propellant to be pumped inside the core and then ejected: from a propulsion perspective, this propellant required for cooling in idling mode is considered a loss, because of its low exit temperature and the resulting low efficiency.

In the past, focus was on fast reactors with high enrichment (97%), allowing for a compact design and no need of moderator materials; in the last decades the interest moved toward LEU (Low-Enriched Uranium) reactors (enrichment < 20%) due to both safety and proliferation concerns for HEU (High-Enriched Uranium) reactors. An important side effect of the

development of LEU reactors for space propulsion is the possibility for private companies to join the work in this sector.

An advanced concept related to NTP is the bimodal hybrid (Nuclear Thermal/Nuclear Electric) propulsion: in this configuration, a solid core such as the one described previously is used for large thrust manoeuvres, while, when the rocket is far from gravitational fields, the reactor is run at low thermal power level, allowing a simple cooling by a closed-loop flow of coolant. The power is then extracted by a conversion system that feeds the electric propulsion.

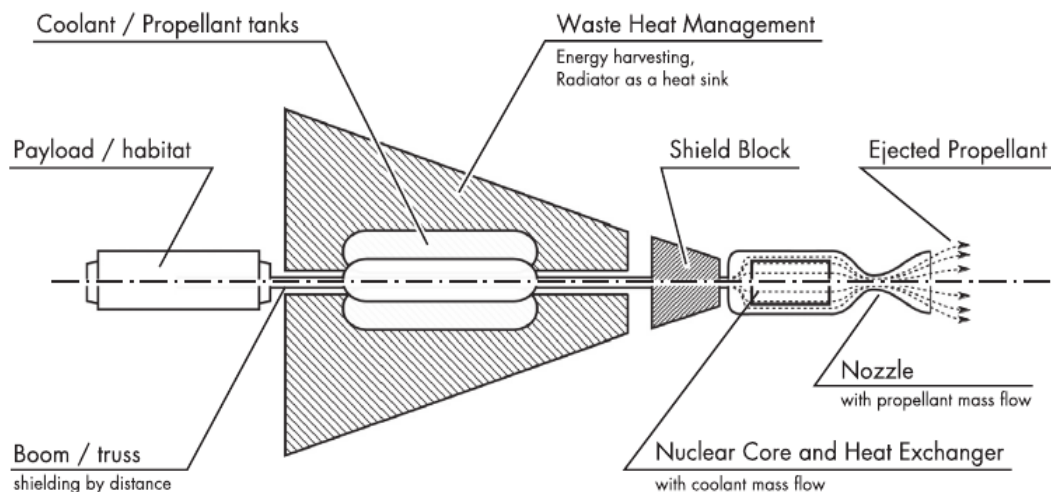


Fig. 1.2 - Schematic view of a rocket for NTP [6].

The development of NASA Design Reference Architecture (DRA) 5.0 highlighted the importance of nuclear thermal propulsion through performance assessments of both NTP and advanced chemical propulsion. While the second concept is still mandatory to escape Earth gravity, NTP is the preferred propulsion system for the interplanetary travel to Mars. Therefore, deep and complete studies on NTP are desirable to finally unlock this key technology.

1.2 Reactor configuration

Solid, liquid and gaseous cores have been proposed along the past years; however, at the moment, solid core looks as the most feasible and realistic option [5].

In this work, the reactor configuration is derived from Rover/NERVA program: a cylindrical core, with hexagonal fuel and moderating elements. Both fuel and moderating elements have a 1.905 flat-to-flat distance. Each fuel element is crossed by 19 coolant channels, in which liquid hydrogen flows. The fuel is a $(U,Zr)C$ composite, with 2 different enrichments, 17% and 20%. Many studies were performed on composite fuels during the above-mentioned program and a vast literature is available [7]. Moderating elements have a concentric structure; starting from the centre, the structure is: coolant channel, Zircaloy-4 cladding, $ZrH_{1.8}$ moderator, coolant channel, Zircaloy-4 cladding, thermal insulator; the region outside the thermal insulator is made of graphite. There is a specific reason for this choice of materials, which will be analysed in the following sections.

The core is a 35 cm radius and 75 cm height cylinder, with 2 different enrichment zones and a radial and axial reflector. Both radial and axial reflectors are 20 cm thick, but the axial reflector is present only on the core upper region: indeed, the axial reflector is crossed by the coolant channels, and the high coolant outlet temperature is incompatible with the reflector material. To achieve a uniform propellant temperature, a lower plenum is placed below the active region. Reactor control is performed by 12 beryllium control drums, equipped with a neutron absorber plate, specifically B_4C .

Finally, reactor power is set to 450MW: this value should provide the thrust and i_{sp} required by NASA DRA 5.0.

In the following figures (**Fig. 1.3** to **Fig. 1.6**) the reactor geometry is presented. The images were obtained by Serpent *plot* option, and the geometry was generated by Serpent geometry model. This geometry will be used as Serpent input for the NERVA derived reactor (Section 2.1).

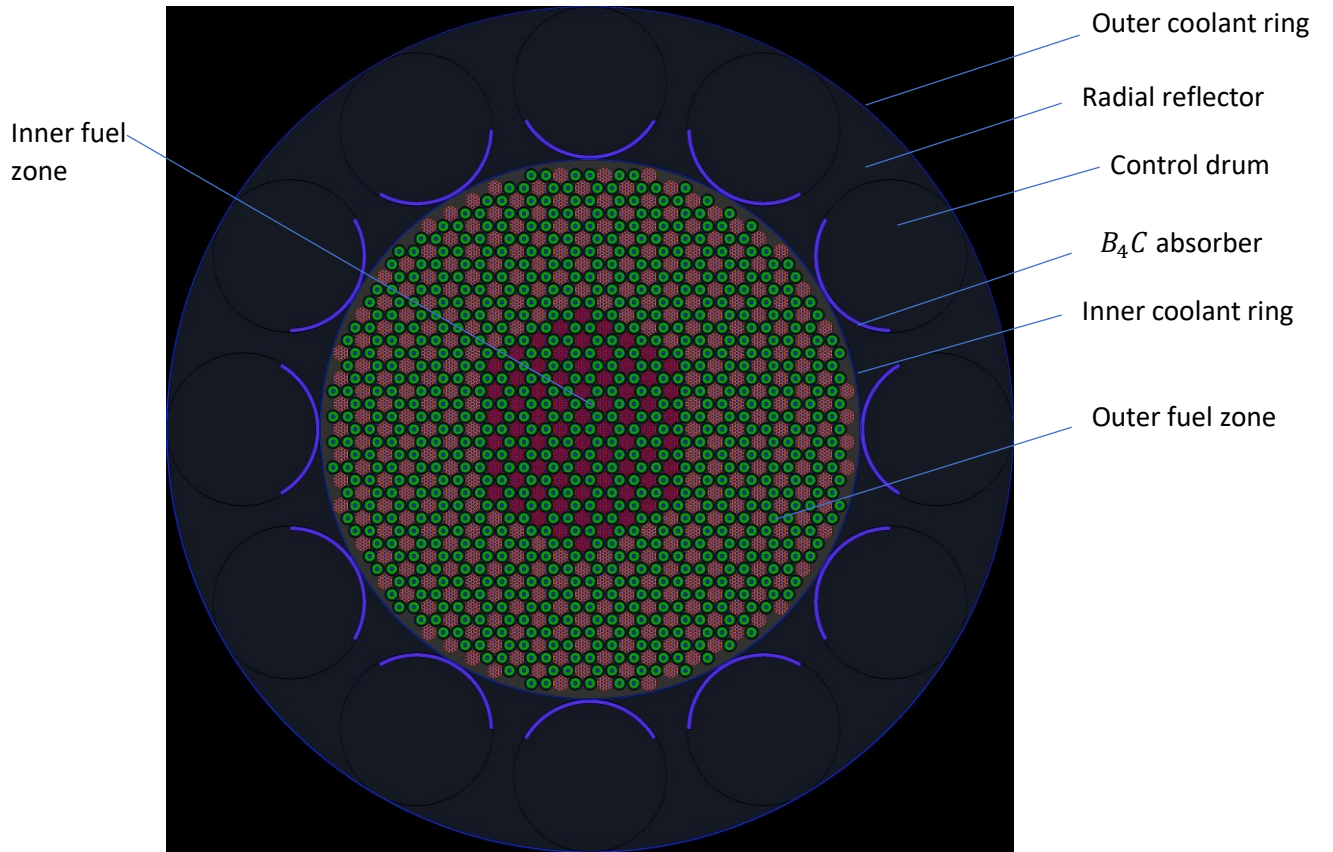


Fig. 1.3 - Core poloidal section – NERVA derived reactor (Serpent input).

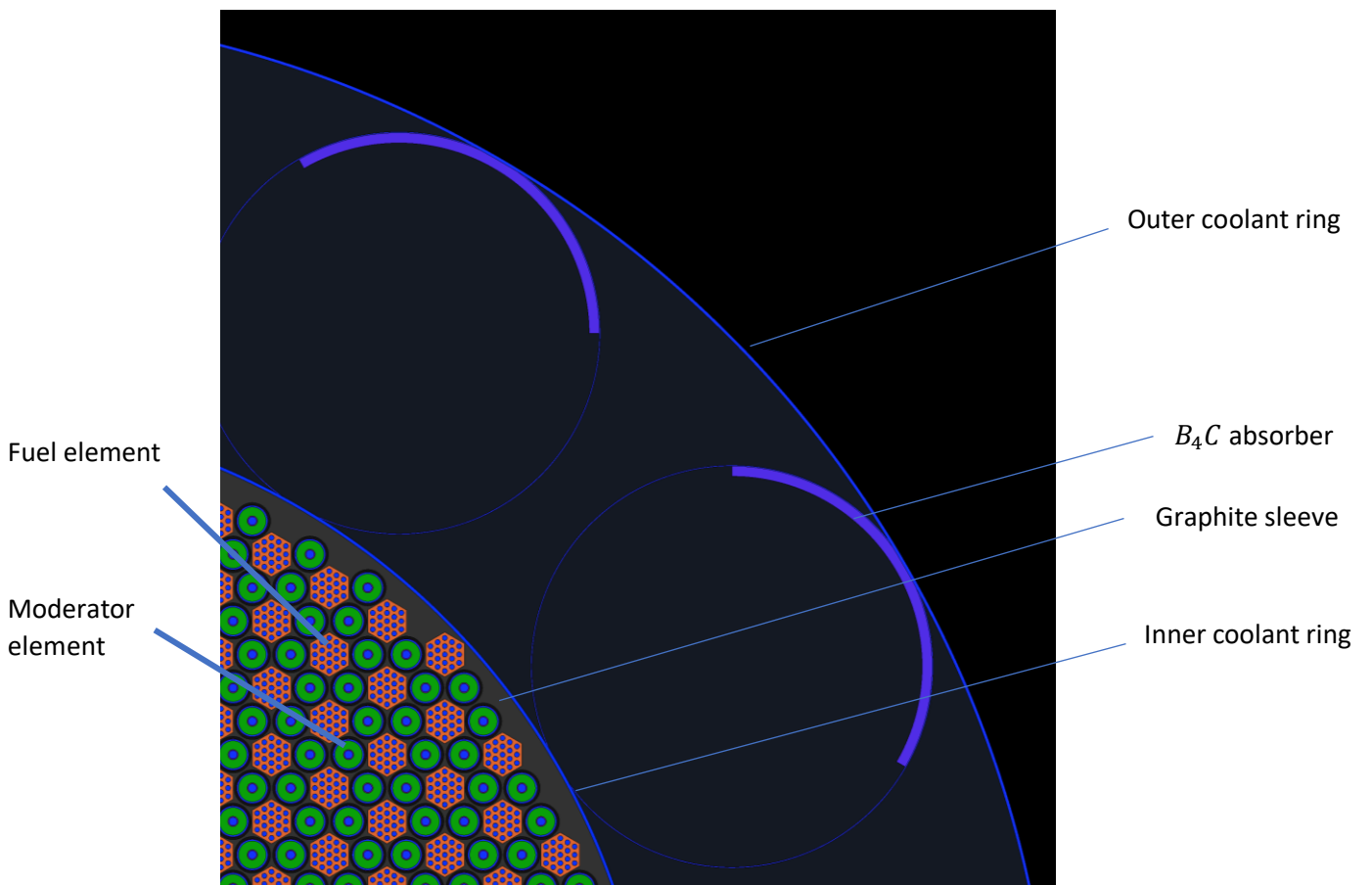


Fig. 1.4 – Core poloidal section detail – NERVA derived reactor (Serpent input).

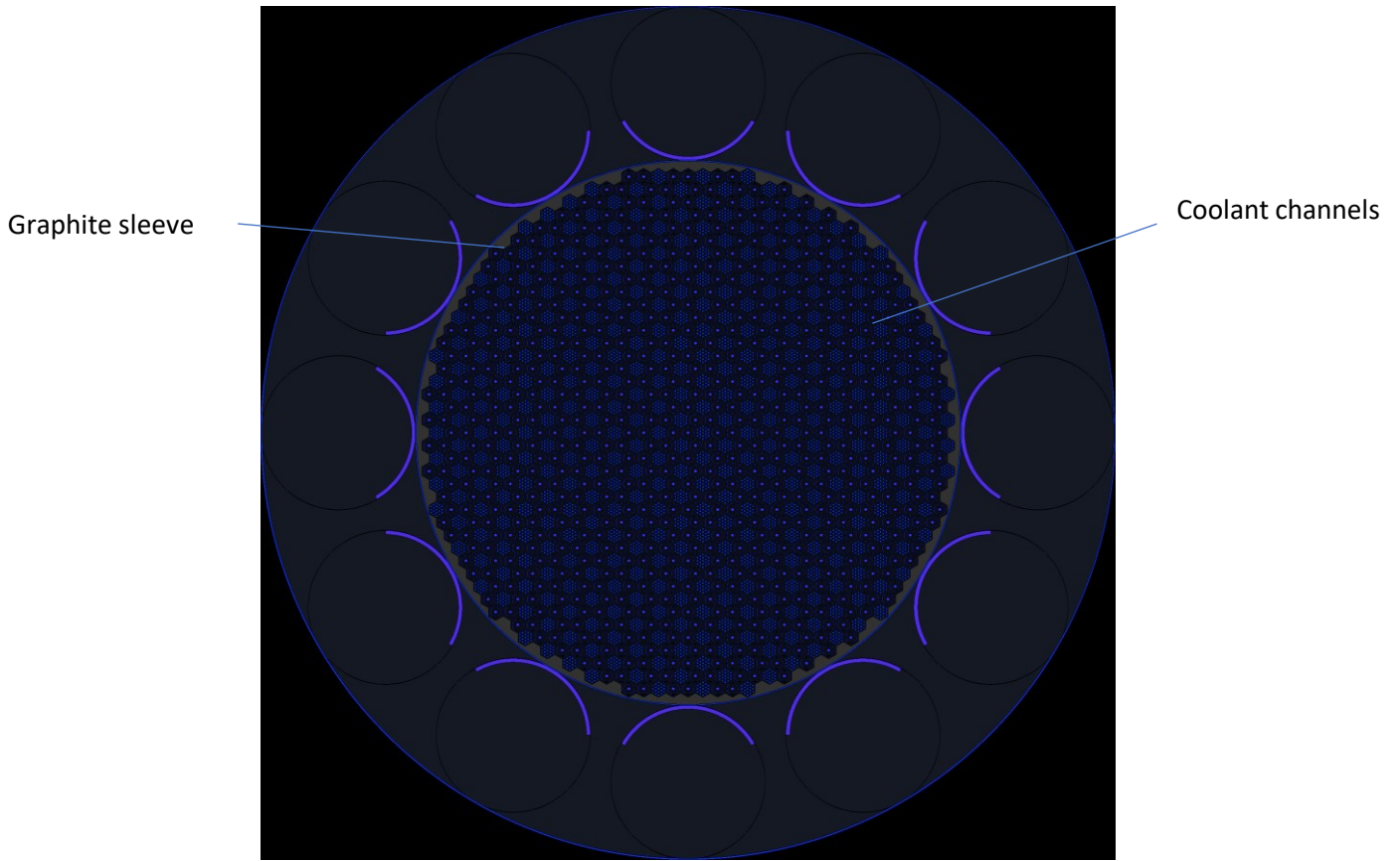


Fig. 1.5 - Axial reflector poloidal section – NERVA derived reactor (Serpent input).

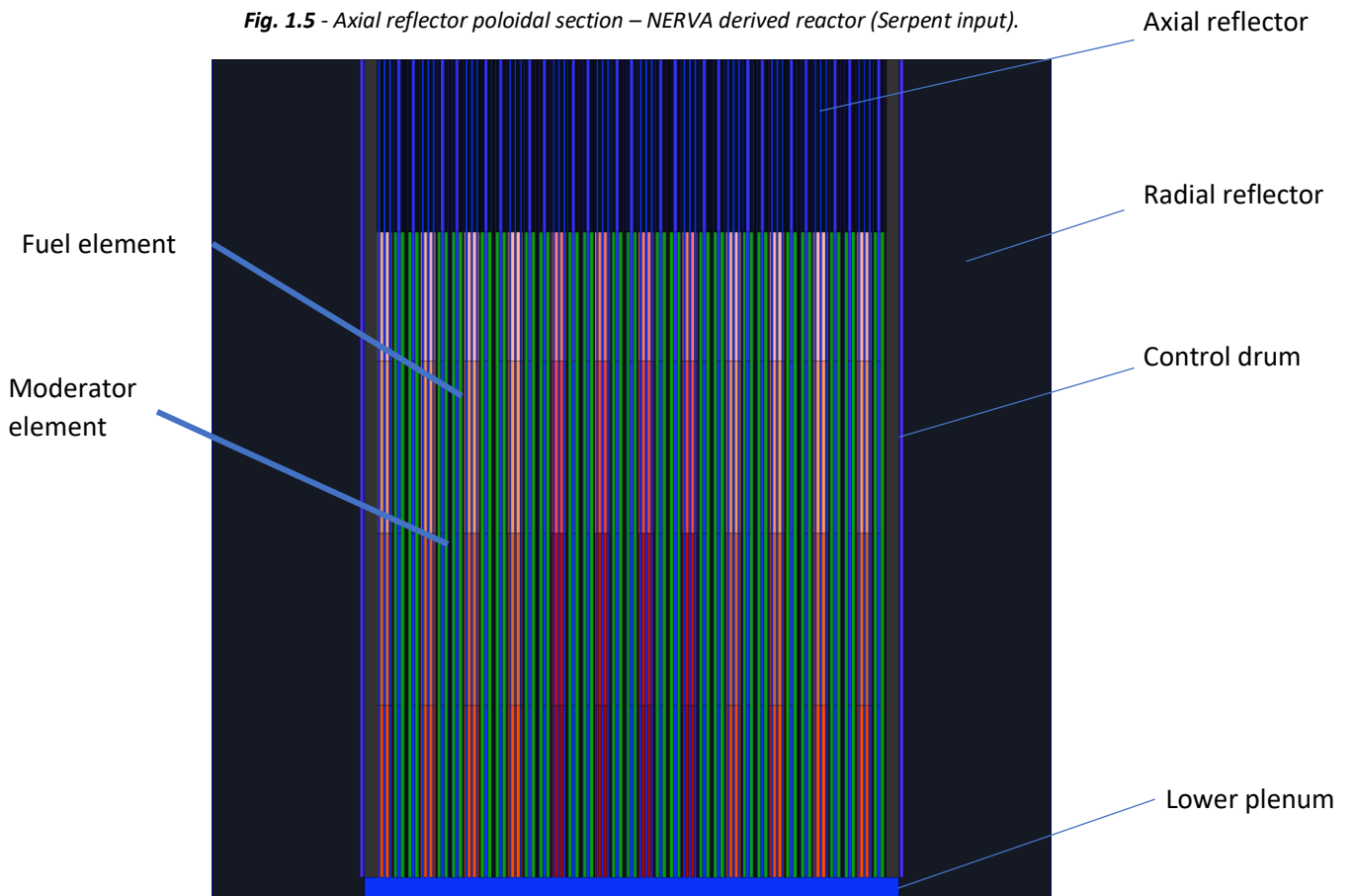


Fig. 1.6 - Core axial section (Different colours on the axial direction refer to different fuel temperature, on the radial direction to different enrichments) – NERVA derived reactor (Serpent input).

1.2.1 Fuel elements

Four generic requirements must be satisfied by the fuel:

- High melting point (operational temperature larger than 2500K)
- Chemical compatibility with coolant and cladding
- Low neutrons absorption cross section
- Good structural properties

Many fuels were tested during Rover and NERVA programs [7]: *UC* pebble bed, with a pyrolytic coating, was found as one of the most suitable. Further tests showed the feasibility of $(U,Zr)C$ hexagonal fuel elements with a graphite matrix, which have higher melting temperature thanks to the *Zr* addition.

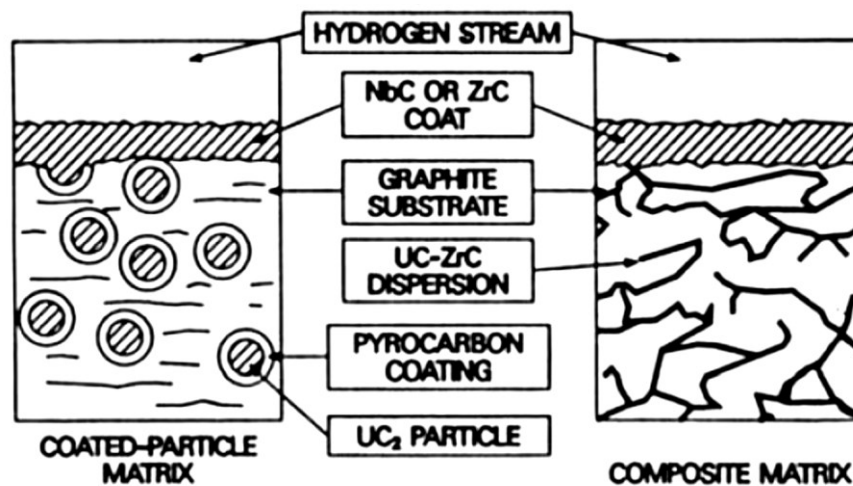


Fig. 1.7 - Coated-particle and composite fuel detail [8].

Graphite has a low absorption cross section and good scattering properties, but it reacts with hydrogen, especially at the high temperatures expected in the reactor, leading to a fast matrix erosion; for this reason, a *ZrC* or *NbC* coating is required. A technological issue related to that is the discrepancy between fuel and coating thermal expansion coefficients: their value should be as similar as possible, to avoid cracks formation during the production process; *NbC* and *ZrC* have similar thermal expansion coefficients, making them almost interchangeable. *ZrC* has better neutronic properties (lower neutrons absorption), but its melting temperature is lower than *NbC* melting temperature (3450K versus 3770K), at least for standard production techniques [2]: novel techniques seems capable to bring *ZrC* melting temperature up to 3900K [9]. Even if *ZrC* was demonstrated to be superior to *NbC* [8], both *NbC* and *ZrC*

coatings will be analysed in the following sections. Another limiting property of graphite is its structural resistance: to maintain a sufficiently high matrix resistance, fuel volume inside the matrix should not exceed 35 % of the total volume, leading to a maximum fuel loading of 0.64 g/cm³ [7].

Another viable fuel option for nuclear thermal propulsion are CERMET (Ceramic-Metallic) fuels: these fuels are usually composed by UO_2 or UC and a refractory metal. The following refractory metals have been tested for space applications [9]: Ir , Nb , Ta , Re , Mo and W . Their main advantage is the extremely high melting temperature, combined with high thermal conductivity and strength. When adopted for a LEU reactor, they should clearly have a low absorption cross section and chemical compatibility with fuel. High absorption cross section (Ir), hydrogen uptake at relatively low temperatures (Nb and Ta), chemical incompatibility with fuel at high temperature (Re), low performances as alloying element at high temperatures (Mo), leads to the selection of Tungsten based fuels. It should be noted that W is not exempt by issues: absorption cross section must be reduced by enrichment in $W-184$ and Ductile to Brittle Transition Temperature must be taken in serious consideration when designing the fuel elements, especially for a space reactor that will operate in many burn cycles with consequent large temperature excursions. Considering the advantages, W based fuels have good self-shielding properties, very effective fission product retention and they are proliferation resistant, because it is really hard to extract uranium from their matrix (in contrast with composite fuels, which can be easily fractured) [10]. The fuels considered in this work are the $(U,Zr)C$ carbide and UO_2-ThO_2-W .

As already said, the fuel element is a hexagon with 1.905cm flat-to-flat distance with 19 cooling channels: this geometry is a heritage from NERVA project, and it was successfully tested during that program.

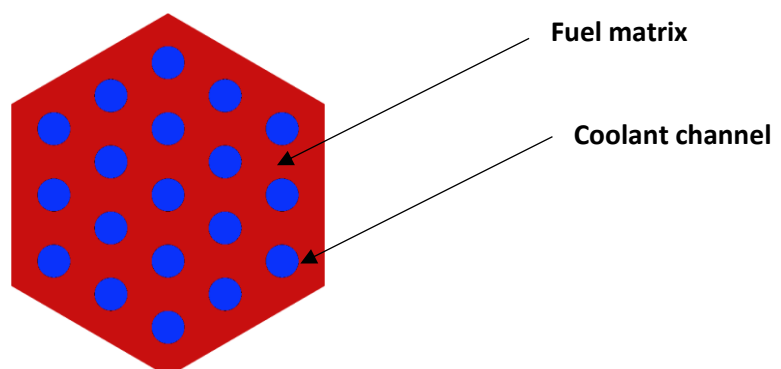


Fig. 1.8 - Core fuel element – NERVA derived reactor (Serpent input).

1.2.2 Moderator elements

Moderator elements are extremely important in a thermal reactor, since they allow neutrons to be slowed down to thermal energies: indeed, at these energies the fission cross section of U_{235} increases. The difference between an unmoderated and a moderated core is shown in **Fig. 1.9**. The neutron spectrum was obtained by Serpent detector *dt*.

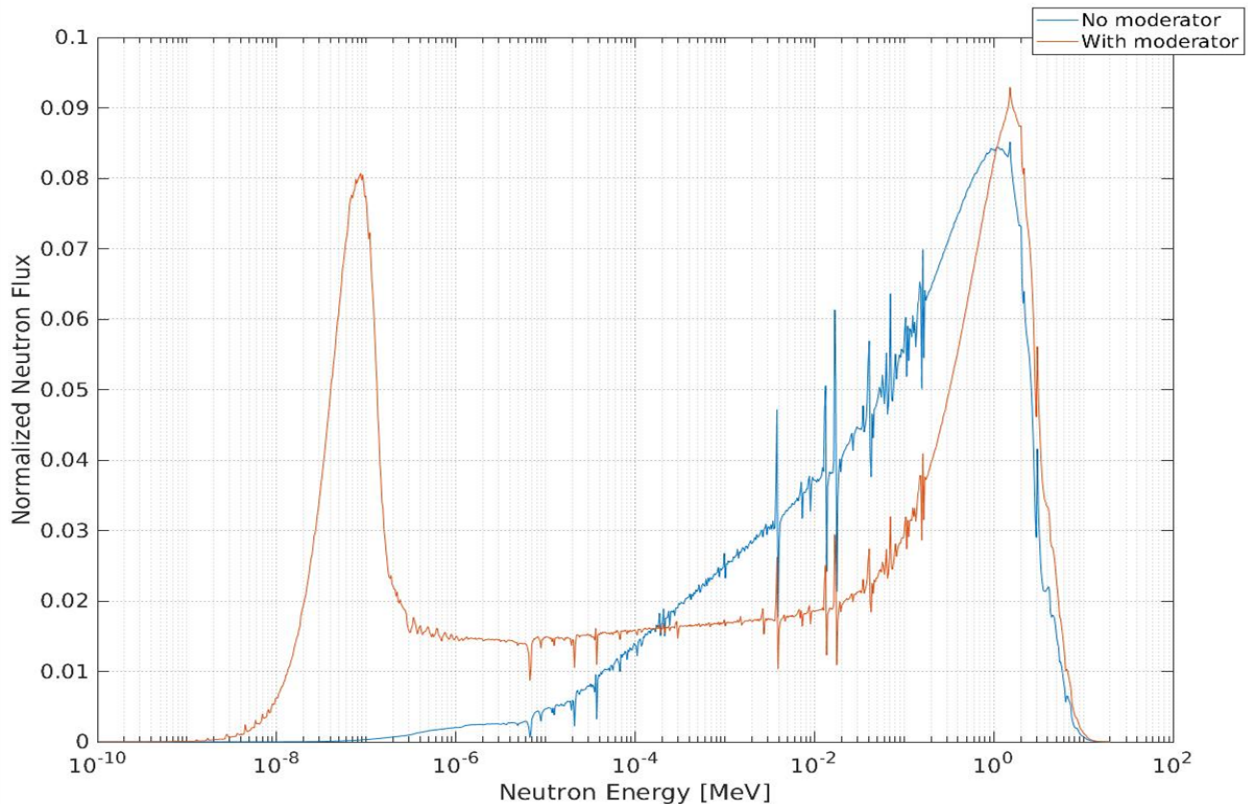


Fig. 1.9 - Neutron spectrum for moderated and unmoderated core – NERVA derived reactor.

The choice of moderator elements' material is limited to solid, because of volume constraints. Among solid moderators, the most promising are graphite, beryllium, zirconium hydrate ($ZrH_{1.8}$) and Lithium Hydrate (7LiH). The first two materials have high melting temperature, making them particularly suitable for such a reactor; however, graphite undergoes to chemical reactions when it comes in contact with high temperature hydrogen, while beryllium, even being a neutron multiplier (due to $(n,2n)$ reaction), suffers from loss of structural integrity because of He production. Lithium presents a similar issue, having the 6Li a very large absorption cross section, which leads to tritium and helium production. Therefore, $ZrH_{1.8}$ is the most suitable moderator, even if its thermo-mechanical properties are not comparable to

those of graphite and beryllium, and its moderating capability is lower than ${}^7\text{Li}$ capability. Moderator elements structure is designed to prevent the $\text{ZrH}_{1.8}$ moderator to reach high temperatures; indeed, the insulator (ZrC 50% TD [11]) protects the $\text{ZrH}_{1.8}$ from the large power produced in fuel elements, while the inner Zircaloy cladding prevents interactions between the coolant hydrogen and the moderator. The standard NERVA moderating element is shown in **Fig. 1.10**, where the outer radius of each Serpent geometric surface is reported.

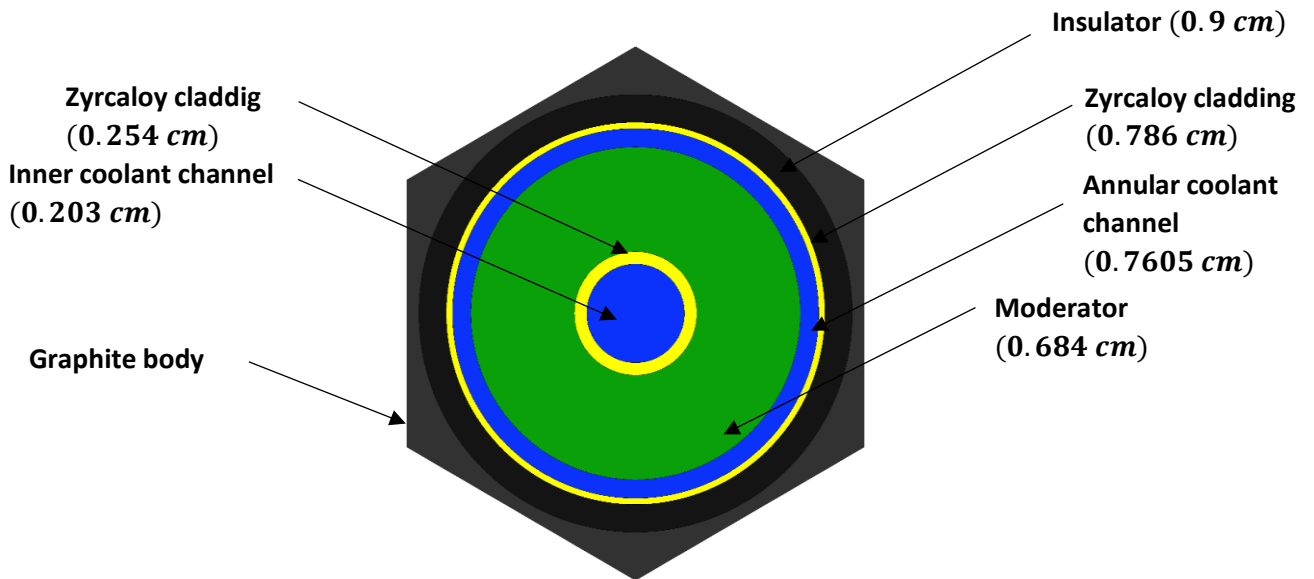


Fig. 1.10 - Core moderating element and surfaces outer radii – NERVA derived reactor (Serpent input).

1.2.3 Reflector and control drums

In space propulsion reactors, the reflector is extremely important not only for the neutron leakage decrease that it provides, but also for its reactivity active control. Its mass gives a large contribution to the total reactor mass, making it a component of interest when dealing with mass reduction optimization.

The radial reflector is made of metallic beryllium, which combines acceptable density (1.85 g/cm^3) with good reflective and moderating properties. It surrounds the core for the entire length, and it is equipped with 12 rotating control drums (CD), made of metallic *Be*, with a 120° circular sector in B_4C absorber. CD working principle is simple: when the absorber is facing the core, the neutron absorption is maximum, allowing to bring the reactor in a subcritical state; when the absorber is facing outward, the positive reactivity insertion is maximum. Tuning the rotational angle keeps the reactor critical. It is clear that the CD control worth should be high enough to compensate reactivity losses due to burnup and to bring the reactor subcritical even in accidental scenarios. Many different control systems have been proposed in the past: control shutter, slats or petals layout and the widely adopted (in terrestrial applications) control rods. However, control drums are the most endorsed technology, thanks to their easy implementation (both from the technological and engineering viewpoint) and to their widespread adoption in previous design. For these reasons, control drums are the selected reactivity control system in this work.

The axial reflector is crossed by the totality of the coolant channels and it is located only on the top of the core, being the temperature around the core bottom too high for both *Be* metal and *BeO*.

Metallic beryllium is not suitable for the upper axial reflector either, because at temperatures $T > 600K$ it is prone to interact with the hydrogen flowing in coolant channels [12]; the problem is overcome using *BeO* instead of *Be*.

1.3 Methodology and goals

Many previous works focused only on a specific design topic, such as neutronics or thermal-hydraulics, without exploring possible interactions between different areas. The accidental scenarios analysis is usually tackled as a standalone problem, and not as an issue that actually leads the design, strongly affecting both neutronics and thermal-hydraulics. Trying to overcome these limitations, the present work approaches the design in a more complete way, investigating various configurations until a reactor design that is safe, highly performing and that fulfils NASA requirements is found.

In doing so, a rigorous model is developed and then applied to this innovative and still scarcely investigated class of reactors: the LEU, CERMET fuelled reactor. A strong effort was made to elaborate a code which eliminates user intervention (and consequently user errors), minimizes time between simulations and handles all the simulation phases integrating different software. The ultimate objective is clearly designing a reactor with comparable, or even higher, propulsive performances with respect to the cases available in literature. As already stated, realistic results are sought, but due to the lack of computational resources these results are not intended to be real design quantities.

A complete neutronic and thermal-hydraulic analysis of the reactor implies the adoption of different software and models. Among the possible software, Serpent is the one chosen for the neutronic simulation. Serpent is a 3D continuous-energy Monte Carlo based code [13] for reactor physics and burnup simulation, which returns all the main neutronics quantities and is highly customisable to satisfy user requirements thanks to detectors implementation. The advantages related to the adoption of a MC code instead of a deterministic one derive from the MC capability to catch specific and local phenomena that would require extremely high computational efforts to be retrieved with a deterministic code. Indeed, the transport process is handled at neutron interaction level, without major approximations, while the method itself can be applied to different fuels and reactors without losing the reliability of the calculation scheme [14]. Thermal-hydraulic calculations are performed by MATLAB: its choice, instead of a thermal-hydraulic code or a CFD software, is justified by the fact that this is a preliminary design, without any ambition to provide definitive results for a real reactor design. This consideration leads to the adoption of a self-developed MATLAB code, which evaluates only the quantities of interest; it also proves to be much more efficient (from a computational time

perspective) and flexible than other software. Since it turns out that the pre-processing and post-processing of both neutronic and thermal-hydraulic simulations is heavily time consuming, especially when dealing with several core configurations, a Python code was developed to handle the whole process. This will be discussed in detail later in the work.

From the above considerations, it looks reasonable to check the validity of the entire model against an available case in literature; furthermore, there are other reasons which may be of concern for the model development, as shown hereafter.

The core contains a huge number of materials, each one with its properties and chemical composition. Values slightly differ depending on the reference, and this will reflect on results. There are many ways to model the reactor when dealing with the thermal-hydraulic simulations, many applicable correlations and possible simplifying assumptions. In addition to that, the geometry and layout of the core is not unique, and small differences are found among the authors.

For all these reasons, the following approach is outlined before starting the work: first of all, a core from literature is selected and the own model is built and tested. Once the model can be considered correct, the optimization of the core is performed: this involves geometry and layout modifications, materials substitutions, enrichment variations. Performing the optimization on a core with a long history in literature allows to check at any step whether the results are reasonable or not and gives many information on the best way to approach the optimization itself. Finally, with the experience gained from this preliminary work, a LEU reactor fuelled with CERMET is designed and optimized to meet the thrust and specific impulse requirements: this last step reveals the necessity to develop a fully automated model, which can handle the whole simulation (from Serpent input creation to results post-processing) without user intervention. The analysis may be divided in three sections: neutronics, safety and thermal-hydraulics. Even if these sections are linked together (the reader can easily follow the logical path behind the reactor design), each one is intended to be self-consistent: hypothesis, modellization and procedures may be applied independently to the other sections and to any reactor of this class.

2. Neutronic Analysis

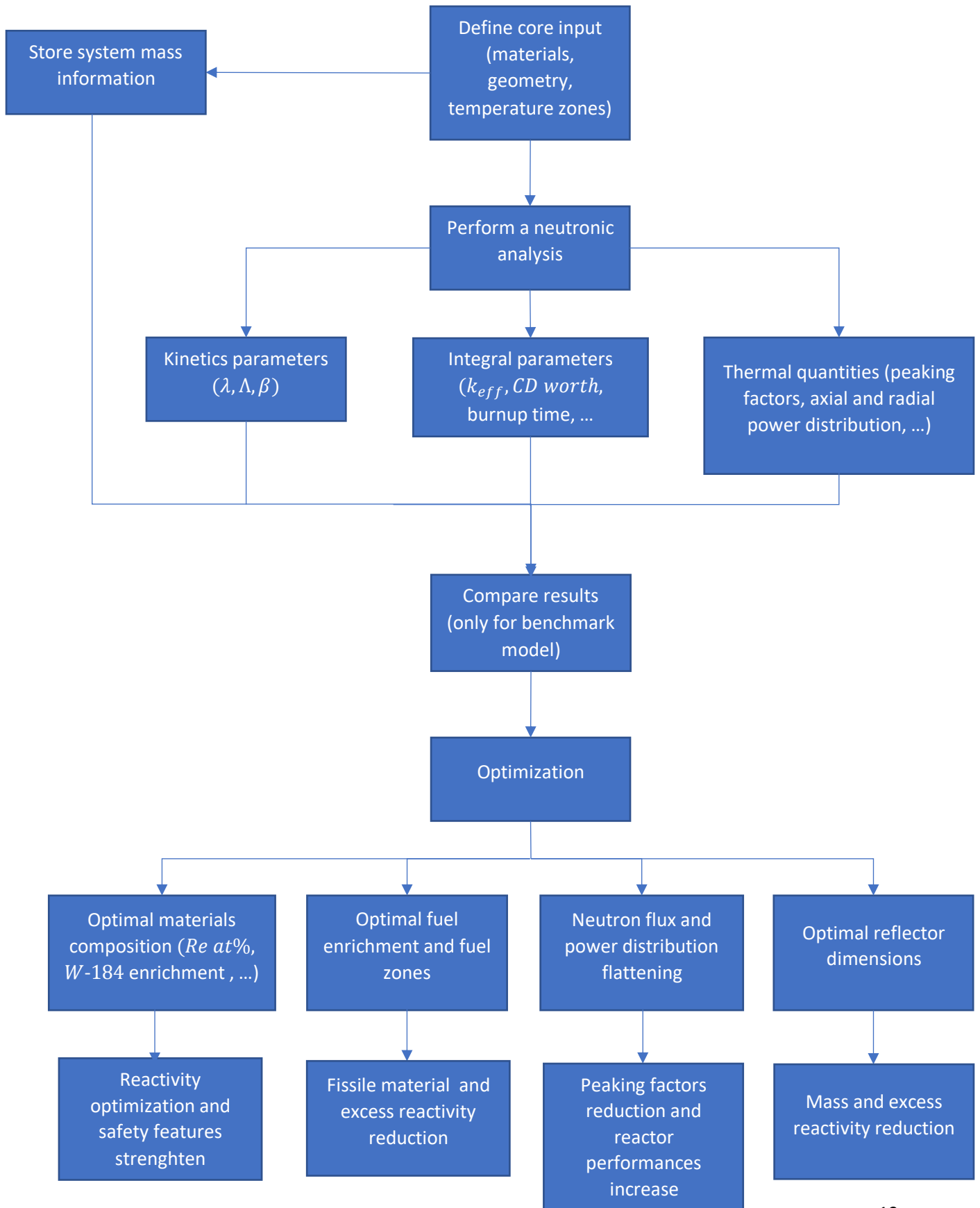
A neutronic analysis and the consequent optimization of a reactor is a challenging work, which implies the investigation of both neutronics and core materials. It is the starting point for the reactor design, because the neutronic analysis returns important information on core criticality, fuel depletion, neutron flux and power distributions, control system reactivity worth and dynamics parameters; furthermore, it allows for a comparison among different materials. All those parameters heavily affect reactor behaviour: if the excess reactivity is too low, the reactor cannot operate for the required mission time; conversely, if it is too large, supercriticality issues arise in accidental scenarios, thus leaving space for an optimization focused on fuel enrichment and layout. Neutron flux and the consequent power distribution highlight possible optimizations from the thermal viewpoint, which can be performed acting on fuel enrichment and fuel zones, reflector design and core thermal-hydraulics, with an increase of the overall rocket performances. Since the reactor will operate in space without any human intervention, the control system must be capable to handle any possible scenario: this implies that the CD reactivity worth must be known and tuned precisely. Kinetics parameters are fundamental for the reactor dynamics description, allowing for a transient modelling of the reactor. From a theoretical viewpoint, reactor dynamics can be described by the point kinetics equations, which read as [15]:

$$\begin{cases} \frac{dn}{dt} = \frac{\rho - \beta}{\Lambda} n + \sum_{k=1}^6 \lambda_k C_k \\ \frac{dC_k}{dt} = \frac{\beta_k}{\Lambda} n - \lambda_k C_k \end{cases} \quad k = 1, \dots, 6 \quad (2.1)$$

Where n is the neutron density, C_k is the k -th precursor concentration and ρ the reactivity. The main kinetics quantities appearing in the kinetics equations are the decay constant λ_k for each precursor group, the delayed neutron fraction β_k and the mean generation time Λ . The knowledge of β is extremely important, since it defines the threshold for reactor prompt criticality, while λ and Λ define the timescale of the neutron population evolution.

The nuclear data library chosen for the simulation is the JEFF-3.3 library [16]: since the results may show dramatical differences depending on the library, a future work on results sensitivity

implementing various libraries is advisable. The procedure and the reasoning behind the neutronic analysis is summarized in the following flowgraph.



For a thermal, LEU reactor there are several issues that must be faced: first, the excess reactivity should be high enough to ensure criticality for the whole mission time, but reasonably low to avoid supercriticality in accidental scenarios. Secondly, the only active control system is the control drums (CD) system: this means that the CD reactivity worth must be known for every possible angle of rotation, and the CD absorber thickness needs to be tuned to find the optimal value of control worth. Furthermore, reflector thickness has a dramatical impact on both safety and performances, being the heaviest component and strongly affecting neutron flux distribution. Finally, peaking factor must be evaluated and kept as low as possible, since any hotspot would reduce the overall reactor performances. In a system where the mass is a primary constraint, and refuelling is not possible, finding a configuration that can deal with the previously issues requires a systematic approach. To achieve that goal, the reactor model for Serpent was firstly implemented with the most performing materials, according to literature, except for the fuel elements channels' coatings, for which both *ZrC* and *NbC* were tested. Then, a parametric study on reflector thickness, both radial and axial, was carried out to investigate the effects on core neutronics. CD control worth could be easily evaluated by multiple simulations, while a burnup analysis was required to check whether the reactor could handle the 2 hours of expected mission time. The above procedure was successfully applied on a NERVA type reactor, and the results were compared to those available in literature to check model validity. Once the model is shown to be correct, a more systematic approach was followed for a CERMET fuelled reactor analysis, by writing a Python code which handles Serpent simulations. All the work was developed from the basis, since no previous Serpent models or external scripts were available for this class of reactor. Many configurations with different reflector thickness, fuel enrichment and enrichment zones were simulated: implementing a procedure that could modify the last two features efficiently is challenging when dealing with a software like Serpent, but the effort allowed a proper flux flattening, low peaking factors and fissile material saving.

2.1 Base case: NERVA derived reactor

The goal of this section is the development of a neutronic model on Serpent and its application to a system, a reactor for NTP, which presents peculiarities and differences from a common commercial reactor. This procedure will give an insight on that class of reactors, allowing for a model benchmarking too. As previously described, a core from literature is selected to approach the work: the choice falls on C-LEU-NTR [17]. This reactor is an evolution of SNRE (Small Nuclear Rocket Engine) and shows many improvements with respect to previous designs. The reference data are reported below.

	SNRE	C-LEU-NTR
Power [MW]	500	375
Total system mass [kg]	2545	2364
I_{sp} [s]	940	775
Thrust [kN]	72.95	110.89
T/W [–]	2.92	4.8
Mass flow rate in the fuel element [kg/s]	8.5	14.58
^{235}U mass [kg]	59.6	7.18
Number of moderator elements/tie tubes [–]	241	774
Number of fuel elements [–]	564	374
Average fuel exit temperature [K]	2695	1748

Table 2.1 - Reference data for SNRE and C-LEU-NTR [18].

Once the basic design is set, a first group of simulations was run, in order to get the main information which may be of interest for a neutronic and thermal-hydraulic optimization: these data include k_{eff} for both cold and clean and hot reactor, radial and axial reflector thickness effects on k_{eff} , CD worth, radial and axial peaking factor and core power distribution; furthermore, a depletion simulation was run to account for burnup.

Materials composition and properties were retrieved from [7] and [12]. Temperature effects, such as doppler broadening, are handled by Serpent by adding the *temp* entry to materials definition [13]: as initial guess, temperature profiles from SNRE were used. It will be shown that these profiles do not really differ from the ones produced by thermal-hydraulic analysis. Thus, the core was divided axially in four zones, in which a mean temperature was assigned to

the fuel and the coolant. Even if in some zone the temperature exceeds the value used to evaluate fuel cross sections [16], Serpent implements a proper treatment for data extrapolation at higher temperatures. Since the other core materials experience lower temperature variation along the axis, for *Be* reflector, *ZrH_{1.8}* moderator, insulator and graphite a single mean temperature was assigned.

	Coolant temperature in fuel channels [K]	Coolant temperature in moderator channels [K]	Fuel temperature [K]
Zone 1	900	120	1000
Zone 2	1500	220	1600
Zone 3	2300	300	2400
Zone 4	2650	450	2750

Table 2.2 - Mean temperature for different core axial zones.

Coolant density is evaluated for each zone assuming different pressures, according to literature [19]:

	Coolant density in fuel channels (g/cm ³)	Coolant density in moderator channel (g/cm ³)
Zone 1	$9.527 \cdot 10^{-2}$	$1.953 \cdot 10^{-3}$
Zone 2	$2.762 \cdot 10^{-2}$	$1.066 \cdot 10^{-3}$
Zone 3	$1.240 \cdot 10^{-3}$	$6.094 \cdot 10^{-4}$
Zone 4	$5.524 \cdot 10^{-3}$	$4.432 \cdot 10^{-4}$

Table 2.3 - Coolant density along channels [19].

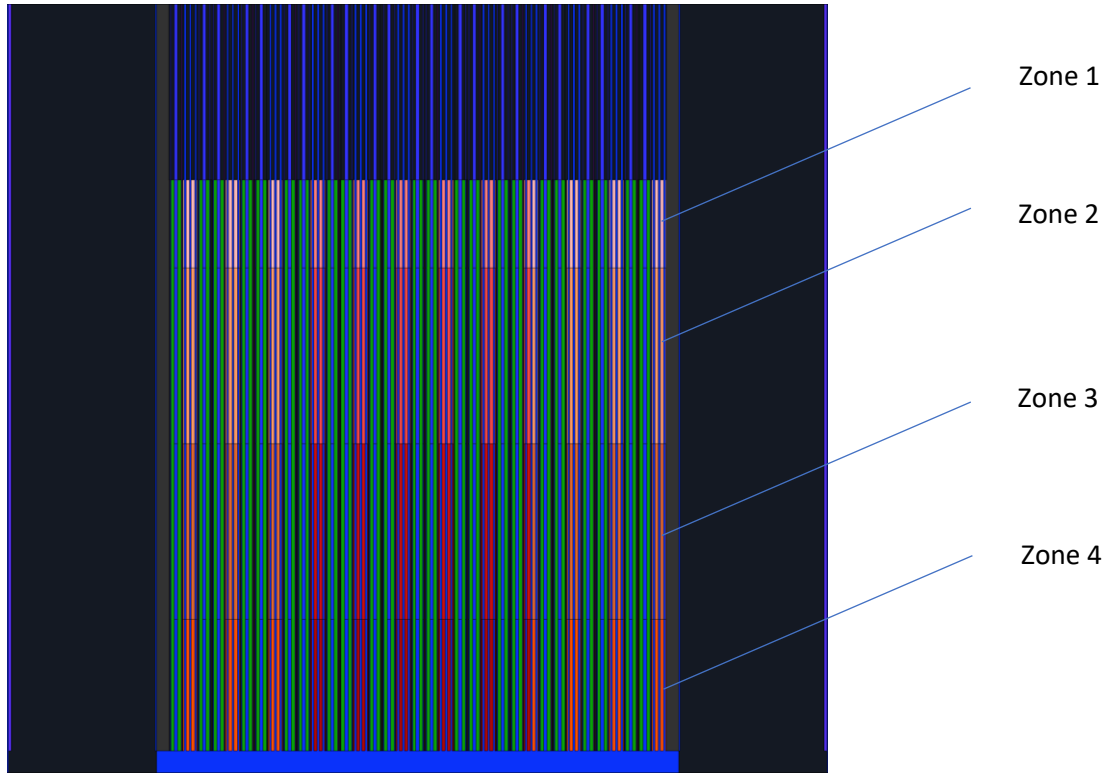


Fig. 2.1 - Core temperature zones division – NERVA derived reactor (Serpent input).

With this basic design, k_{eff} values are very large, both for the *NbC* and thr *ZrC* cladding options, either for cold core or hot core. For the 20 cm thick reflector (both axial and radial), k_{eff} values are reported in the table below.

	Hot reactor k_{eff}	Cold reactor k_{eff}	Hot reactor excess reactivity (\$)
Control drums out	1.12744 ± 0.00040	1.22253 ± 0.00040	21.0
Control drums in	0.96483 ± 0.00040	1.04248 ± 0.00040	–

Table 2.4 - k_{eff} for hot and cold reactor, *NbC* coating (50 inactive cycles, 75 active cycles, 100000 neutrons per cycle).

	Hot reactor k_{eff}	Cold reactor k_{eff}	Hot reactor excess reactivity (\$)
Control drums out	1.19606 ± 0.00040	1.24363 ± 0.00040	32.3
Control drums in	1.02761 ± 0.00040	1.18216 ± 0.00040	4.5

Table 2.5 - k_{eff} for hot and cold reactor, *ZrC* coating (50 inactive cycles, 75 active cycles, 100000 neutrons per cycle).

Temperature effects reduce core reactivity by an amount of 15.7 \$ for *NbC* case and by 7.8 \$ for *ZrC* case: in both cases, the CD are not able to bring the reactor subcritical, highlighting serious control issues at start-up.

ZrC shows better neutronics properties, granting a higher excess reactivity. Large excess reactivity, even for the hot reactor, implies that with this core configuration a coating with good structural and thermomechanical properties should be preferred to a neutronics advantageous cladding. However, if the *ZrC* melting temperature is assumed to be $T_m = 3910$ K [20], zirconium carbide is a reasonable choice as coating material.

For what concerns solution validity, the correct convergence is assured by Shannon entropy: indeed, not only the k_{eff} value should be affected by low error, but the fission source too. Serpent criticality mode relies on a power iteration procedure, with an initial guess on the fission source; it has been shown that the fission source usually converges more slowly than k_{eff} [21]. For this reason, a proper number of inactive cycles must be set in the simulation. Shannon entropy is a suitable quantity to assess convergence, due to its simplicity for both calculation and results interpretation: a 3D grid is superimposed over all the fissionable regions and in each cell the number of fissions is tallied. Being N_s the number of grid boxes and P_j the relative number of source sites in j -th box with respect to the total source sites, Shannon entropy is defined as:

$$H_{fsrc} = - \sum_{i=1}^N P_j \cdot \ln_2 P_j \quad (2.2)$$

and H_{fsrc} converges to a single value when the source distributions approaches stationarity. In the current simulations, 50 inactive cycles may be considered suitable to ensure fission source convergence, as shown in **Fig. 2.2**. The Shannon entropy was obtained as Serpent output by the *set his* card.

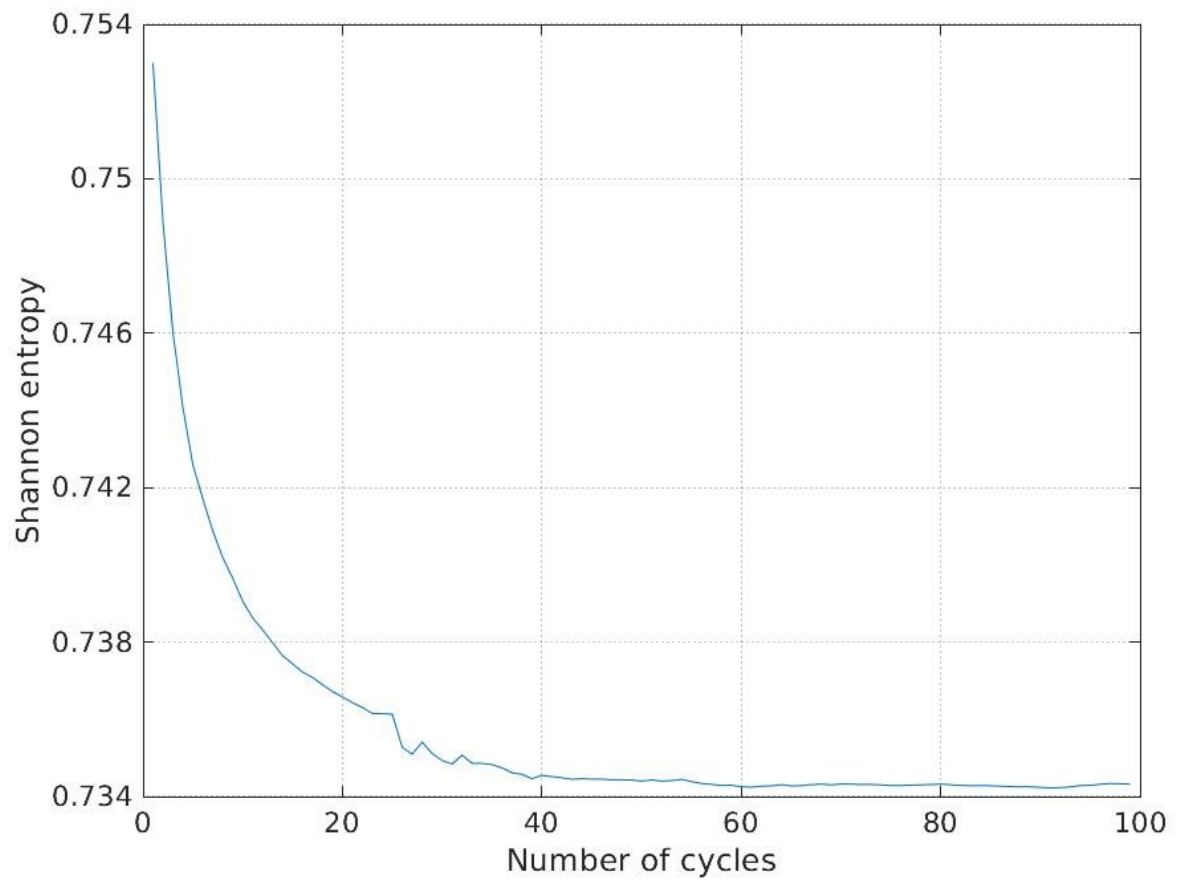


Fig. 2.2 - Shannon entropy vs. cycles number – NERVA derived reactor.

2.1.1 Control Drums reactivity worth

As already said, the reactivity related to control drums rotation is a crucial parameter, being the CD the only component which provides an active control of the reactor. The CD reactivity worth is about 15845 pcm, or 26.1 \$, which may be considered a suitable value, provided that the excess reactivity is reduced: even if the reactor can be brought subcritical, a proper shutdown margin must be foreseen, to face a possible submersion accident. It should be noted that CD reactivity worth may be increased or decreased by changing the B_4C absorber thickness, or by shifting the drums to different radial distances from the core centre. However, while the second option implies a layout modification that is not necessary for the purpose of this analysis, the increase of absorber thickness above a threshold value has no impact on core neutronics: indeed, since CD occupy a peripheral position, any increase in neutron absorption would affect mainly the neutron flux at core boundary; once the flux in that region has been completely depressed, the neutron population becomes almost indifferent to further increase of B_4C in CD. Needless to say, this may be a relevant issue when dealing with accidents.

The following graph shows the CD reactivity worth for different rotation angles: there is not a significant behaviour difference between the ZrC and NbC coating options, leading again to a preference for ZrC coating.

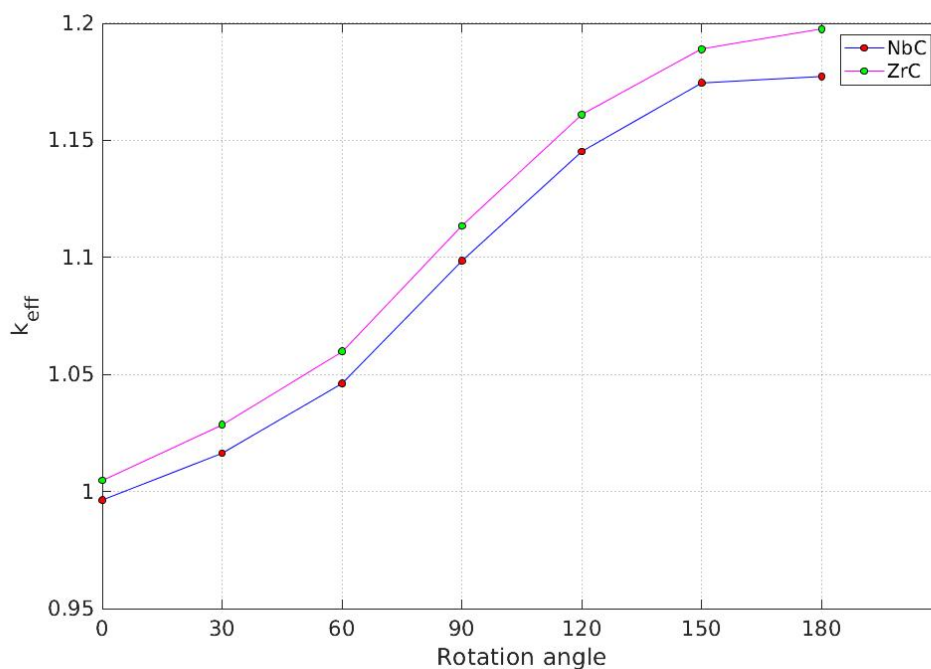


Fig. 2.3 - k_{eff} as a function of rotation angle ($\sigma=20$ pcm) – NERVA derived reactor.

2.1.2 Reactor mass

In a terrestrial reactor design the reactor mass is not a key parameter, since the reactor is not moved from its ground position; this is not the case for a space reactor, which has to be brought outside the Earth sphere of influence, overcoming the gravitational attraction of our planet. Therefore, reactor mass should be kept as low as possible. In the following table, each components contribution (except for the neutron shielding) to the total reactor mass is reported.

	Mass (Kg)
<i>U235</i>	7.37
Fuel	231
Moderator	656
Axial reflector (<i>BeO</i>)	189
Radial reflector (<i>Be</i>)	978
Additional graphite	≈ 30
Total	2054

Table 2.6 - Reactor component mass.

The main contribution is given by the radial reflector: even if Beryllium density is fairly low, its large volume leads to a high mass. The second biggest contribution is related to moderator elements, while the fuel and the axial reflector, which are the densest components in the reactor, accounts for about 200 *kg* each. Moderator composition may be considered almost fixed, in the sense that it is already the best option available. Furthermore, removing some moderator element from the core would drastically change the core layout, which is not the present purpose. Acting on fuel density may be a viable option, but it will not lead to a remarkable mass reduction, because of its low relative contribution.

Those considerations, together with the large k_{eff} previously evaluated, suggest a possible way to optimize the reactor configuration: a reduction in reflector thickness is expected to lower considerably the total mass. Anyway, this operation must be carried out carefully, because the reflector thickness, both axial and radial, strongly affects the core power distribution: thinning too much the reflector generates hot spots in the inner zone of the core, leaving the peripheral region lowly utilized. This implies a lower outlet coolant temperature

and a consequent lower reactor efficiency, making the optimization useless, or even damaging.

2.1.3 Reflector thickness and power distribution

A parametric study on axial and radial reflector thickness is presented in the following; the power distribution for the corresponding thickness reduction is then used to check whether the optimization is feasible or not from a thermal-hydraulic viewpoint.

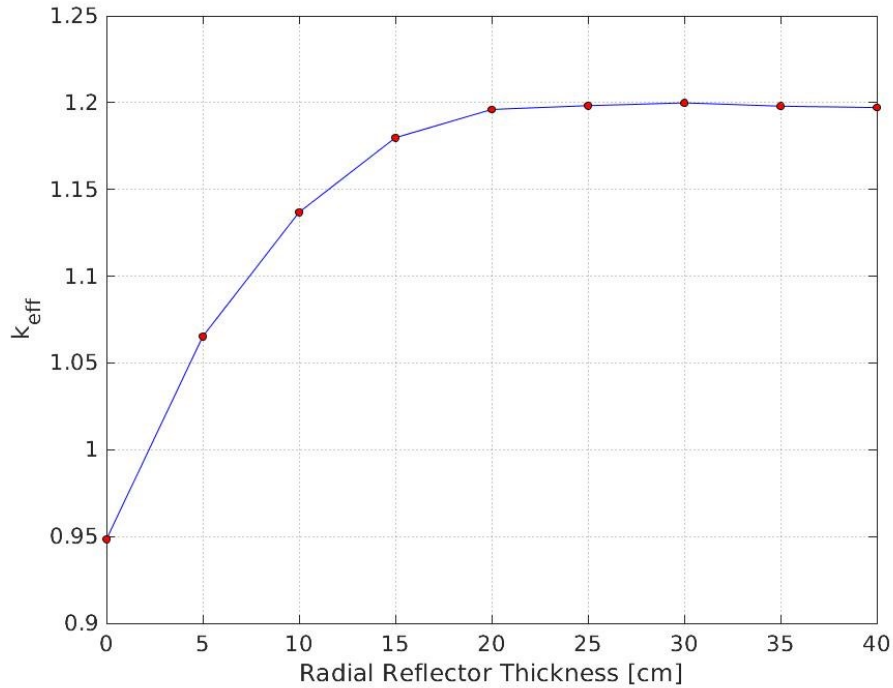


Fig. 2.4 - k_{eff} as a function of radial reflector thickness ($\sigma=20$ pcm) - NERVA derived reactor.

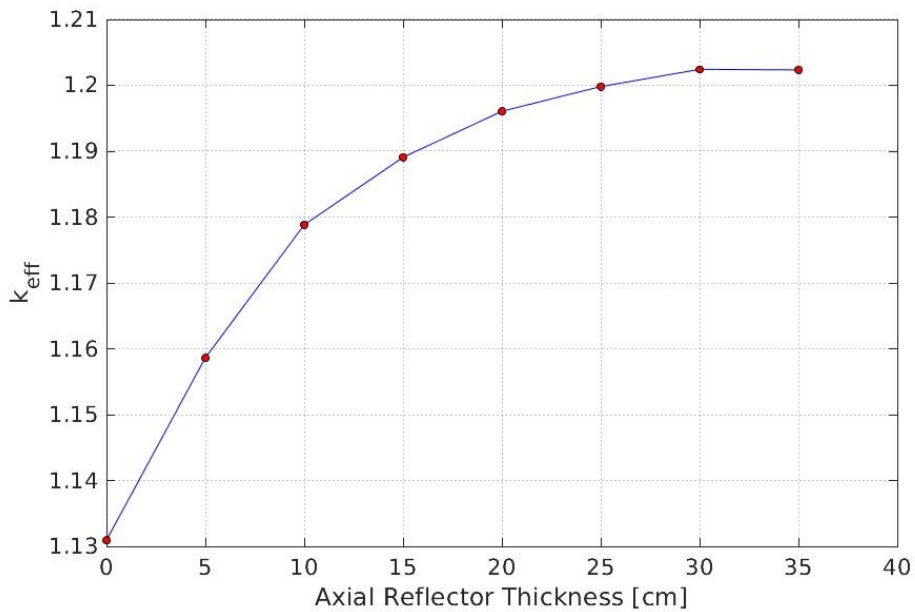


Fig. 2.5 - k_{eff} as a function of axial reflector thickness ($\sigma=20$ pcm) - NERVA derived reactor.

Few comments on these results: the radial reflector thickness influence much more the k_{eff} than the axial reflector thickness, which is reasonable since the radial reflector covers a larger surface; moreover, the axial reflector is placed only on the upper boundary of the core. Above 20 cm of thickness, the radial reflector thickness is basically ineffective, because the neutron flux is almost negligible at this distance from the core centre. A reduction higher than 5 cm seems not advisable for the radial reflector, while a much more consistent reduction looks reasonable for the axial reflector. However, neutron flux at the axial reflector outer edge should be evaluated: a reduction in axial thickness may lead to an increase of neutrons escaping the reactor, which in turn will require an increase of neutron shielding, to ensure crew safety. Since the neutron shielding is made of materials heavier than BeO , the overall result may be an increment of system mass.

The flux distribution for a 5 cm radial reduction and 15 cm axial reduction is shown in

Fig. 2.6.

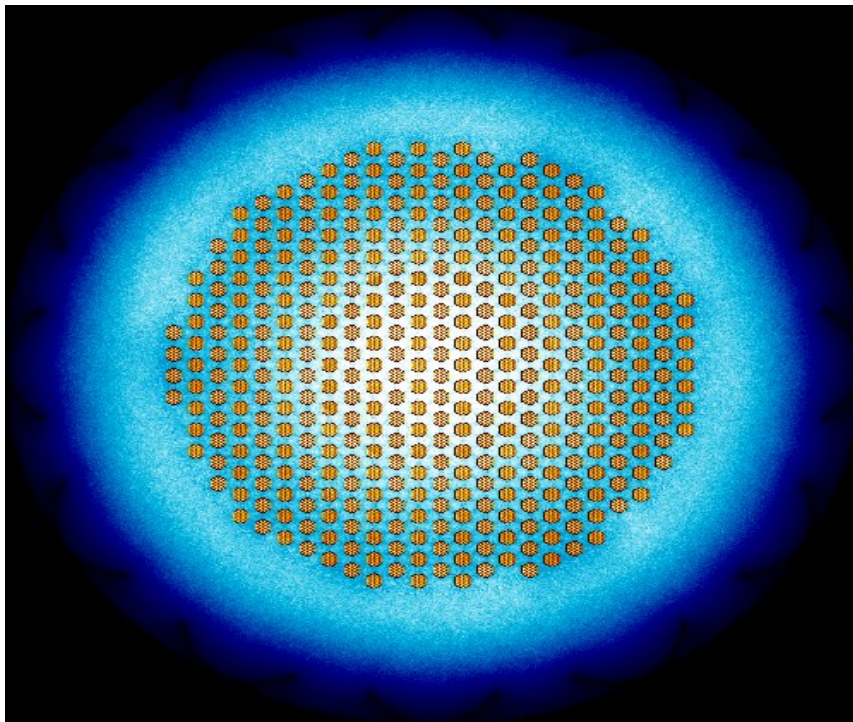


Fig. 2.6 - Neutron flux distribution (Serpent mesh detector) - NERVA derived reactor.

Light areas refer to higher flux zones.

As expected, the neutron flux is higher in the inner region, while decreasing toward the core periphery. Furthermore, when rotated outward the CD absorber effect is almost negligible. Radial power distribution is shown in the following pictures, for two different axial reflector

thickness: clearly, the axial reflector variation does not affect the radial power distribution. Moreover, it is possible to note that the outer core region is not properly utilized for both cases, leading to a high radial peaking factor and consequently lower reactor performances.

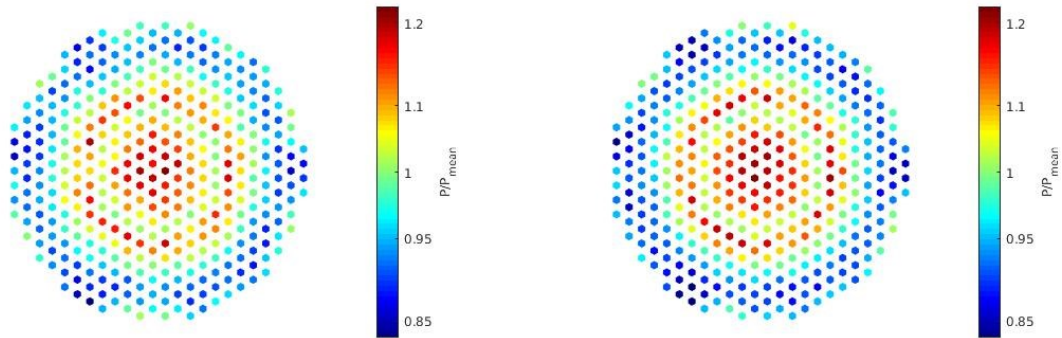


Fig. 2.7 - Fuel element power distribution. 15 cm axial reflector thickness (left), 5cm axial reflector thickness (right).

Conversely, axial neutron flux results heavily affected by the axial reflector cutting, presenting a sharp reduction in the core upper region. The flux (**Fig. 2.8**) is clearly asymmetric, due to the lack of a bottom axial reflector.

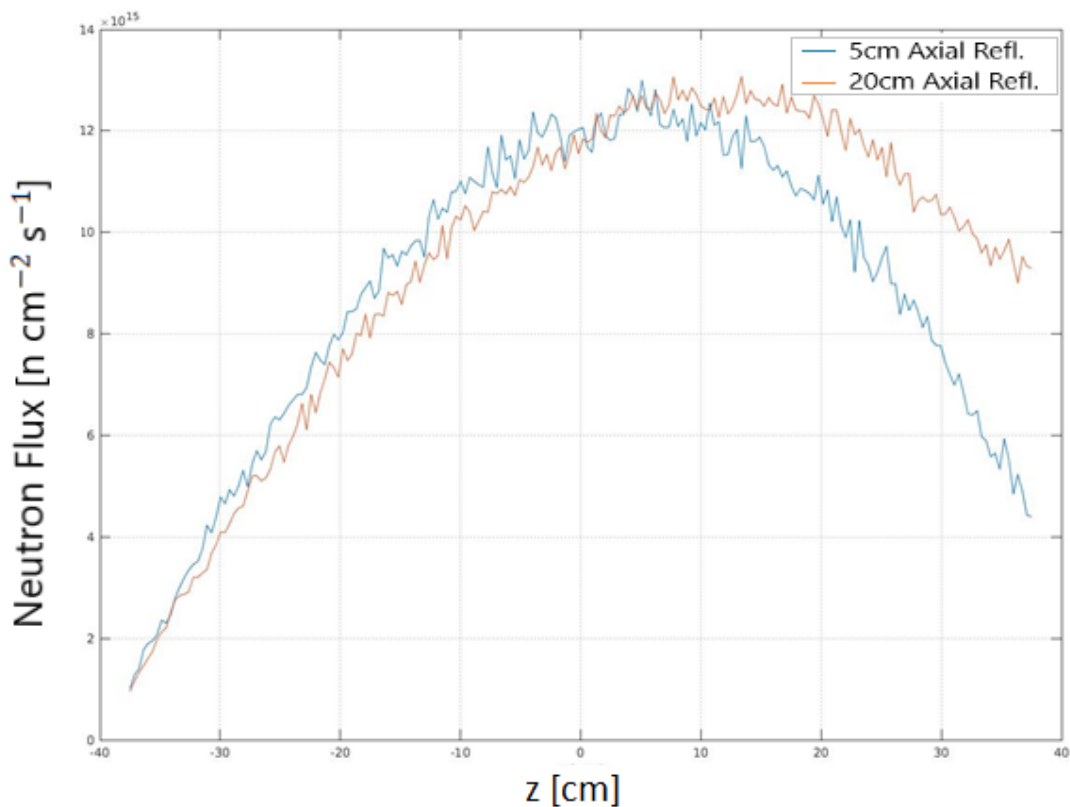


Fig. 2.8 - Neutron flux along the z-axis in a fuel element (Serpent cartesian detector) - NERVA derived reactor.

Even if the reduction leads to a higher axial peak factor, this should not impact considerably on the overall reactor performances. **Table 2.7** summarizes the results.

	Radial peaking factor	Axial peaking factor	Hot channel factor
R: 20 cm, A: 20 cm	1.14	1.38	1.57
R: 20cm, A: 5 cm	1.14	1.46	1.66
R: 15cm, A: 5 cm	1.17	1.63	1.92

Table 2.7 - Peaking factors for different configurations of radial (R) and axial (A) reflectors - NERVA derived reactor.

Peaking factors give a synthetic, very useful information on power distribution inside the core: knowing their value, even if a thermal-hydraulics analysis has not been performed yet, different configuration may be compared from a thermal viewpoint, allowing a huge computational time saving. For those configurations, the axial reflector cut weakly affects the hot channel factor, being a viable option. A much more relevant dependence is shown by the hot channel factor when both reflector thickness changes: this behaviour should be taken under consideration when dealing with the thickness optimization, which may lead to thermal issues inside the fuel elements, such as local melting or deformations.

2.1.4 Burnup analysis

A burnup analysis investigates elements depletion inside the core. Particular attention is paid on fissile materials depletion (in that case, $U235$), but also the behaviour of burnable poison and spectral shift absorbers should be taken in account because of their strong influence on core reactivity. Furthermore, as burnup proceeds, the neutron flux shape may be altered by materials depletion, shifting the hot spots among different locations. Finally, fission products build-up generates mechanical stresses inside the fuel, enhancing possible failure mechanisms. A fission product that arises specific concern is the $Xe-135$, which is a strong neutron absorber: its effect on the reactor capability to perform multiple startup in short timeframes was already assessed by [18]. However, this last topic will not be investigated in the present work, due to the limited computational resources.

The expected mission time for a NTP reactor designed for a Mars mission will be about 2 hours [22], so it is reasonable to assume that fissile materials depletion should not be an issue, with reactor criticality assured by a small excess reactivity. Similarly, fission products are not of concern from a thermomechanical viewpoint, due to their limited production. In this framework, a burnup analysis aims to check whether the criticality is granted for the whole mission time. It is well known that the time steps input for Serpent should be small enough to avoid convergence issue and misleading results [13]: thus, they were chosen as $t = (2, 14, 26, 50, 98)h$. The standard output from a Serpent simulation in burnup mode is shown from **Fig. 2.9** to **Fig. 2.11**.

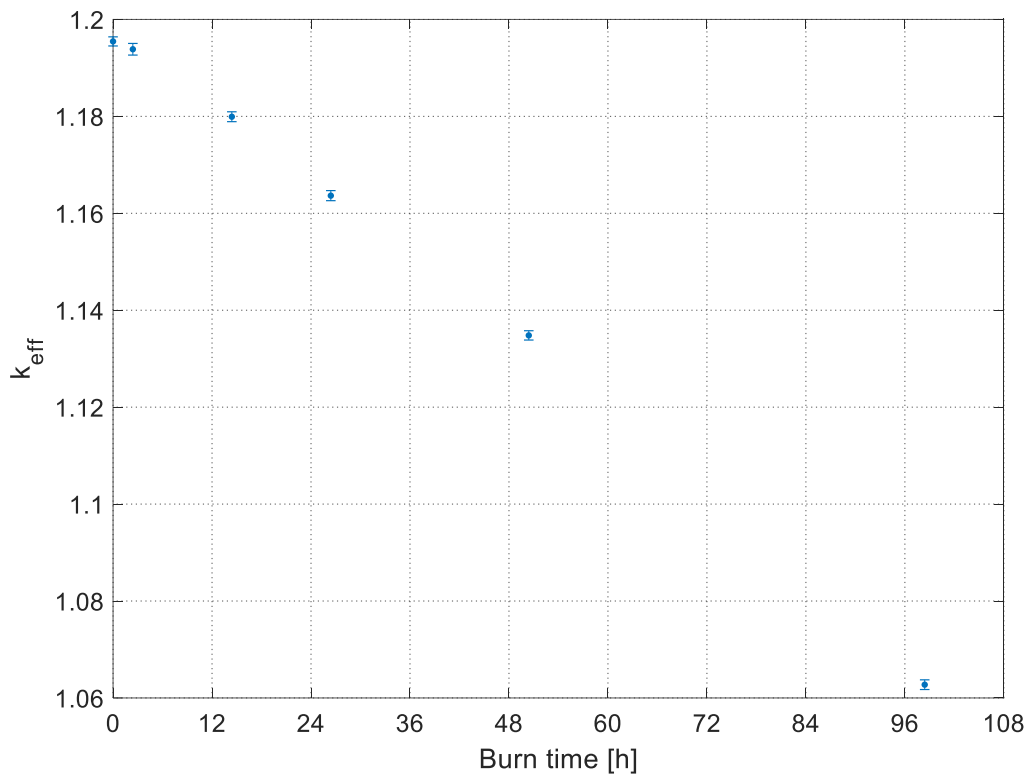


Fig. 2.9 - k_{eff} at different burnup steps - NERVA derived reactor.

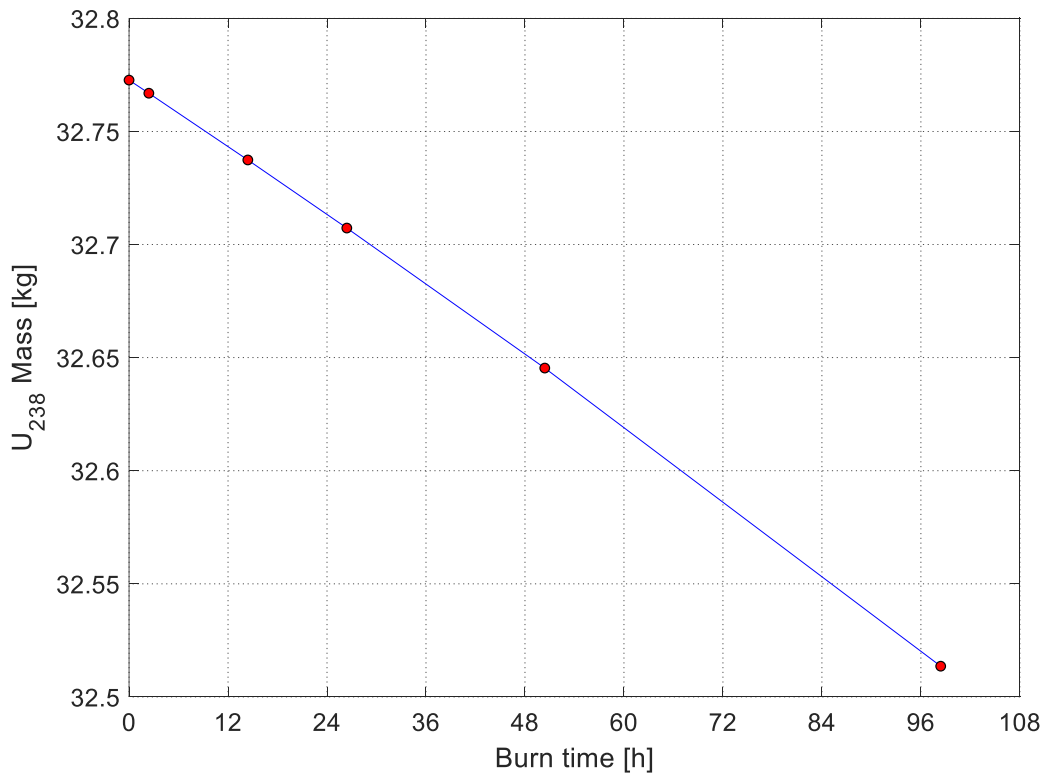


Fig. 2.10 – Uranium-238 mass in the core at different burnup steps - NERVA derived reactor.

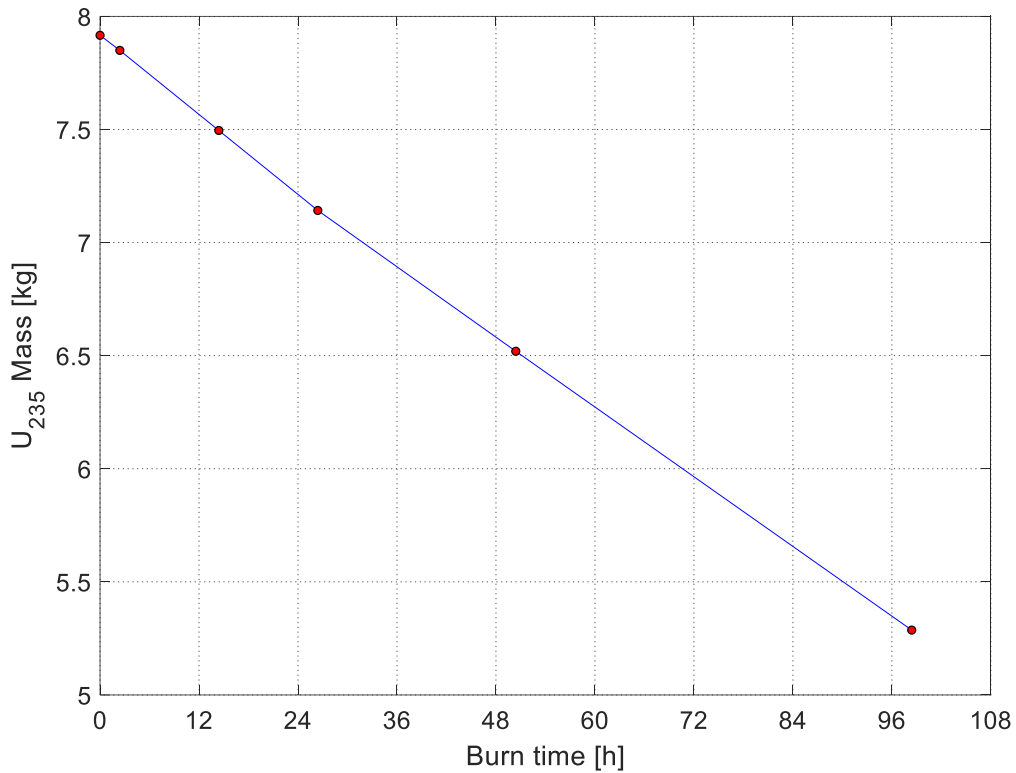


Fig. 2.11 - Uranium-235 mass in the core at different burnup steps - NERVA derived reactor.

As expected, a small reactivity reduction ($\Delta k_{eff} = 163 pcm$) is experienced by the reactor after 2 hours of operations; in addition, after 4 days of full power operations there is still a large reactivity excess. Furthermore, a relevant contribution to the reactivity loss is related to fission products build-up: provided that enough time is left between different full power burns, it is reasonable to expect longer reactor operational time. Therefore, an optimization focused on excess reactivity reduction, and possible neutron flux flattening is desirable.

2.1.5 Results comparison and conclusions

The analysis so far produced enough results to be compared to literature data, in order to check the validity of the model. There is only one uncertainty related to the k_{eff} value of the reference reactor: it is not specified whether the coating is *NbC* or *ZrC*; however, the error associated to both cases is fairly low.

	C-LEU-NTR	Current model	Error
k_{eff} (NbC coating)	1.11610	1.12744	1.0%
k_{eff} (ZrC coating)		1.19606	7.1%
β_{eff} [-]	0.00717	0.00713	0.5%
Λ [μ s]	106	109	2%
Reactor mass (no shielding) [kg]	2016	2054	1.8%

Table 2.8 - Results comparison of the reference and the current model.

It should be recalled that the reference model adopted MCNP for neutronic simulations, while the current work choice was Serpent: therefore, even an error of 7% on k_{eff} may be considered reasonable. For what concerns reactor mass, small differences in the model, such as “cut elements” on the core boundaries or additional components considered may lead to mass discrepancies. Kinetics parameters, namely the delayed neutron fraction β_{eff} and the mean generation time Λ , show a fairly good agreement with C-LEU-NTR data: this is an important outcome, because it is known that Serpent may produce misleading results when computing kinetics parameters, especially the neutron generation time. A proper evaluation of kinetics parameters is fundamental, since they describe reactor dynamics, which is related in turn with reactor control and safety. Thus, from these considerations, the model can be assumed to be correct.

Before starting the CERMET reactor design, few further considerations could be made: the large excess reactivity is an issue in terms of safety and startup, because the reactor can be brought barely subcritical when cold; however, this opens a window on possible optimizations, aimed at reducing fissile material mass. A 2-zone enrichment core seems not very performing, leading to high peaking factor: therefore, fuel zoning will be taken in serious consideration in the next section. With the experience gained from the analysis of this base case, it is possible to proceed to the CERMET reactor.

2.2 CERMET reactor

In the present section, the neutronics of a CERMET reactor is analysed, unveiling its main features; then, an optimization procedure is proposed to increase the overall reactor performances, leading to substantial improvements with respect to the initial configuration. The reflector and the moderating elements are the same as NERVA reactor, while CERMET fuel is composed by $UO_2 - ThO_2$ (60% volume fraction, with 8% molar fraction of ThO_2) and W (40% volume fraction). As already said, tungsten has to be enriched at least to 99%at of $W-184$, to reduce parasitic absorptions, while ThO_2 ensures chemical stability at high temperatures. Fuel coating is a $W-Re$ alloy: Re atomic fraction inside the coating is a crucial parameter, because on one hand it enhances thermomechanical properties, on the other hand it contributes to neutrons absorption. The effects of Re addition and $W-184$ enrichment are shown in **Fig. 2.12**.

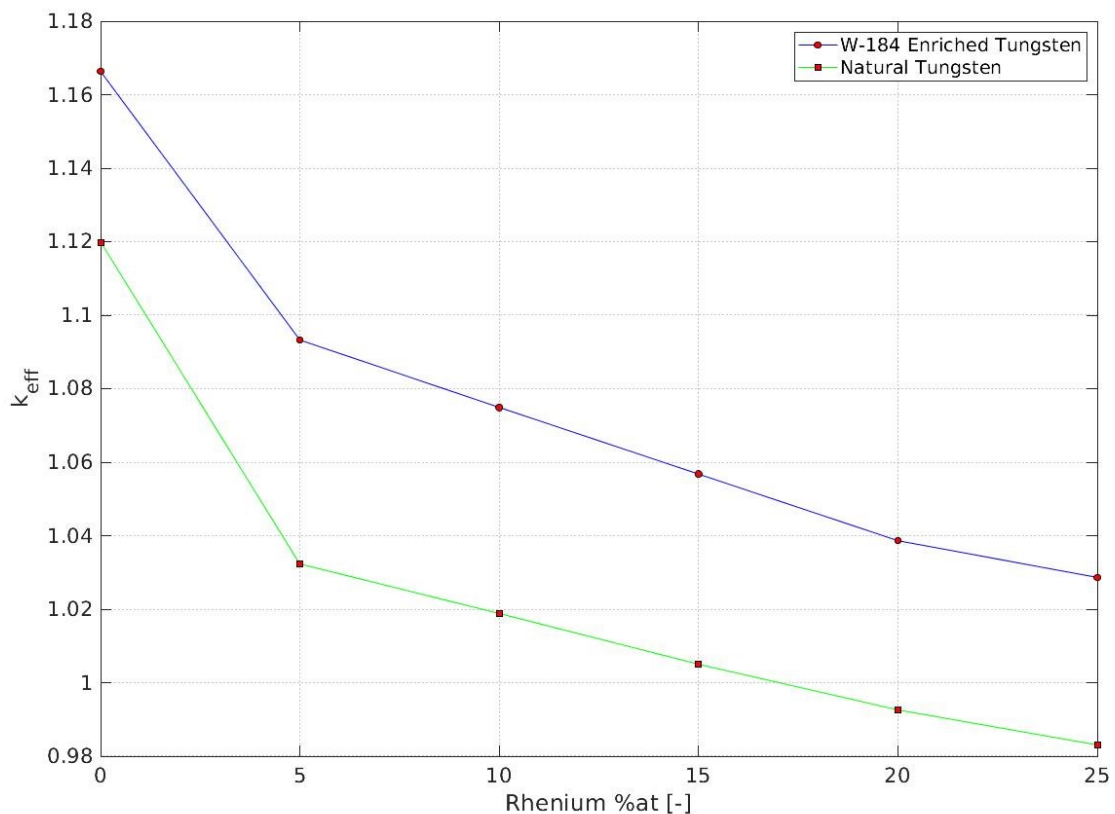


Fig. 2.12- k_{eff} vs. Rhenium atomic fraction for natural and enriched tungsten ($\sigma=20 pcm$) – CERMET reactor.

$W-184$ enrichment greatly reduces absorption, with a gain of about 5000 pcm . Furthermore, both materials exhibit an almost linear dependence on rhenium atomic fraction. Density is

another relevant feature of CERMET fuel: while composite fuel has a density of 3.65 g/cm^3 , with an uranium loading of 0.64 g/cm^3 , CERMET is a 14.27 g/cm^3 dense material, with 5.4 g/cm^3 uranium loading. Being the fuel volume the same in both reactors, one may ask why the reactivity is comparable, even if the uranium content in CERMET reactor is about 9 times the content in NERVA reactor. The answer lies, again, in the presence of *Re* and *W* inside the core: because of their large absorption, much more fuel is needed to ensure criticality. Apart from these differences, the reactor model is quite similar to the previous one, therefore the results will be just briefly summarized hereunder.

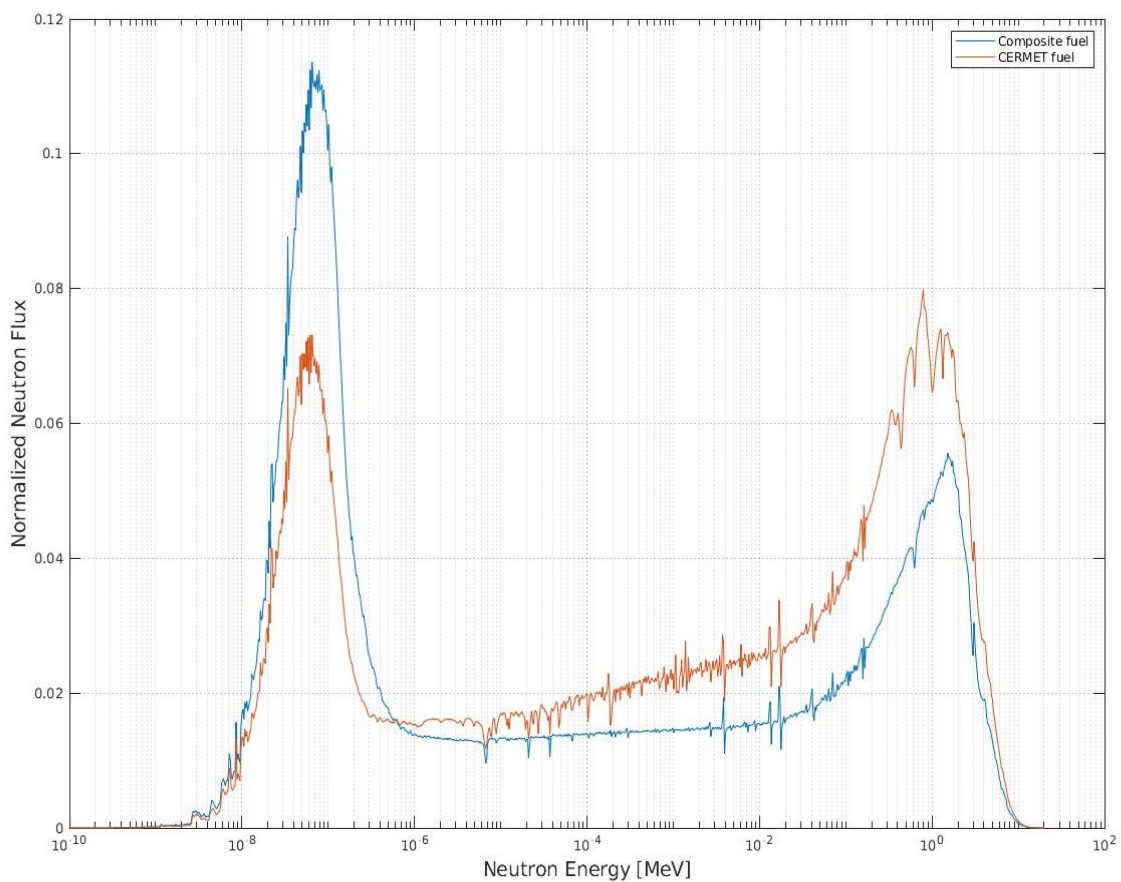


Fig. 2.13 - Neutron spectrum comparison between composite and CERMET fuel.

CERMET fuel neutron spectrum slightly differs from the composite fuel, revealing a spectrum shifted to high energies: this feature has a strong impact on accidental scenarios, such as submersion in seawater, because the moderating effect of water is be much more relevant, resulting in larger positive reactivity insertions. One way to mitigate this behaviour is to modify the moderator-to-fuel ratio: however, that procedure would alter the entire core layout, going beyond the scope of this work.

The main quantities of a reactor with $Re\ 5at\%$ are summarized in **Table 2.9**.

	CERMET reactor
k_{eff}	1.16791 ± 0.00040
$Re\ at\%$	5%
Excess reactivity [\$]	27.4
β_{eff}	0.00731 ± 0.00016
CDs reactivity worth [\$]	20.2
Shutdown margin	Not Available
Hot channel factor	2.04
Total mass (without shielding) [Kg]	2756

Table 2.9 - CERMET reactor parameters.

With a k_{eff} value above 16000 pcm , it is evident that with this configuration the reactor cannot be brought subcritical; however, there is a huge amount of reactivity that can be absorbed just by adding rhenium to the coating, enhancing safety as well.

The delayed neutron fraction results in an appropriate value, granting a suitable safety margin between criticality and prompt criticality.

The total system mass is larger than the NERVA type reactor, owing to the higher fuel density: this translates in the need for greater thrust to satisfy the TWR (thrust-to-weight ratio) requirement, making the outlet coolant temperature a crucial parameter to monitor.

Reflector reduction is again a viable option to reduce core reactivity, as shown in the following pictures.

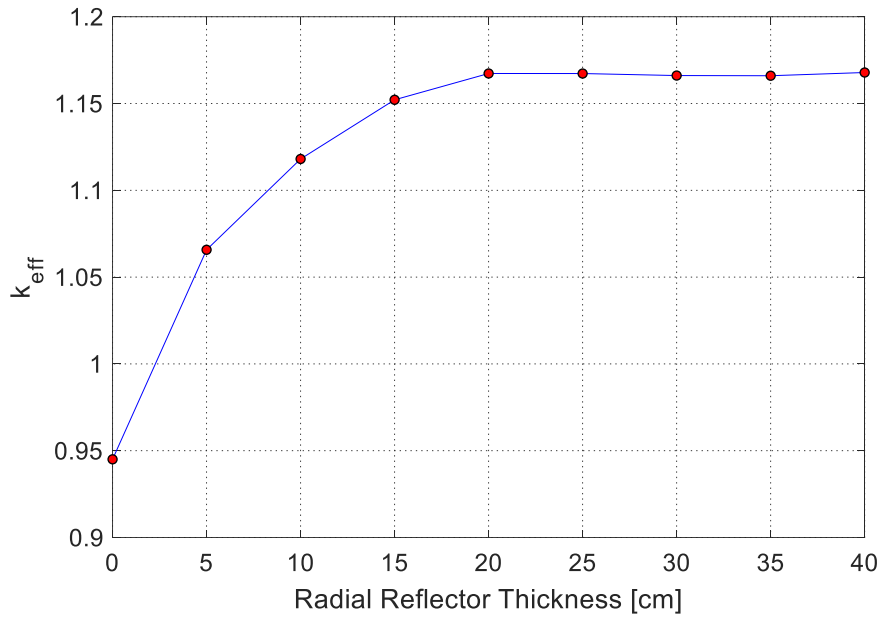


Fig. 2.14 - k_{eff} as a function of radial reflector thickness ($\sigma=20\text{ pcm}$) – CERMET reactor.

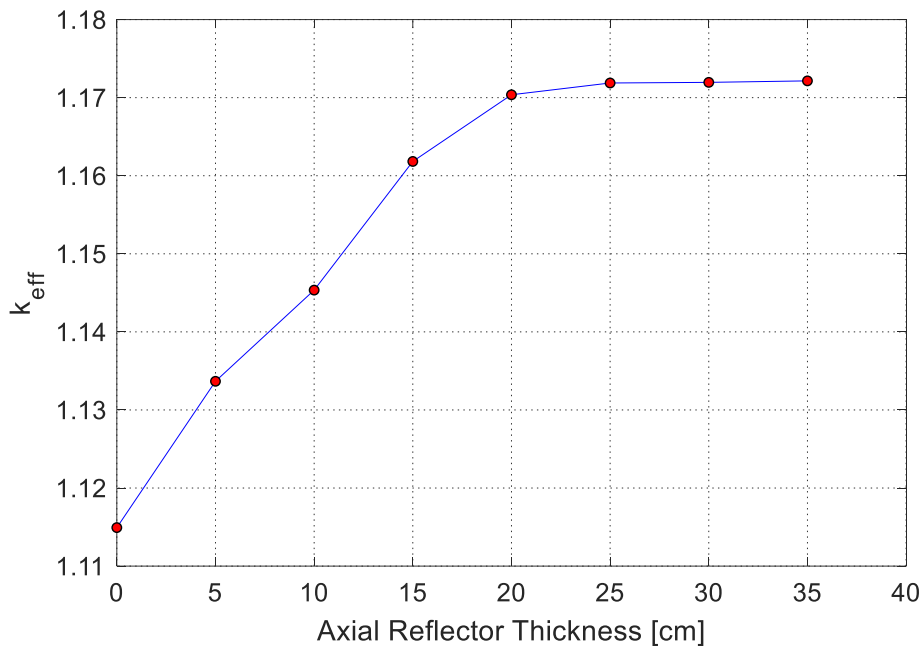


Fig. 2.15 - k_{eff} as a function of axial reflector thickness ($\sigma=20\text{ pcm}$) – CERMET reactor.

Both a reduction of radial reflector and axial reflector seem feasible, keeping in mind their effect on peaking factors. Since in CERMET reactor the fuel (848 Kg, of which 62.3 Kg are $U235$) gives a large contribution to the total system mass, acting on fuel enrichment could be a better option than reducing reflector thickness. Furthermore, keeping a thick reflector enhances safety, since the shielding provided by the submersion medium does not affect the already minimized core leakages.

Concerning neutron flux and power distribution, the simulations produced the following results.

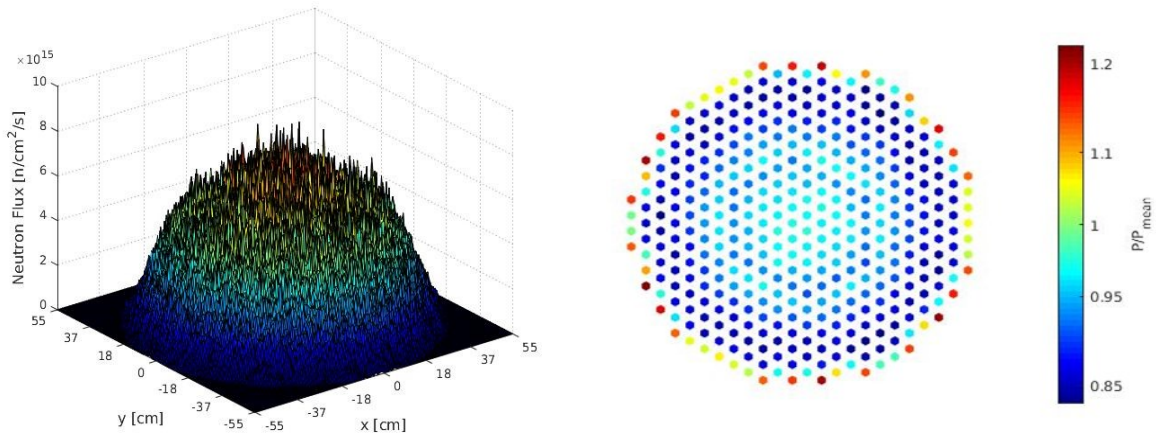


Fig. 2.16 - Neutron flux and power distribution at $z=0$ – CERMET reactor.

Neutron flux and power distribution may look discordant, being the flux higher in the core inner region, while the power raises on the core boundary. However, decomposing the flux in its thermal and fast components, the situation becomes clear.

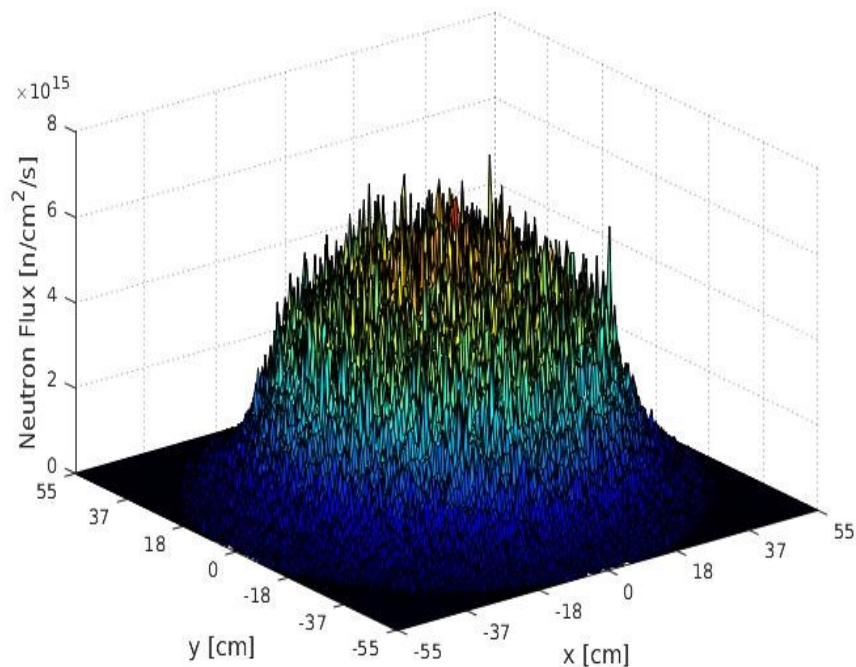


Fig. 2.17 - Fast neutron flux at $z=0$ – CERMET reactor.

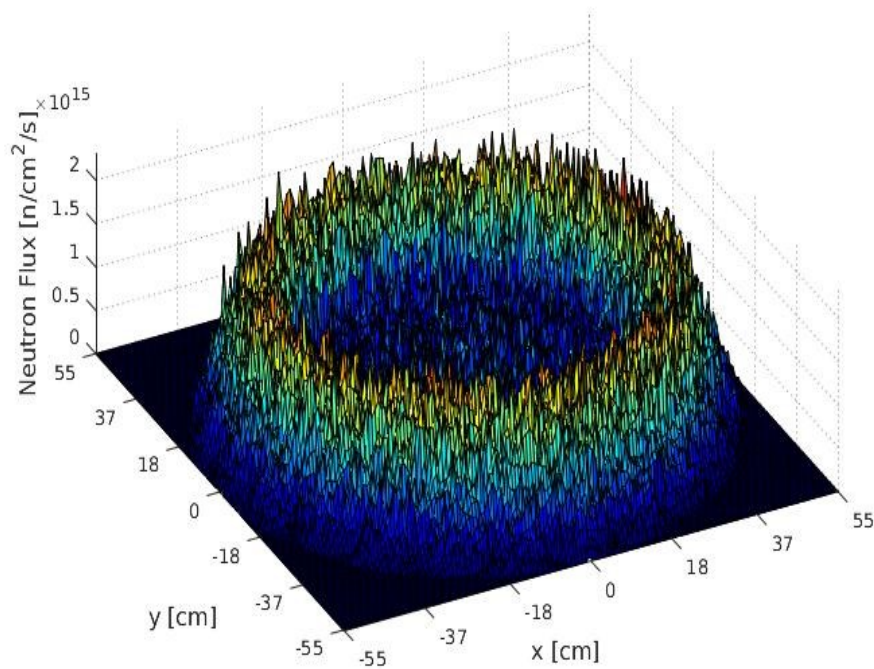


Fig. 2.18 - Thermal neutron flux at $z=0$ – CERMET reactor.

Most of fast neutrons populate the central region, while thermal neutrons are located mainly on the peripheral region: thus, the flux is peaked in the centre, but a huge number of fissions occurs near the boundary, resulting in the above power distribution. This behaviour emphasizes the radial reflector relevance: indeed, neutrons flow toward the reflector; here they are moderated and reflected back to the core, undergoing fission in the outer fuel elements. Since the hot spots are located close to the core boundary, power flattening can be achieved easily by slightly reducing radial reflector thickness or by redistributing core fissile material.

Finally, the burnup analysis does not add any significant consideration, since with such a huge excess reactivity the reactor can clearly sustain 2 hours of operations.

All the relevant information on the CERMET reactor have been presented, therefore it is now possible to carry out a systematic reactor optimization.

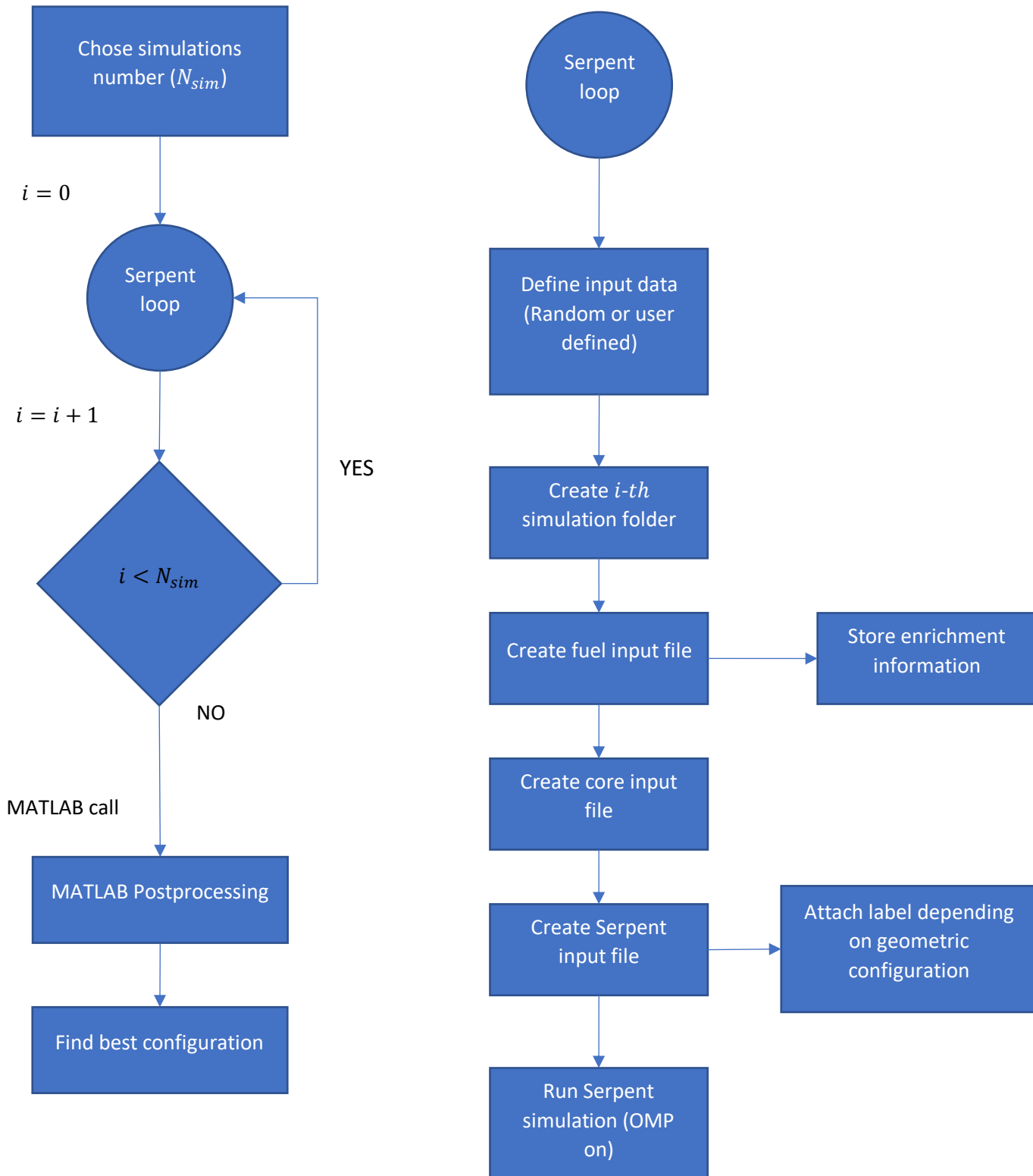
2.2.1 Optimization

An optimization procedure applied to a reactor for NTP should aim to reduce overall and fissile mass, flatten flux distribution to lower peaking factors and, finally, increase reactor performances (both i_{sp} and Thrust). Furthermore, in this framework, safety during submersion accidents must be ensured.

To achieve these goals, it is possible to act on the following parameters: axial and radial reflector thickness, fuel enrichment, Re fraction inside coating, spectral shift absorbers addition, enrichment zones number and fuel element layout. However, because of the high number of possible configurations which may be obtained by varying these parameters, an automated procedure is required. Since Serpent input and output files are basically text files, a Python code able to manipulate those files, thus pre-processing and postprocessing, seems an obvious choice. Therefore, once the input parameters are selected, the optimization procedure should explore the widest domain region reasonably achievable, with the lowest possible computational effort. A brute force approach is not reasonable, due to the extremely high number of possible combinations among all the parameters: for this reason, the following criteria were chosen to reduce the allowable configurations.

- Reflector thickness varies in the range $[20; 5]cm$ for both radial and axial reflector, with 5 cm steps;
- The standard enrichment zones number were set to 7, which resulted in the most promising value from the NERVA reactor analysis. Six or five enrichment zones were tested anyway, in particular cases;
- The maximum fuel enrichment is randomly chosen between 20% and 12%. Below this lower bound, the fissile mass inside the core is not enough to achieve criticality;
- Fuel enrichment from one zone to the adjacent differs by 1% or 2%. Larger steps lead to higher peaking factor;
- The spectral shift absorbers that have been tested are: Eu_2O_3 , Gd_2O_3 , Ir , Re , Sm_3O_2 . Only one at a time was tested.

The following flow diagram highlights the main steps of the code.



The first step is the choice of the desired neutronic simulations: once this is done, no more user inputs are required, strongly reducing user related errors. The code generates input data for the i -th simulation, create a folder to store all the required files, writes two *.txt* files, according to the input, which contain information on fuel composition and core layout and that will be included in the main Serpent input file. The choice of the number of axial (thermal) zones and fuel enrichment zones are left to the user. Each of the core elements can be labelled, allowing for any kind of element-wise operation: even if a core imported from CAD software may simplify the first core definition, once this procedure is done by text files a relevant group of core manipulations become available for the user. For instance, one may be interested to act on the enrichment of a single fuel element instead of the entire zone, or just to multiple elements which are not linked by any geometric pattern: if any element has its own label, this procedure is straightforward. The same method can be adopted to rotate each CD as desired. Fuel enrichment for each zone and geometric information are stored, to allow an easier classification during postprocessing. Finally, the main Serpent input file is created, and the simulation is run. It is possible to enable parallel computing prior to simulation start. Serpent provides many kind of detectors to investigate the quantities of interest, or to track specific reactions: thus, a set of detectors is made available for each simulation; keeping in mind the figures of merit relevant for this class of reactors, all the required information can be gathered by these detectors. Among the possible choices, cartesian detectors are used to evaluate both 1D axial and 2D radial flux, neutron spectrum and power deposition inside the whole core. Similarly, the *set cpd* option allows for fuel-element-wise power deposition. Once the required number of simulation is reached, MATLAB is called by bash to gather and process simulations results: k_{eff} is stored, mass saving coming from reflector and fissile material reduction are calculated, power distribution and axial profile are evaluated to obtain the peaking factors. The whole process is extremely fast, thanks to the lightness of Python scripts (replacing MATLAB postprocessing with a Python script implementing its scientific libraries makes the code even faster) and the proper choice of simulation settings which maximize speed without losing precision. Specifically, thanks to the Shannon entropy evaluation, the inactive cycles are set to 50, while active cycles to 100; neutron population at each iteration should be high enough to allow statistically relevant detectors data: owing to the small reactor dimensions, 25000 ÷ 75000 particles are sufficient. Detectors mesh should result in no more than 1 million cells, otherwise it will constitute a bottleneck for

postprocessing. At the end of this process, a simple *.txt* file summarizes all the relevant features for each configuration, each one labelled depending on its own reflector thickness. A global result of this procedure is shown below.

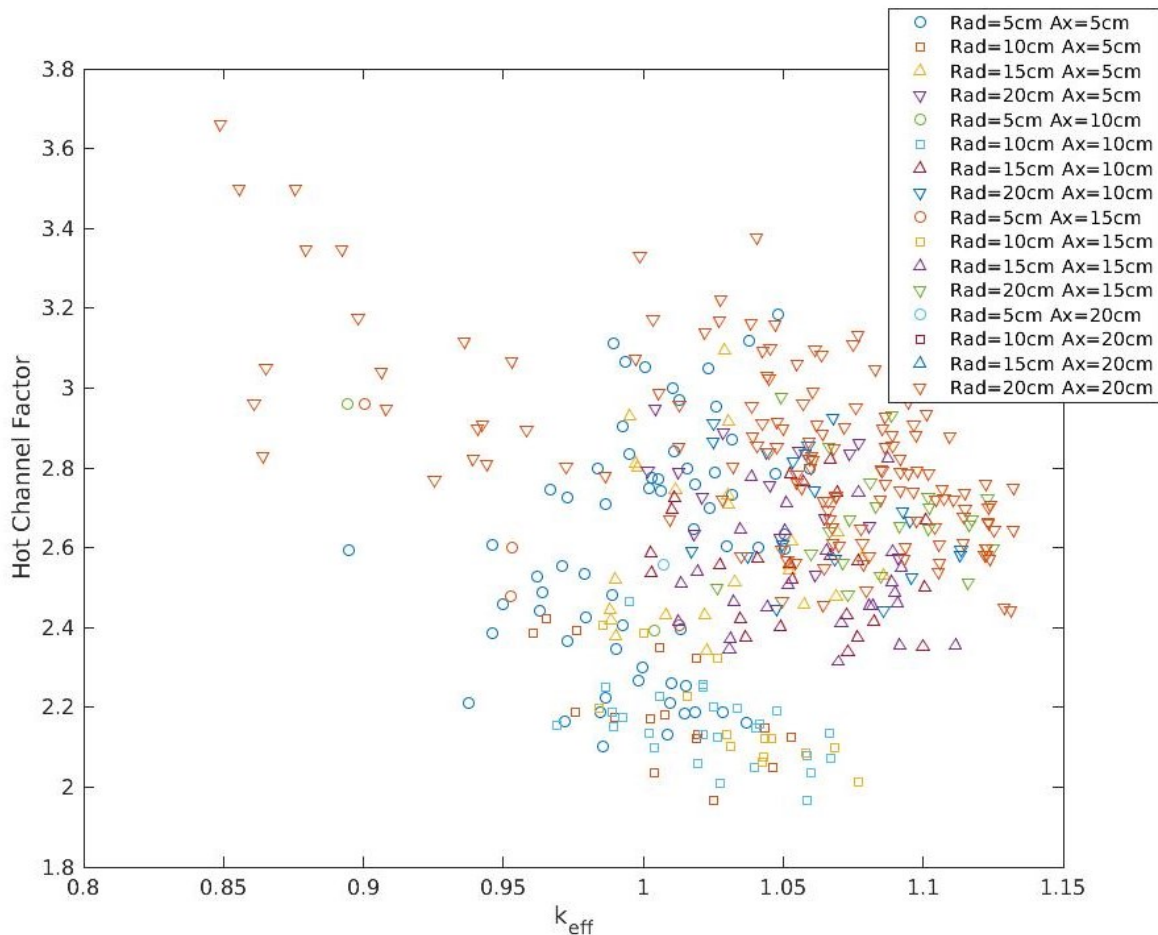


Fig. 2.19 - k_{eff} and F_{hc} for various reactor configurations obtained through the optimization procedure.

The point distribution as a function of reflector thicknesses shows how these two parameters heavily affects the output. Specifically, radial reflector thickness looks as the most relevant input: a 10 cm thickness leads to low hot channel factor (F_{hc}) values and an acceptable k_{eff} , while configurations with a 20 cm thick radial reflector cover a wide region of k_{eff} and present higher F_{hc} . Furthermore, the radial reflector importance is in accordance with the neutronic considerations made in the previous section. Fuel enrichment and fuel zoning weakly affect the output values (in the range in which those two inputs are modified): simulations with the same reflector thickness are confined in relatively small regions (apart from a thickness of 20 cm), revealing that different enrichment values and different

enrichment zones do not influence k_{eff} and F_{hc} significantly.

Among all these configurations, the most promising returns the following results, with a consistent mass saving, a moderate excess reactivity which allows reactor control and a slightly better F_{hc} if compared to the standard configuration.

	Optimized configuration
k_{eff}	1.05855 ± 0.00040
Inactive cycles – Active cycles	50 – 75
Neutron population per cycle	50000
Excess reactivity (\$)	9.64
β_{eff} [–]	0.00712 ± 0.00010
Λ [μs]	22
Enrichment zones (% U_{235} enrichment)	7 ([19 18 17 16 15 14 13])
Reflector thickness (radial/axial) [cm]	10/10
Radial peaking factor [–]	1.29
Axial peaking factor [–]	1.51
Hot channel factor [–]	1.96
U_{235} mass saving (%)	7.6
Axial reflector mass saving [Kg]	94 (–56%)
Radial reflector mass saving [Kg]	588 (–60%)
Total mass [Kg]	2074 (–25%)

Table 2.10 - Optimal configuration results – CERMET reactor.

Even if this is the optimal configuration from the performance viewpoint, an accidental scenarios analysis is mandatory to check core safety. Specifically, a 10 cm radial reflector may result too thin to provide a proper neutrons leakage reduction, implying a large positive reactivity insertion when the core becomes surrounded by a reflective medium.

2.2.3 Conclusions

Starting from the base configuration of a CERMET reactor, which presented high excess reactivity, control issues, large mass and unoptimized fuel loading, an optimization procedure was successfully applied to find the best configurations. Total system mass is reduced by a factor of 1/4 and hot channel factor lies below 2; k_{eff} is low enough to allow reactor control in nominal conditions, but sufficiently large to ensure 2h of continuous operations. Delayed neutron fraction is still above 700 pcm, while Λ is about a fifth of the value obtained by the composite-fuelled reactor, meaning that the neutron spectrum is slightly faster, as expected by looking at **Fig. 2.13**.

The code results in a powerful tool to explore an extremely wide area of the possible configurations' domain, with a mean execution time of 6.5 min for each Serpent loop iteration. Computational time sharply increases when accidental scenarios analysis and thermal-hydraulics calculations are performed: postprocessing becomes a fundamental step, since it reduces the configurations to be further analysed from hundreds (or thousands) to few cases. These few optimal configurations are then tested for the submersion accidents and thermal-hydraulics, as described in detail in the next chapters.

3. Accidental scenarios analysis

An accidental scenarios analysis is mandatory when designing a nuclear reactor. Safety must be ensured in any possible reactor operation and failure scenario, maintaining k_{eff} below criticality. There are many concerns related to nuclear reactors for space applications, related to the possible failure of the first mission stage, when the rocket is escaping Earth gravity. In this framework, a specific class of scenarios that must be taken in account are submersion accidents: following a launch abort scenario, the reactor falls back to the Earth, where it gets submerged in different materials. This situation is extremely dangerous for both population and environment, because the core may reach supercriticality and increase its power exponentially until the core melts, with a consequent release of radioactive elements. Thus, prior to reactor construction, it must be proved that reactor safety can be assured in any accidental scenario.

Among these scenarios, the most relevant are submersion in dry sand, submersion in wet sand, submersion in seawater and, finally, submersion in seawater followed by reflector dismantling. In those scenarios reactor temperature is brought below room temperature, an infinite reflective medium surrounds the core and, moreover, each of those scenarios adds moderator inside the channels, resulting in a large burst of positive reactivity. CD must be designed properly to provide enough shutdown margin; however, if the reflector gets dismantled, the reactor loses its only active control component. In this situation, the core may rely only on its passive reactivity control system, namely spectral shift absorbers (SSA). Indeed, even if design implementing control rods have been proposed [23], it is preferable to avoid such safety systems, due to unavoidable increase of system complexity and reliability related issues. Alternative active control techniques, like propellant pressure control [24], are interesting from a fine regulation viewpoint, but their reactivity control worth is too limited for an effective implementation in accidental scenarios.

CERMET neutron spectrum from neutronic analysis (**Fig. 2.13**) shows a large fraction of fast neutrons: it is foreseeable that those neutrons will be slowed down when submersion occurs, and the consequent reactivity increase may be too large to be absorbed by CD alone. This behaviour is presented in the following sections, with a detailed description of each accidental scenarios.

3.1 Accidental scenarios

In this section the four accidental scenarios previously introduced are analysed, highlighting reactor weakness to a particular class of scenarios. In a submersion in dry sand scenario, the reactor is assumed to be surrounded by a 5m radius sphere made of sand (SiO_2 with 30% porosity, $\rho = 1.855 \text{ g/cm}^3$), while moderator and fuel channels remains empty : it is actually the less dangerous scenarios, because no moderation is added in the inner region of the core. This is not the case for the wet sand (SiO_2 with 30% porosity, voids filled by H_2O , $\rho = 2.162 \text{ g/cm}^3$) scenario, in which seawater floods the channels, leading to a much larger reactivity increase. Submersion in seawater (3 wt% $NaCl$ in H_2O , $\rho = 1.025 \text{ g/cm}^3$) shows small differences with the wet sand scenario, while the reflector dismantled scenario results in the hardest scenario. Indeed, the water that fills the channels in the core inner region strongly thermalizes the neutrons in that zone (**Fig. 3.1**), with a consequent increase of the local power and k_{eff} . The B_4C absorbers of the CD cannot act effectively on these neutrons because they are too far from the core boundary, leading to a supercritical core. This situation gets worse when the reflector is lost due to the impact. It should be noted that in submersion accidents not only the reactor moderating capability raises up, but also neutrons reflection, which is provided by the additional surrounding medium. However, it is easy to show that this surrounding medium weakly affects core reactivity, because of the reflector that already reflects most outgoing neutrons.

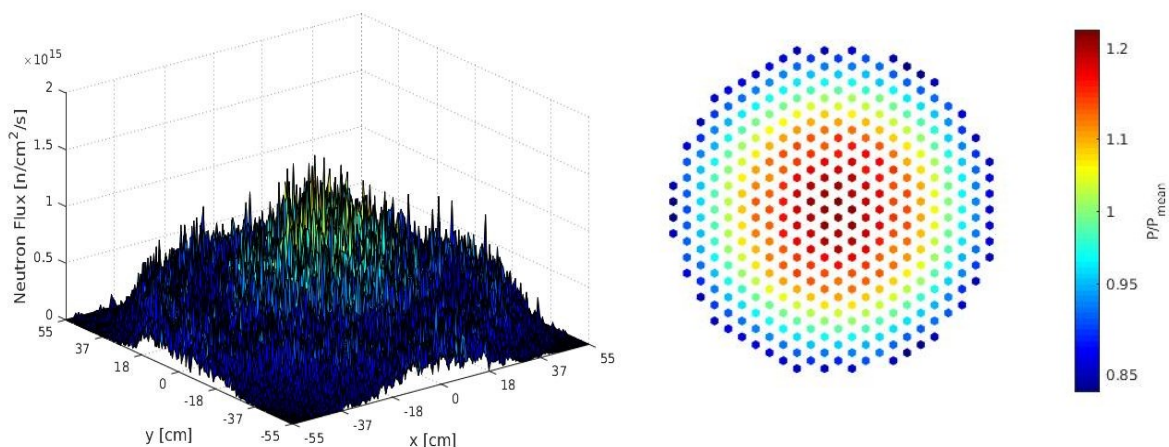


Fig. 3.1 - Thermal neutron flux and power distribution following an accidental scenario – CEREMET optimized configuration.

The results from accidental scenarios analysis (50 inactive cycles, 75 active cycles, 100000 neutrons per cycle) are summarized in the following table:

	CD position	Channels	Reflecting medium	k_{eff}
Submersion in dry sand	Inward	Empty	Sand	1.04746 ± 0.00060
Submersion in wet sand	Inward	Water	Sand	1.20173 ± 0.00060
Submersion in seawater	Inward	Seawater	Seawater	1.20040 ± 0.00060
Reflector dismantled	NA	Seawater	Seawater	1.20794 ± 0.00060

Table 3.1 - k_{eff} following submersion accidents – CERMET optimized configuration.

In all the four accidental scenarios the reactor cannot be brought subcritical, meaning that the reactor design must be modified, at expenses of rocket performances. However, even reducing the excess reactivity to values close to criticality ($k_{eff} \cong 1$), the positive reactivity insertion related to the submersion is extremely large. Thus, an additional safety system is required. Three main choices available are: spectral shift absorbers (which are in part already present due to the *Re* coating), control rods or an advanced CD system.

From now on, all the simulations on accidental scenarios are run with 50 inactive cycles, 75 cycles and 100000 neutrons per cycle.

3.2 Spectral shift absorbers

Spectral shift absorbers (SSA) have been successfully implemented in many HEU NTP reactors, but their effectiveness reduces when dealing with LEU reactors. SSA are burnable poisons that are depleted as burnup proceeds: when neutrons absorption occurs, the SSA is converted to a low-absorbing isotope. As stated by their name, the absorption cross section is maximum at medium energy, in the transition zone between thermal and fast spectrum. If their concentration is tuned properly, SSA depletion follows fissile materials burnup, ensuring an almost constant reactivity. Furthermore, in submersion accidents, moderation addition is directly compensated by an increased neutrons absorption provided by the SSA, keeping the reactor subcritical. This mechanism works extremely well with fast spectrum reactors, because in normal operations the SSA absorptions are almost negligible: for some reactor design, it is even possible to assist to a reactivity inversion when the reactor gets submerged [25]. Conversely, when this solution is brought to thermal reactors reactivity issues in normal operations arise. This behaviour has been already shown in **Fig. 2.12** when the *Re* coating concentration was analysed: similar trends may be expected for the SSA tested, namely Sm_3O_2 , *Ir*, Gd_2O_3 , Eu_2O_3 [26].

SSA may be placed at the core boundary, as a sleeve in contact with the reflector, around the channels as additional layer or dispersed inside the fuel. The effect of a sleeve on core reactivity is shown in **Fig. 3.2**.

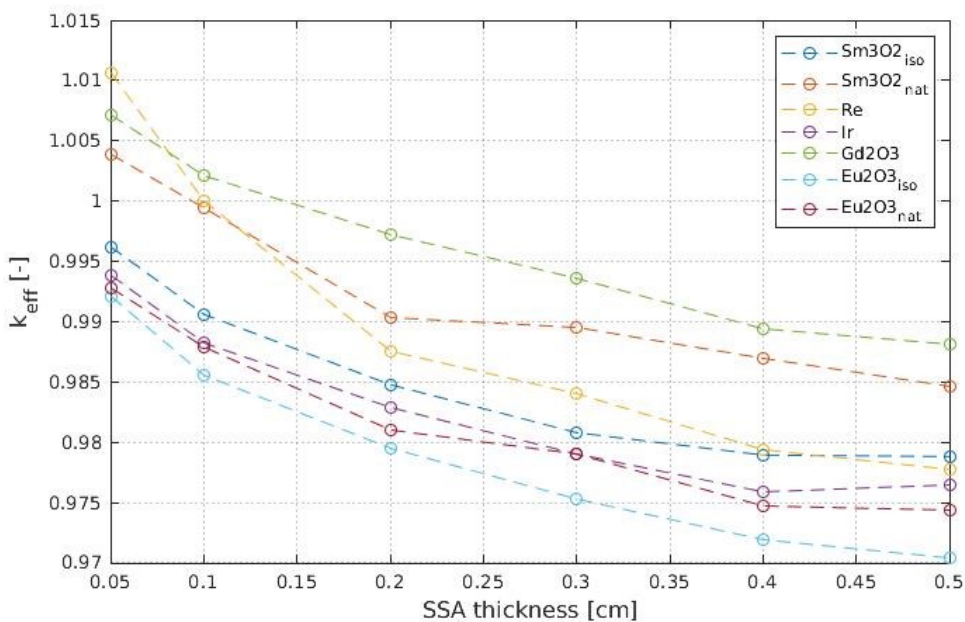


Fig. 3.2 - Effect of different SSA on reactor reactivity (normal operations) – CERMET optimized configuration.

Samarium and Europium were tested both in their natural isotope and its high-absorbing isotope. For the most absorbing materials even a 0.05 cm sleeve leads to a subcritical reactor in operating conditions. Other SSA may be implemented as 0.1 cm sleeve, but their contribution in accidental scenarios is still not enough to ensure subcriticality. The best configuration implementing SSA presents the following values of k_{eff} .

				No SSA	With SSA
	CD position	Channels	Reflecting medium	k_{eff}	
Submersion in dry sand	Inward	Empty	Sand	1.04746 ± 0.00060	1.00206 ± 0.00060
Submersion in wet sand	Inward	Water	Sand	1.20173 ± 0.00060	1.12532 ± 0.00060
Submersion in seawater	Inward	Seawater	Seawater	1.20040 ± 0.00060	1.16477 ± 0.00060
Reflector dismantled	NA	Seawater	Seawater	1.20794 ± 0.00060	1.16651 ± 0.00060

Table 3.2 - Comparison between base configuration and optimized configuration with SSA sleeve.

It is evident that SSA sleeve cannot be the solution; dispersion inside the fuel is not effective as well, thus a layer of SSA inside the moderator elements is proposed. The most effective SSA results to be rhenium, with a layer of 50 μm between the Zircaloy cladding and the $ZrH_{1.8}$ moderator. This configuration has low impact on nominal operations, both for the small quantity of SSA added to the core and its location, but strongly reduces reactivity in accidental scenarios: indeed, being the SSA close to the coolant channels, it is extremely effective when the seawater fills the channels, absorbing most of the thermalized neutrons.

The combination of *Re* layer and CD ensure safety for the dry and wet sand submersion accident, with a core that is slightly supercritical in case of submersion in seawater ($k_{eff} = 1.01003$). The 1000 pcm excess reactivity from the last case can be still absorbed in some way, but the reflector dismantled case is still an open issue, with a $k_{eff} = 1.12600$.

3.3 Control rods

To face this last class of accidents the introduction of control rods is analysed: as already stated, that choice increases system complexity, but it is worth to understand the reactor response to large, negative reactivity insertion. Thus, an increasing number of control rods was inserted inside the core, replacing fuel elements, up to 7: this is the minimum number of control rods required to ensure subcriticality. Their position was chosen arbitrarily, in the sense that no sensitivity analysis was performed to find the better location for each one; however, since one is placed in the middle and the remaining six at half the core radius, 60 degrees spaced, one may expect little variations from the following results.

	CD position	Channels	Reflecting medium	k_{eff}
Submersion in dry sand	Inward	Empty	Sand	0.95440 ± 0.00060
Submersion in wet sand	Inward	Water	Sand	0.99819 ± 0.00060
Submersion in seawater	Inward	Seawater	Seawater	0.99412 ± 0.00060
Reflector dismantled	NA	Seawater	Seawater	0.99348 ± 0.00060

Table 3.3 - Effect of seven B_4C control rods on core reactivity following submersion accidents – CERMET optimized configuration.

From a theoretical viewpoint, control rods are an effective system to maintain the reactor under safe conditions even in the worst accidental scenarios. Shutdown margin may be increased by adding another rod or by optimizing safety rod design. Nonetheless, introducing moving rods in a nuclear thermal rocket with a solid core poses engineering challenges. Failure of both control rods and CD system should be investigated, because an impact strong enough to dismantle the reflector could reasonably damage control rods' moving mechanism as well. If these two systems fail, the situation will not be much different from a core with reflector dismantled and without control rods. This is the reason to analyse an advanced CD system.

3.4 Advanced control drums system

The most important outcome from the previous analysis is that, no matter how much negative reactivity can be inserted following a submersion accident, there is always the probability that the reactor becomes subcritical. Thus, the problem should be tackled from a different direction: the underlying idea is to make control drums indispensable components for reactor criticality. This translates in fuel addition to the CD and a shifting toward the core centre. An advanced CD system has been already proposed [27], though not widely analysed in literature.

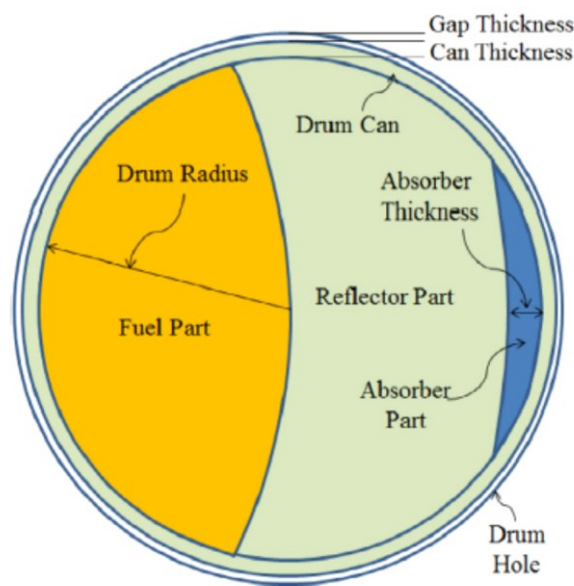


Fig. 3.3 - Advanced tolerant control drum [27]

The advanced tolerant control drum (ATCD) presents a fuel sector, a reflector part and the absorber. Its main difference from a simple control drum is the fuel sector, which is rotated inward when the reactor is operating, while it is pointed outward when shutdown is required. This configuration not only increases CD worth, but it also leads to a large reactivity loss in the event of reflector dismantling. To enhance the reactivity worth, the ATCD is placed deeper in the core, with its centre lying on the core outer radius (**Fig. 3.4**)

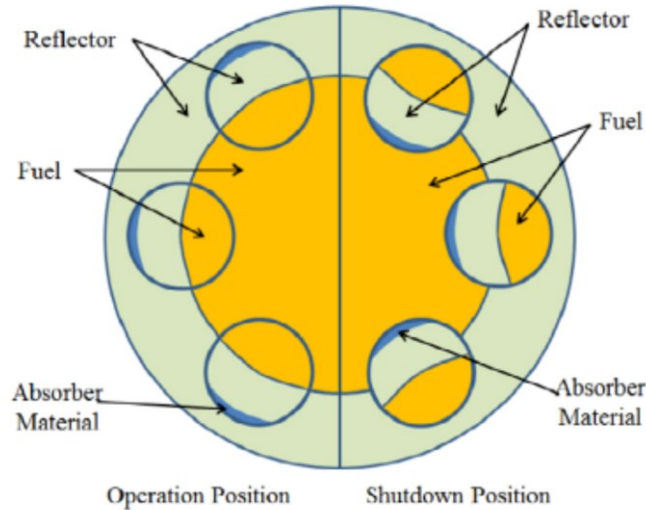


Fig. 3.4 - ATCD position for reactor operation and shutdown [26].

In the present work, a slightly more sophisticated control drum is proposed. Basically, layers of fuel and moderator replace the simple fuel sector: the combined effect of moderator and reflector ensure a high neutron flux even in the CD. Even if engineering issues may arise from a control system like this (for instance, its cooling), it is worth to investigate its effect on neutronics and to check whether it could be a definitive solution to solve supercriticality in submersion accidents or different systems should be adopted.

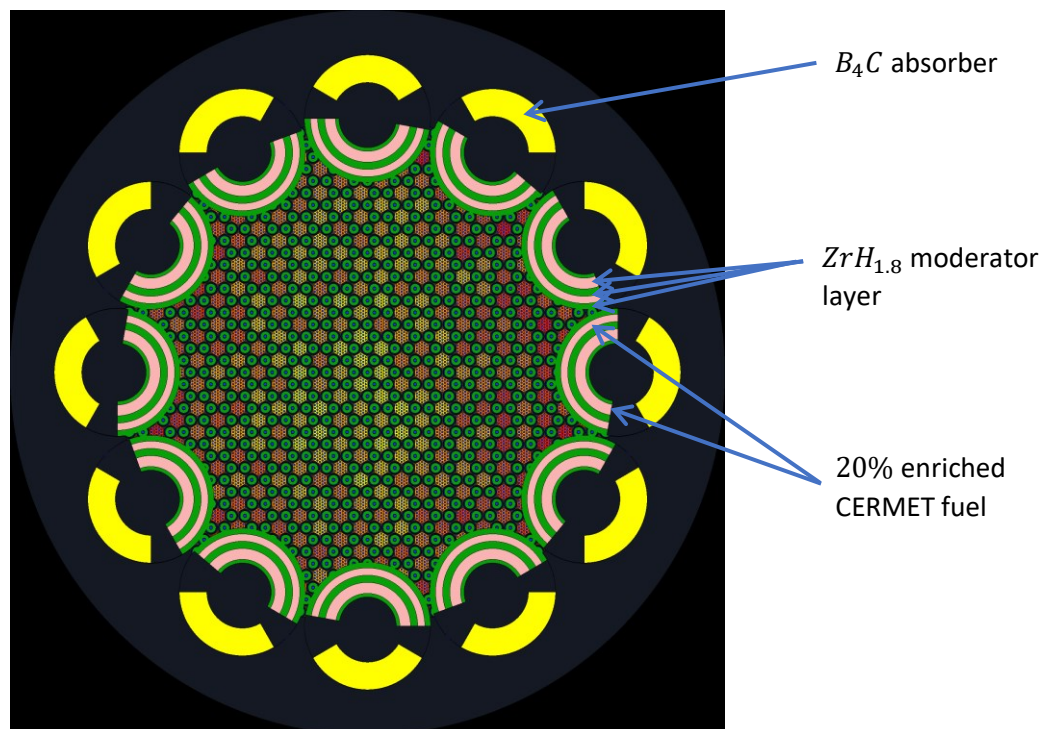


Fig. 3.5 - ATCD core. Absorber (yellow), moderator (green), fuel (pink). (Serpent input).

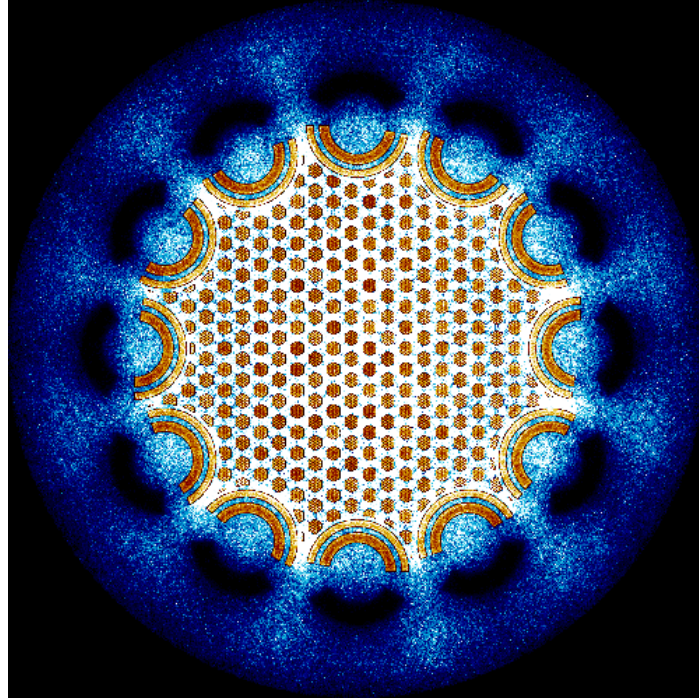


Fig. 3.6 - Mesh detector for neutron flux. ATCD core. Dark zones are related to absorbers presence.

From the previous neutronic analysis it was found that increasing absorber thickness above a certain value has no effect on core neutronics, because of the peripheral location occupied by CD. Now that they have been moved closer to the inner region of the core, absorbers thickness was increased up to 4 cm, to provide a much relevant negative reactivity insertion. Concerning the fuel and the moderator layers, moderator occupies three sectors with the following inner and outer radii: 9cm/8 cm, 7cm/6 cm, 4.5cm/4 cm. The zones between moderator layers are filled with fuel 20% enriched: this configuration helps to maximize the CD reactivity contribution.

	CD position	Channels	Reflecting medium	k_{eff}
Submersion in dry sand	Inward	Empty	Sand	0.84227 ± 0.00040
Submersion in wet sand	Inward	Water	Sand	0.95294 ± 0.00040
Submersion in seawater	Inward	Seawater	Seawater	0.95031 ± 0.00040
Reflector dismantled	NA	Seawater	Seawater	0.98564 ± 0.00040

Table 3.4 - k_{eff} for ATCD core following a submersion accident.

In the end, for the totality of possible submersion accidents the core is kept subcritical, with a minimum shutdown margin of -1436 pcm, or -1.99 \$, from the reflector-dismantled scenario.

3.5 Conclusions

In this section, an accidental scenarios analysis has been performed to verify reactor capability of withstanding submersion accidents. It is found that when submersion occurs, a large burst in reactivity is experienced by the system. To bring the core subcritical, three different solutions have been investigated: spectral shift absorbers, control rods and advanced control drums. Spectral shift absorbers result hardly implementable in LEU reactors, due to their negative effect during normal operations. For each of the SSA tested, there was no configuration that can ensure subcriticality in case of accidents and criticality in nominal operations. However, this does not mean that SSA should not be used for reactivity control, rather they must be combined with a different control system to maintain the reactor under safety conditions in any situation.

Control rods may be a viable option, at least from a theoretical viewpoint, since it was demonstrated that they manage to bring the reactor subcritical in all the accidental scenarios. Only their effect on neutronics was studied, leaving practical issues to more detailed analysis. Thus, possible engineering complications may lead to a preference for simpler systems, such as advanced control drums.

The ATCD are shown to be an effective control system which can be successfully adopted to face submersion accidents. By minor changes to the ATCD already proposed by [27], a core capable to maintain a k_{eff} lower than unity for every possible submersion scenario is found. Such a system should be tested on a real reactor, but thanks to its similarity with common CD, the design and the reactor behaviour should not show dramatic changes. The main data related to this new configuration are summarized in **Table 3.5**.

	ATCD reactor configuration
k_{eff}	1.00215 ± 0.00020
Excess reactivity [β]	0.29
β_{eff} [–]	0.00727 ± 0.00010
Λ [μs]	17
Enrichment zones (% U_{235} enrichment)	7 ([19 18 17 16 15 14 13])
Reflector thickness (radial/axial) [cm]	10/10
Radial peaking factor [–]	1.25
Axial peaking factor [–]	1.49
Hot channel factor [–]	1.86
U_{235} mass saving (%)	7.6
Axial reflector mass saving [Kg]	94 (–56%)
Radial reflector mass saving [Kg]	588 (–60%)
Total mass [Kg]	2074 (–25%)

Table 3.5 - Reactor data for the ATCD configuration.

4. Thermal-hydraulics analysis

Thermal-hydraulics analysis is the last step for a preliminary design of a reactor for space propulsion. The main goals of this analysis are to check whether thermal limits are not exceeded in any core element and to evaluate (or increase, if possible) the overall rocket performances. The first objective is mandatory for safety reason: if the temperature raises up to materials melting point, local melting occurs; this is an extremely dangerous situation, because the whole reactor may be compromised and radioactive elements may escape the core. Furthermore, ensuring that the temperature remains below safety limits, at least for nominal operations, has a direct impact on propulsion performances: indeed, for large values of the hot channel factor F_{hc} , the high temperatures along the hot channel limit the average outlet coolant temperature, bounding both the specific impulse i_{sp} and the thrust F . Concerning the second goal, the performances evaluation highlights reactor weakness (e.g., a low TWR may suggest an additional mass cut) and allows for a comparison with other design. Many successfully attempts have been made in this direction in the previous neutronic analysis: fuel enrichment was varied to find the optimal value that minimizes excess reactivity, reactor mass and peaking factors. This process leads to a 7-zones layout, which provides substantial power distribution flattening. At this stage, possible optimizations may be carried out from the thermal-hydraulic viewpoint, such as mass flow rate tuning and orificing. Thus, the present section is organized as follow: firstly, a simple fuel element model is built, in such a way that its analysis is feasible with basic thermal-fluid dynamics concepts implemented in MATLAB; secondly, a 0-D analysis is performed, in order to define inlet and outlet coolant conditions, both for fuel elements and moderator elements. Then, the temperature profile along the hot channel is evaluated, reconstructing the axial power profile from Serpent output. This is done for the last CERMET configuration obtained in Section 3, which is the only one that satisfies safety requirements. Finally, rocket performances are estimated, the definitive design is compared to others available in literature and improvements for future works are proposed.

4.1 Fuel element model

A thermal-hydraulics analysis may be executed by CFD software that return almost any attainable quantity of interest, with a complete view of both fluid dynamics and heat exchange process. However, this approach does not fit with the philosophy of this work, which aims to develop a model for space reactor design that must result light, applicable even with limited computational resources and easily integrable with other codes. In this perspective, the fuel elements cannot be analysed as they are, because of their geometry complexity.

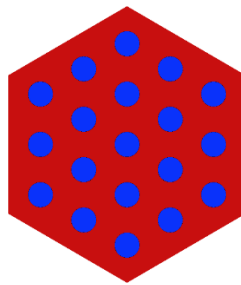


Fig. 4.1 – CERMET core fuel element section (Serpent input).

A reasonable, simple modellization of the fuel element is proposed as follow: each channel is assumed to be surrounded (radial-symmetrically) by 1/19 of the total fuel element mass, to conserve both the fuel mass and the heat exchange surface. Since the pitch among the channels and the distance from the outer channels to the edge of the element is comparable, this geometric simplification should not introduce large errors. Furthermore, this approach returns an equivalent radius for the fuel and a cylindrical concentric structure that can be readily investigated, still preserving the essential feature of the heat exchange phenomena in the fuel.

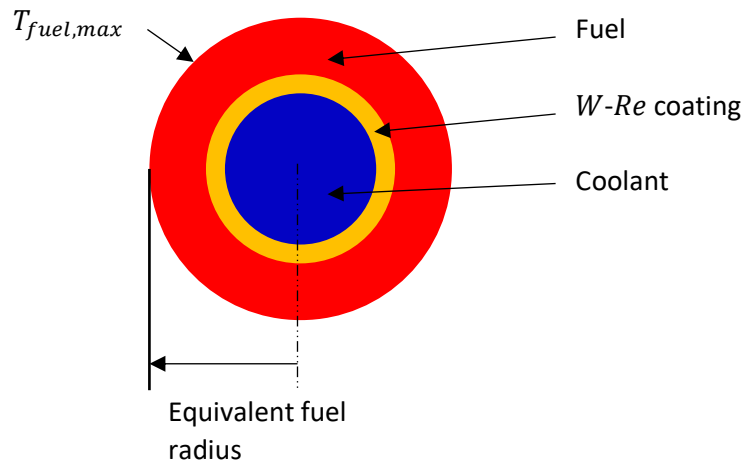


Fig. 4.2 - Fuel coolant channel model (not in scale).

Once the geometry is simplified, some modelling assumptions are introduced:

1. Radial symmetry;
2. Axial conduction negligible inside fuel elements;
3. Adiabatic fuel element outer boundaries;
4. Power deposition inside the fuel elements equal to 89% of the total reactor power;
5. *W-Re* coating thermal conductivity constant;
6. Steady state conditions.

Before going on, it is worth to motivate the above assumptions. The first hypothesis is directly related to the geometric simplification performed, because, as far as the fuel element is modelled by 19 cylindrical concentric subsystems, there is no reason to think that the system is not radial-symmetric. The second assumption is a common one when dealing with 1D or 2D radial-symmetric analysis, being the heat flux orders of magnitude greater along the element transversal section. The third hypothesis is probably the strongest: the fuel element is in contact with the surrounding moderator elements, along an interface made of graphite on moderator side and fuel matrix on the other side, which is not adiabatic. However, the inner coolant channels are surrounded by fuel matrix only: modelling the channels as concentric cylinders, and assuming that along each of the 19 channels the fuel releases the same power, the outer fuel temperature ($T_{fuel,max}$) will be the same, thus heat will not flow from one channel subsystem to another. In addition to that, the adiabatic hypothesis will produce conservative results. The fourth assumption could be verified by exploiting Serpent detectors: evaluating the power deposition inside the fuel elements and knowing that the total power is

450 MW, computing the power fraction released inside the fuel is straightforward. The lack of computational resources leads to an uncertain power fraction, ranging from 86% to 92%, hence its value was set to 89%. The fifth hypothesis is completely justified by the infinitesimal thickness of *Re* coating: as a matter of fact, doubling or halving coating conductivity did not produce any appreciable fuel temperature variation. Finally, since the study of a power transient is out of the scope of this work, a steady state condition is assumed.

For reader convenience the main reactor feature involved in the thermal-hydraulics analysis are reported in the following table.

	ATCD reactor configuration
Reactor power [MW]	450
Power fraction deposited in fuel elements	0.89
Radial peaking factor [–]	1.25
Axial peaking factor [–]	1.49
Hot channel factor [–]	1.86
Active length [cm]	75
Number of fuel elements	389
Fuel element flat-to-flat distance [cm]	1.905
Number of channels for fuel element	19
Coolant channel radius [cm]	0.12292
Coating thickness [cm]	$5.08 \cdot 10^{-3}$
Equivalent fuel radius [cm]	0.2295

Table 4.1 - Summary of ATCD reactor features.

4.2 0-D analysis

When dealing with complex systems, approaching the analysis starting from a simple model and then increasing the complexity is a reasonable, effective practice. Thus, before proceeding with the hot channel study, a 0-D reactor analysis is presented. The main goal of this section is to compute the inlet and outlet coolant temperature, for both moderator and fuel elements. While the inlet coolant temperature is a necessary boundary conditions for the following hot channel analysis, the outlet coolant temperature can be used to check the consistency of the 2D radial-symmetric model, comparing the outlet coolant temperature from an average channel to that obtained by 0-D analysis. It should be recalled (Section 1.1.3) that the coolant flow, once its pressure is raised to the operational value, is split in two flows: a fraction is sent back and forth in the moderator elements (\dot{m}_{mod}), while the remaining coolant (\dot{m}_{pl}) goes directly inside the upper plenum, where it mixes with the fraction returning from the moderator elements. From the upper plenum the coolant flows inside the fuel element, reaching the lower plenum and finally entering the nozzle. Hence, from basic thermodynamics, the following system may be easily obtained:

$$\begin{cases} T_{out,mod} = \frac{P_{tot} - P_{fuel}}{\dot{m}_{mod} \cdot c_{p,mean}} + T_{in,mod} \\ T_{in,fuel} = \frac{\dot{m}_{mod} T_{out,mod} + \dot{m}_{pl} T_{inlet}}{\dot{m}_{mod} + \dot{m}_{pl}} \end{cases} \quad (4.1)$$

Where $P_{fuel} = 0.89 P_{tot}$ is the power fraction released in the fuel elements and $c_{p,mean}$ is the mean value of the coolant specific heat [28]. $T_{in,mod}$ is the inlet moderator coolant temperature: assuming that $T_{in,mod}$ is equal to the inlet reactor coolant temperature, its value can be retrieved from literature [2] or inferred from previous design. Specifically, $T_{in,mod} = 125\text{K}$. Obviously, there are many combinations of \dot{m}_{mod} and \dot{m}_{pl} once the total mass flow rate is set, with the main constraint that \dot{m}_{mod} should be sufficiently high to avoid moderator elements melting. The total mass flow rate directly affects both the specific impulse and the thrust, so its value must be chosen carefully: as a first attempt, it is set as $\dot{m}_{tot} = 12.5 \text{ kg/s}$.

Solving the system for different values of the partial mass flow rates until the $T_{out,mod}$ is

sufficiently low, one obtains the following results.

	ATCD reactor configuration
Total coolant mass flow rate \dot{m}_{tot} [kg/s]	12.5
Coolant mass flow rate inside moderator elements \dot{m}_{mod} [kg/s]	4.5
Moderator inlet coolant temperature $T_{mod,in}$ [K]	125
Moderator outlet coolant temperature $T_{mod,out}$ [K]	834
Fuel inlet coolant temperature $T_{fuel,in}$ [K]	380
Fuel outlet coolant temperature $T_{fuel,out}$ [K]	2447

Table 4.2 – Thermal-hydraulic results from 0-D analysis - ATCD reactor configuration.

The moderator mass flow rate should result suitable to ensure sufficient cooling to the moderator elements, while the fuel inlet coolant temperature should be low enough to guarantee that the melting temperature will not be reached in any zone of the fuel. With these basic results it is possible to proceed to the hot channel study.

4.3 Hot channel analysis

In a nuclear reactor, the hot channel is the most loaded channel (from a thermal viewpoint), which limits the maximum power density achievable inside the core and consequently its performances. Thus, the hot channel factor F_{hc} should be lowered as much as possible. The neutronic optimization worked also on that direction, so now this is the right time to check its effect on the hot channel temperature profile. To do so, the power profile must be known in the hot channel: this is not an easy task, because the hot channel location is not known prior to the simulation run. If it had been the case, one would just have set a detector on that position to evaluate the power profile. However, since it is unknown, there are different ways to proceed: a 3-D cartesian detector can be defined in the whole core domain, returning the power distribution; since the fission power is generated only in the fuel elements, it is easy to find the hot channel and the related power profile. The main issue that makes this method inapplicable is the huge computational resources required to store and process the 3-D power distribution: even accepting a very low data resolution, the total bins' number reaches quickly one million (i.e., a 100x100x100 mesh). To avoid such a brute force approach, the card *set cpd* can be inserted in the Serpent input file: *set cpd* returns the core power distribution at different levels, including fuel elements level. Since the power is given as the integral value along each fuel element, the data to handle are much more limited in this case. From the power distribution it is straightforward to find the hot channel (it just requires an algorithm capable to reconstruct the core layout, such as the one developed for the power distributions in Section 2) and to define a detector on that location. Then, a new simulation is run, the power profile in the hot channel is evaluated by the detector and the hot channel analysis can be performed. This method is actually smarter than the brute force approach and can be easily implemented in the global code; however, it requires each simulation to be run twice, which becomes unacceptable when dealing with hundreds of simulations. Therefore, a simpler approach is chosen to tackle the problem: a cartesian detector is placed on a fuel element, to store the power profile. Simultaneously, the *set cpd* card evaluates the power generated inside each fuel element. At this point, the power profile recovered from the detector is normalized to the average channel power profile, and from this the hot channel power profile is reconstructed through the hot channel factor. This procedure is extremely fast because it does not require any additional simulation nor large RAM usage and can be implemented in a

MATLAB script. Once the power profile is available, the temperature profile can be computed. The heat exchange process is modelled as usual with the thermal resistance method: for further information the reader is referred to [29]. The input data for the analysis are summarized in **Table 4.3**.

	ATCD reactor configuration
Hot channel mass flow rate [kg/s]	$1.69 \cdot 10^{-3}$
Inlet coolant temperature [K]	380
Hot channel factor [–]	1.86
Integral hot channel power [MW]	1.49

Table 4.3 - Input data for hot channel analysis – ATCD reactor configuration.

Hydrogen properties are obviously temperature and pressure dependent, and they were taken from [28]. CERMET conductivity is also a function of temperature; it was retrieved from [30]. The *W-Re* coating thermal conductivity was evaluated as a weighted average, being the tungsten thermal conductivity a function of temperature, as reported by [30].

Finally, the heat transfer coefficient was evaluated through the Dittus-Boelter correlation, which is valid in a wide range of Reynolds and Prandtl number:

$$Nu = 0.023 Re^{0.8} Pr^{0.4} \quad (4.2)$$

$$h = Nu \cdot \frac{k_{coolant}}{D_{channel}} \quad (4.3)$$

where Nu , Re , Pr are respectively the Nusselt, Reynolds and Prandtl numbers, h is the heat transfer coefficient between the coolant and the coating surface, $k_{coolant}$ is the hydrogen thermal conductivity and $D_{channel}$ is the channel diameter.

The coolant temperature profile is computed by dividing the channels in n axial bins, where n is the length of the axial power profile array. Thus, at each bin the coolant temperature is evaluated through an energy balance, and the cladding and fuel temperatures are found by iterations, since convergence is reached, according to the general equation:

$$q' = R_{th} \cdot \Delta T \quad (4.3)$$

where q' is the heat flux per unit length, R_{th} the thermal resistance associated to the two

points among which the temperature difference ΔT is calculated. By this basic model the temperature profile for both coolant and fuel can be computed, as shown in **Fig. 4.3**. The calculations were made with the real power profile and the equivalent cosine profile. The z -axis origins is set at the middle of the core, while the direction points toward the bottom of the core.

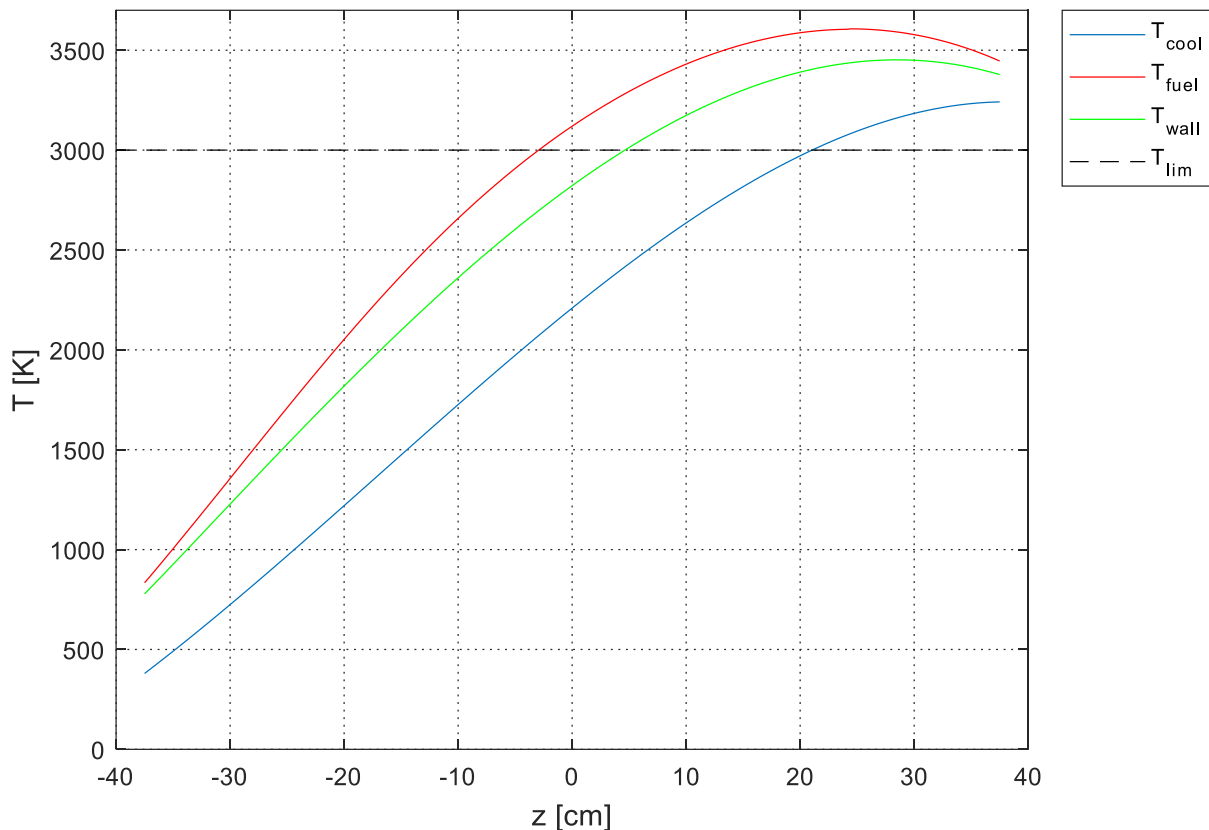


Fig. 4.3 - Fuel and coolant temperature in the hot channel (cosine power profile) – ATCD reactor configuration.

The temperature profiles look as expected, with the typical shape related to a cosine power profile: actually, it is not a real cosine due to the presence of axial reflector only on the upper core, as shown in **Fig. 4.6**; however, for a preliminary calculation an equivalent cosine profile was used. The maximum fuel temperature exceeds the limit of 3000 K [31] with a peak value of 3567 K, which is obviously unacceptable.

Since all the efforts focused on flattening the power distribution have been already made, a thermal-hydraulics optimization may be performed. An effective way to lower the temperatures in the hot channel is the reactor orificing [32]: through the implementation of specific devices, an higher coolant flow rate can be redirected in the hot channel, at expenses

of the other channels. This technique is much more effective than simply increasing the total mass flow rate, which will translate in a worse usage of propellant and in lower propellant temperatures, damaging the overall reactor performances.

Thus, the hot channel mass flow rate is varied simulating an orificing, looking for the value required to bring the peak temperature below 3000 K: this value is found to be $2.0 \cdot 10^{-3} \text{ kg/s}$ for each channel in the hottest element. This procedure raises the peaking temperature in the average channel up to 2829 K (real power profile), that is still acceptable. The new temperature profiles are reported in the following figures.

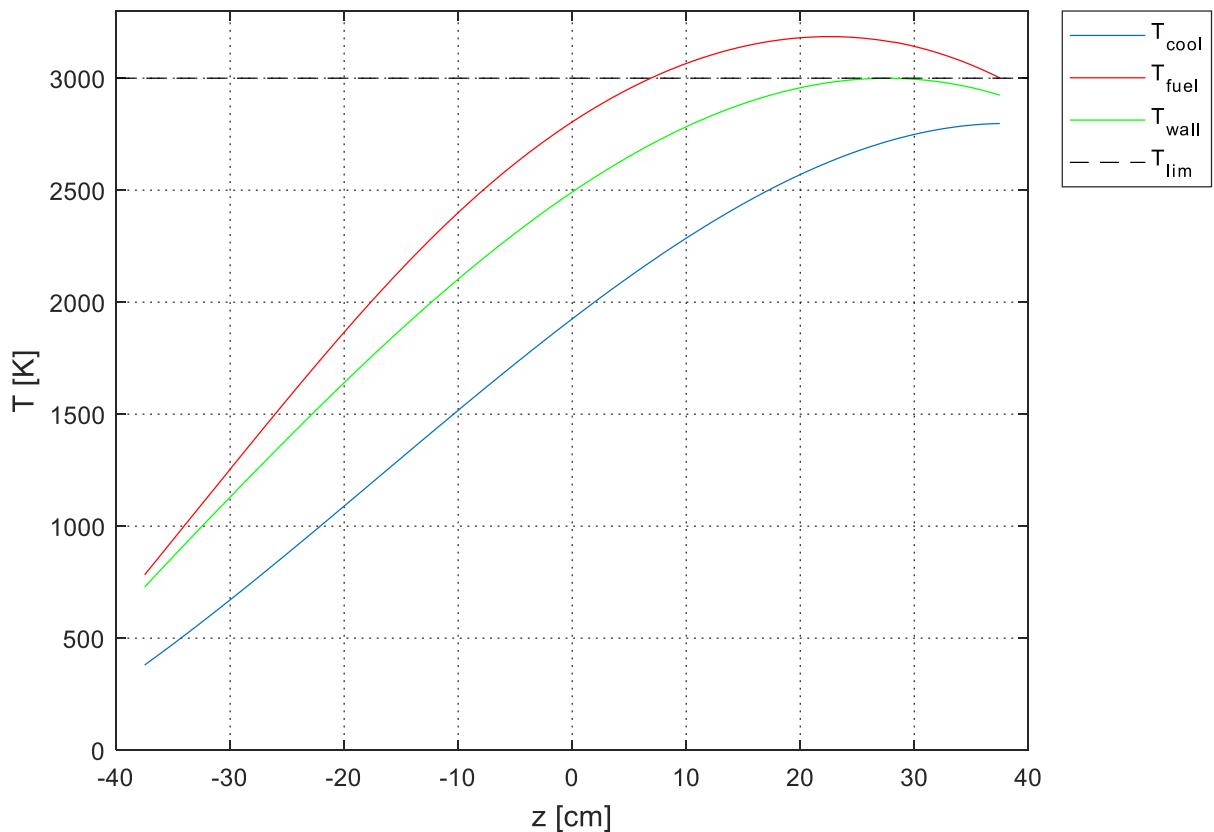


Fig. 4.4 - Fuel and coolant temperature in the hot channel, orificed core (cosine power profile) – ATCD reactor configuration.

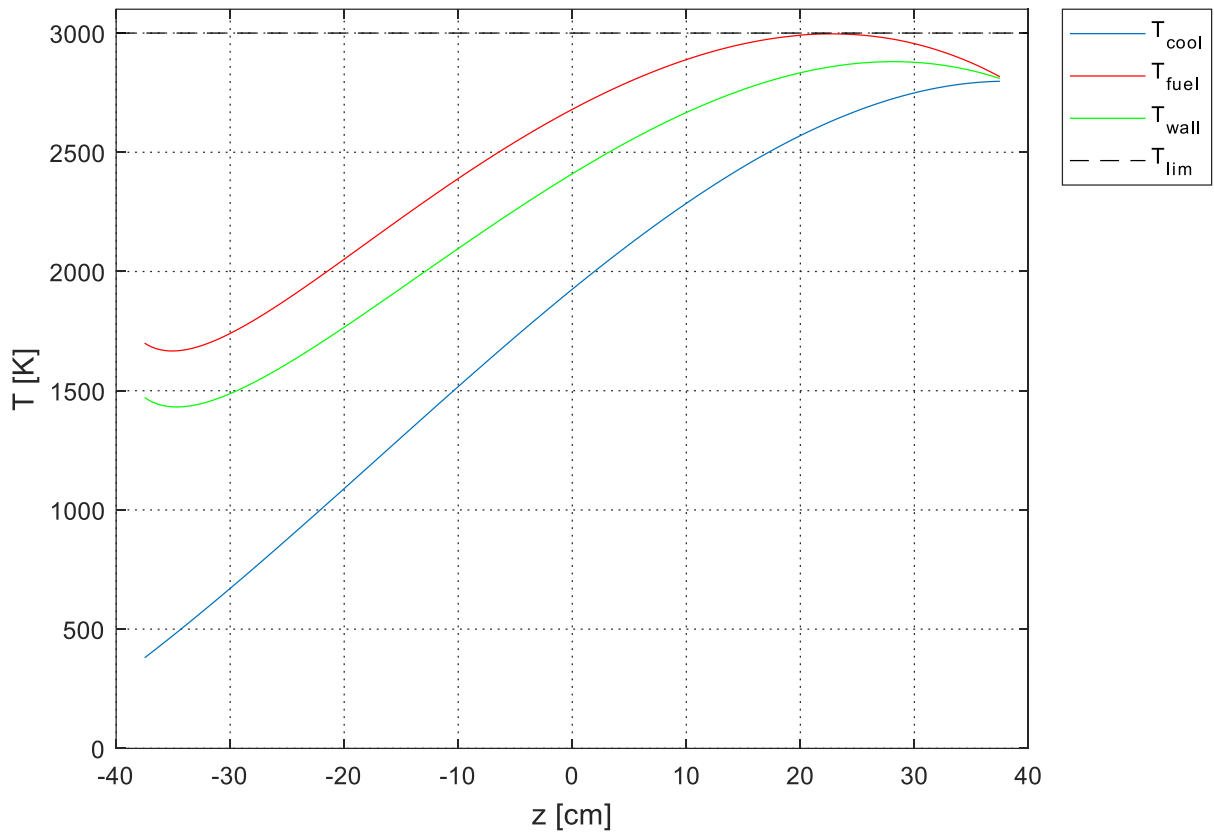


Fig. 4.5 - Fuel and coolant temperature in the hot channel, orificed core (real power profile) – ATCD reactor configuration.

It is interesting to note the difference between the temperatures obtained by a cosine power profile and the one obtained by the real profile. Specifically, the cosine profile leads to a peaking temperature above the limit, while the real profile does not. This is related to the strong shape difference of the two profiles, which affects the resulting temperature.

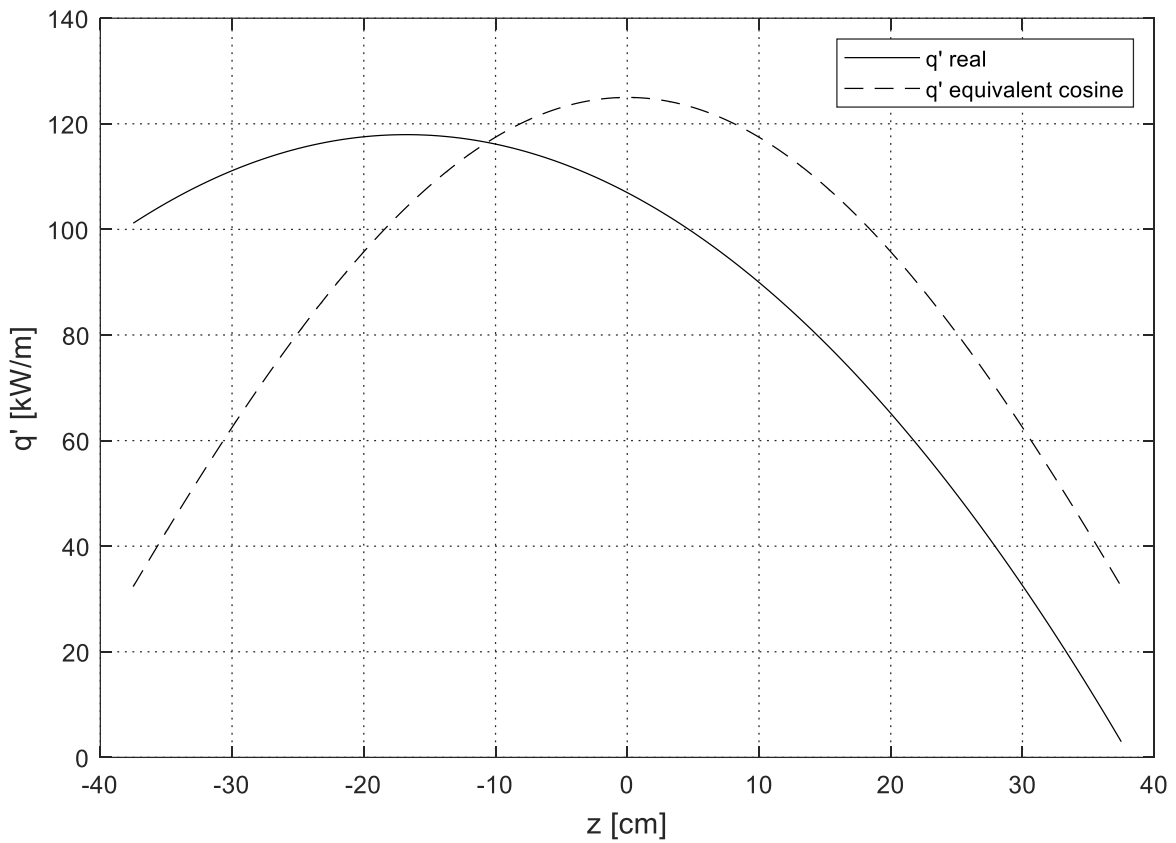


Fig. 4.6 – Hot channel power profile per unit length – ATCD reactor configuration.

The curious tail (**Fig. 4.5**) in the entrance region is probably a combined effect of the asymmetric power profile and the behaviour of the heat transfer coefficient (**Fig. 4.7**), which increases sharply as the temperature rises.

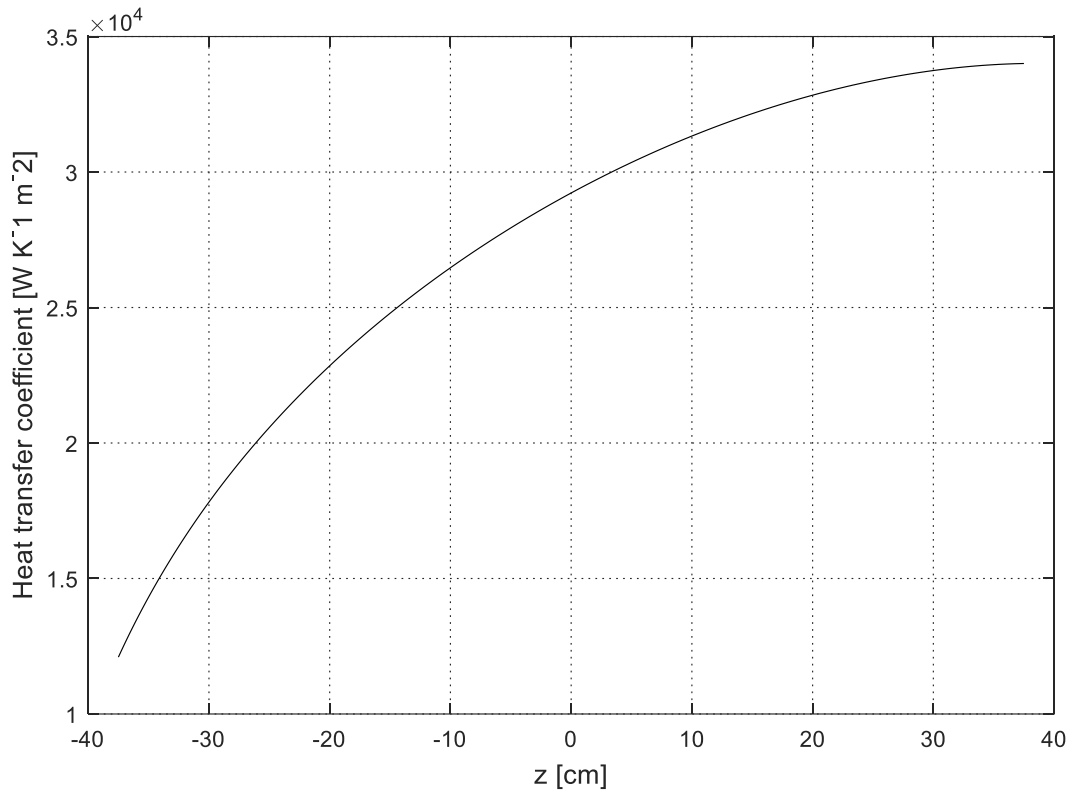


Fig. 4.7 - Heat transfer coefficient along the hot channel – ATCD reactor configuration.

Concerning the average channel, the temperature profiles are the following:

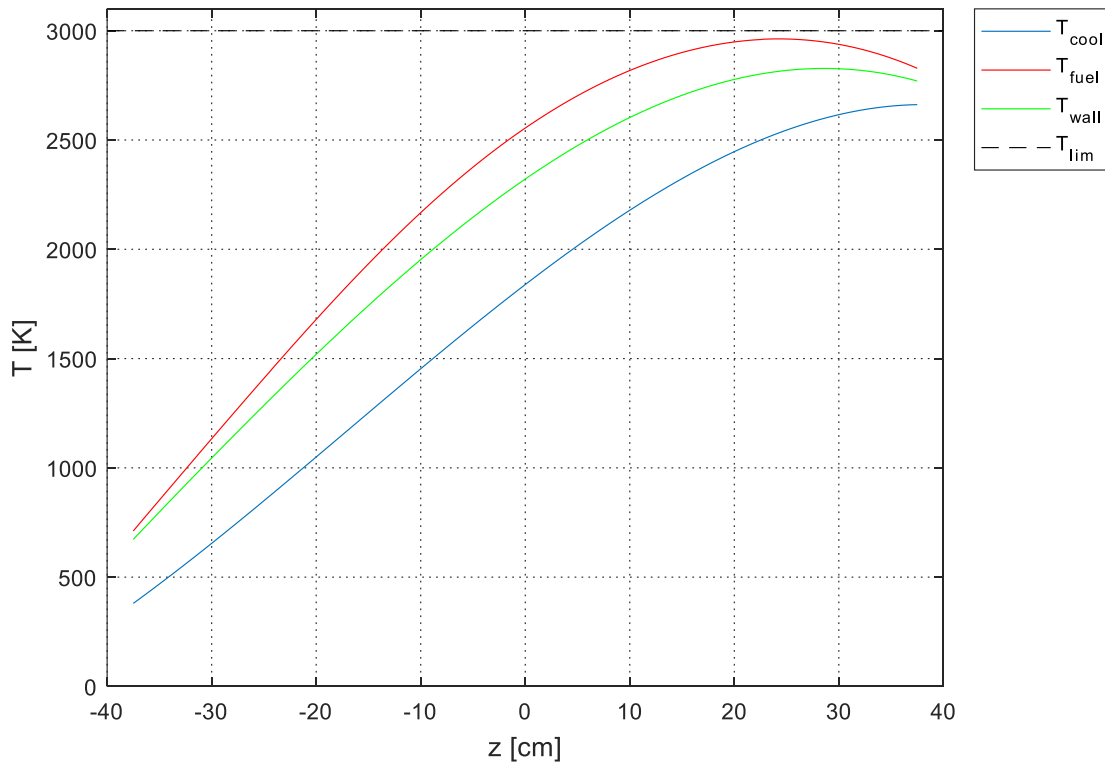


Fig. 4.8 - Fuel and coolant temperature in the average channel, orificed core (cosine power profile) – ATCD reactor configuration.

	ATCD reactor configuration
Hot channel mass flow rate [kg/s]	$2.0 \cdot 10^{-3}$
Peak temperature in the hot channel [K]	2996
Peak temperature in the average channel [K]	2829
Outlet coolant temperature (average channel) [K]	2661

Table 4.4 - Hot channel and average channel data after orificing – ATCD reactor configuration.

The orificing appears to be an extremely effective optimization, which requires a moderate engineering effort to be accomplished. By a mass flow rate increase of approximately 15% in the hot channel the issue related to thermal limits is solved. Furthermore, model consistency can be checked by comparing the outlet coolant temperature from the average channel with the average outlet coolant temperature obtained by the 0-D analysis: the outcome is reasonable, with an error of 8%, which is not so large considering the simplifying assumptions made, both for the 2-D analysis and the 0-D (hydrogen specific heat constant).

At this point of the analysis, the reactor satisfies all the safety requirements that this work proposed to investigate; now, the rocket performances can be evaluated.

4.4 Rocket performances

The analysis so far focused on an optimization of the neutronics and thermal parameters that may affect, both directly and indirectly, rocket performances. Furthermore, the reactor was demonstrated to be safe in any of the conditions studied. However, in the end, the reactor must be competitive from the propulsion viewpoint: its specific impulse, thrust and TWR should make the reactor, and nuclear thermal propulsion in general, an attractive option for spaceflight. The evaluation of those parameters is straightforward, once the thermodynamics data at the nozzle entrance are known. The formulae required for this evaluation are briefly recalled hereunder; for further details on the quantities involved see Subsection 1.1.1.

The rocket thrust is defined as:

$$F = \dot{m} \cdot u_{eq} \quad (4.5)$$

while the specific impulse can be written as:

$$I_{sp} = \frac{F}{\dot{m}g} \quad (4.6)$$

The effective velocity u_{eff} can be obtained from the exit propellant velocity and the pressures at the nozzle exit and in the surrounding environment:

$$u_{eff} = u_{exit} + \frac{(p_e - p_o)A_0}{\dot{m}} \quad (4.7)$$

Finally, the exit velocity can be derived by basic nozzle theory as:

$$u_{exit} = \sqrt{\frac{T_c \cdot R}{MM} \cdot \frac{2\gamma}{\gamma - 1} \left(1 - \left(\frac{p_e}{p_c} \right)^{\frac{\gamma-1}{\gamma}} \right)} \quad (4.8)$$

in which the assumption of ideal nozzle was made.

These equations are the only one required for a preliminary evaluation of rocket performances. It should be noted that the thrust F and the specific impulse i_{sp} are both related to the propellant mass flow rate \dot{m} , showing a competitive behaviour. Furthermore, also the outlet coolant temperature depends on coolant mass flow rate, thus the propellant velocity. A useful visualization of their behaviour as a function of \dot{m} is presented in **Fig. 4.9**, in which NASA requirements are inserted as bounding lines for the mass flow rate. Hydrogen properties for the calculations are available at [28], while the chamber temperature is assumed to be equal to the outlet average coolant temperature.

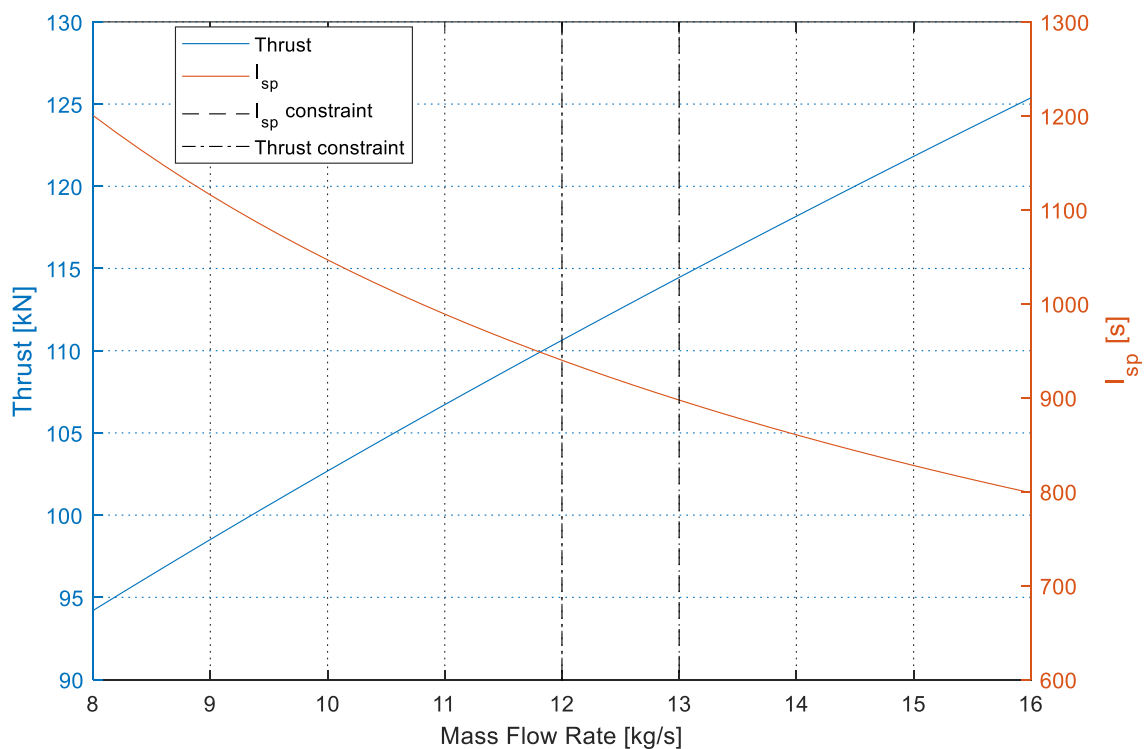


Fig. 4.9 - Thrust and specific impulse vs. propellant mass flow rate ($c_p = \text{const} = 16.5 \frac{\text{kJ}}{\text{kg K}}$).

NASA requirements greatly reduces the possible mass flow rate values for the current design. By reducing the mass flow rate, i_{sp} can be raised up to about 950 s, still producing enough thrust (111 kN). To overcome this limit, multiple reactor engine with lower thrust may be coupled to produce the required rocket thrust: however, reducing the mass flow rate below 12 kg/s may constitute an issue from the thermal viewpoint, being the coolant not able to extract the whole reactor power. Furthermore, the TWR of the single reactor engine must be taken into account: with a thrust of 111 kN, the TWR for this reactor configuration is 5.1, neglecting the shadow shield and other ex-core components. Assuming additional 1000 Kg

from these components, the TWR drops to 3.4, which is quite smaller than the previous value. Clearly, a mass optimization on the ex-core components may be performed: halving the mass allows for a TWR of 4, which is an acceptable value. This brief example shows how the quantities involved in these calculations are correlated, making the optimization of the rocket performances anything but trivial. The core orifice, which greatly enhances core thermal-hydraulics, is ineffective from the propulsion viewpoint: in steady state, the energy balance forces the average outlet coolant temperature to be the same once the total mass flow rate and the inlet temperature are fixed. Assuming an average c_p along the channels:

$$T_{cool,out} = T_{cool,in} + \frac{P_{core}}{\dot{m} c_{p,avg}} \quad (4.9)$$

Thus, whatever happens in the hot and average channels, the average outlet coolant temperature is fixed. Letting $T_{cool,in}$ increase may cause possible damages to the moderator elements, since the inlet coolant temperature is strictly related to the coolant temperature after its flow inside the moderator elements.

All this argument should convince that the best way to approach an NTP system optimization is to start from the very beginning, namely core neutronics and mass reduction, as it was done in this work. With this in mind, the rocket performances are finally evaluated; for the calculations all the properties have been assumed temperature and pressure dependent.

	C-LEU-NTR	ATCD reactor configuration
Reactor mass [kg]	2016	2226
Ex-core components mass [kg]	1000	1000
Thrust [kN]	110	122
Specific impulse [s]	900	996
Thrust to weight ratio - reactor only	<i>N. A.</i>	5.6
Thrust to weight ratio - reactor and ex-core components	3.49	3.9

Table 4.5 – Comparison of reactor figures of merit from the propulsion viewpoint.

4.5 Conclusions

The thermal-hydraulics analysis concludes the preliminary reactor design carried out in this work.

A geometrical modelling of the fuel element was the first step to set up a simulation, reducing the hexagonal domain in a concentric cylindrical structure, which results much easier to analyse. Then, few modelling assumptions were introduced to reduce the complexity of the equations to be solved, allowing a MATLAB script to handle the whole thermal-hydraulics analysis.

A 0-D analysis highlights the main feature of the model, such as the mass flow rate splitting, the resulting inlet temperature and the average outlet coolant temperature. Thus, it both provides the boundary conditions for the hot channel analysis and a benchmark value to check the model.

The hot channel analysis is the core of this section, since it represents on the one hand the accomplishment to all the safety requirements, on the other hand it makes way for possible optimizations that could increase the overall reactor performances. Even if the first results obtained were not encouraging, due to the high temperatures in the hot channel, the introduction of a core orifice greatly improved the thermal-hydraulics mechanism of the core, lowering the maximum temperature below its safety limit.

Finally, the reactor performances from the propulsive viewpoint are evaluated: the complex interaction among the main parameters is shown, and both the thrust and the specific impulse are evaluated by simple algebraic equations. The reactor fulfils NASA requirements for thrust and specific impulse, presenting a variable TWR which will depend on the overall system mass, including ex-core components. **Table 4.6** summarizes the results obtained in this section.

	ATCD reactor configuration
Total coolant mass flow rate \dot{m}_{tot} [kg/s]	12.5
Coolant mass flow rate inside moderator elements \dot{m}_{mod} [kg/s]	4.5
Moderator inlet coolant temperature $T_{mod,in}$ [K]	125
Moderator outlet coolant temperature $T_{mod,out}$ [K]	834
Fuel inlet coolant temperature $T_{fuel,in}$ [K]	380
Fuel outlet coolant temperature $T_{fuel,out}$ [K]	2681
Initial hot channel mass flow rate [kg/s]	$1.69 \cdot 10^{-3}$
Hot channel mass flow rate after orificing [kg/s]	$2.0 \cdot 10^{-3}$
Peak temperature in the hot channel [K]	2996
Peak temperature in the average channel [K]	2829
Thrust [kN]	122
Specific impulse [s]	996
Thrust to weight ratio – reactor only [–]	5.6
Thrust to weight ratio – reactor and ex-core components [–]	3.9

Table 4.6 - Thermal-hydraulics features and performances – ATCD reactor configuration.

5. Conclusions

The main goals of this work were the development of a structured approach to the neutronic and thermal-hydraulics design of a nuclear reactor for NTP and the application of the resulting methodology to a real system: a LEU, CERMET fuelled reactor. All the procedures, models and scripts required have been developed from scratch, with the support of dedicated software such as Serpent for the neutronics and MATLAB for the thermal-hydraulics analysis. Particular attention has been paid on the consistency of both the models and the results: input data were retrieved from established literature sources, uncertainties were considered when possible, simplifying assumptions were made only when strictly necessary and a benchmark case has been included. In this way it has been possible to compare the results with other studies in literature and to check the fulfilment of NASA DRA 5.0 requirements for NTP.

After a review on the state of the art of NTP the work focuses on the neutronics analysis, which has been demonstrated to be an essential step for mass reduction and power distribution optimization. The neutronic model was firstly tested against an available case in literature, then applied to the CERMET reactor. A systematic procedure to investigate and optimize possible reactor configurations was implemented through a Python script which integrates Serpent pre-processing, simulation and MATLAB post-processing. A huge amount of information was available through this method, highlighting the effects of reflector thickness (both axial and radial) and the importance of a precise fuel zoning. From the perspective of rocket performances, the code also acts toward a power profile flattening, reducing hot spots and allowing for higher propellant temperatures. The results of this analysis and the consequent optimization are extremely encouraging: a 25% system mass reduction with a 7.6% fissile material saving is achieved, improving the power distribution as well; excess reactivity is lowered to acceptable values from the safety viewpoint, still ensuring enough reactivity for the whole mission time at full power. Furthermore, the developed code results extremely flexible and may be applied to different cores in future works.

Designing a reactor with high performances and capable to withstand different submersion accidents is a complex task, as highlighted in the accidental scenarios analysis. Spectral shift absorbers, which are widely implemented in fast reactors, have been demonstrated to be hardly applicable in LEU reactors, due to their strong neutron absorption at thermal energies. Thus, control rods effect on core neutronics have been investigated: the introduction of 7

control rods allows to maintain the core subcritical in three of the four accidental scenarios studied. However, in order to limit systems' complexity, an improvement of the well-established concept of control drums have been proposed as an alternative to control rods. The addition of fuel and moderator layers on the CD greatly increases CD reactivity worth, making them a vital component for core criticality: in that way even the worst accidental scenario, the one leading to reflector dismantling, can be handled properly keeping k_{eff} below unity. Thus, the configuration implementing the advanced control drums system is the one chosen for the remaining part of the work.

Finally, a thermal-hydraulics analysis has been carried out to verify that thermal limits are not exceeded inside the core and to evaluate the rocket performances. A possible simplified model for the fuel element has been proposed: with this model the temperature profiles inside both the hot channel and the average channel can be easily evaluated, without the need of more complex CFD codes. The previous optimisation on power profile and peaking factors was not sufficient to limit fuel temperature below 3000K, thus a core orificing has been proposed and investigated. Increasing the coolant mass flow rate up to $2 \cdot 10^3 \text{ kg/s}$ in the hot channel lowered the temperature below safety limit, making the reactor finally safe from both neutronics and thermal viewpoint.

The evaluation of rocket performances paid off all the efforts made in the previous analysis: the reactor has a specific impulse of about 996 s and generates a thrust of 122 kN, resulting in an extremely competitive design if compared to other literature design.

The structured procedure applied, and the code developed as support for the neutronics, accidental scenarios and thermal-hydraulics analysis result in a powerful tool for a fast, rigorous investigation of many different reactor configurations. In the end, a LEU, CERMET reactor design has been demonstrated to be a complex task: however, with a holistic approach, as the one presented in this work, a suitable design from both safety and performances viewpoint can be successfully developed.

Future works should be focused on the extension of the code to other relevant fields, such as thermo-mechanics, the inclusion of ex-core components in the model and a comparison of model results using different nuclear data libraries.

Bibliography

- [1] NASA, "Nasa.gov," 2008. [Online]. Available: https://spinoff.nasa.gov/Spinoff2008/tech_benefits.html.
- [2] M. Turner, "Rocket and Spacecraft Propulsion, Chapter 2 : The Thermal Rocket Engine", II edition, Springer, 2006.
- [3] M. Houts, et al., "Phase 1 Space Fission Propulsion Energy Source Design", in *American Nuclear Society Meeting: International Congress on Advanced Nuclear Power Plants*, Hollywood, FL, United States, 2002.
- [4] M. Cumo, et al., "MAUS/1,5 Nuclear Reactor for Space Electric Power", in *12th International Conference on Emerging Nuclear Energy Systems (ICENES'2005)*, Brussels, Belgium, 2005.
- [5] R. Frisbee, "Advanced Space Propulsion for the 21st Century", *Journal of Propulsion and Power*, vol. 19, n. 6, pp. 1129-1154, 2003.
- [6] R. Gabrielli, G. Herdrich, "Review of Nuclear Thermal Propulsion Systems", *Progress in Aerospace Sciences*, vol. 79, pp. 92-113, 2015.
- [7] J. Taub, "A Review of Fuel Element Development", Los Alamos Scientific Laboratory, Los Alamos, New Mexico, USA, 1975.
- [8] S. Borowski, "A Proven, Growth Technology for 'Fast Transit' Human Missions to Mars", in *AIAA SPACE 2013 Conference and Exposition*, San Diego, California, USA, 2013.
- [9] K. Berensky, "Survey of Fuel System Options for Low Enriched Uranium (LEU) Nuclear Thermal Propulsion", in *2017 Nuclear and Emerging Technologies for Space*, Orlando, Florida, USA, 2017.
- [10] R.C. O' Brien, et al., "Current Development of Nuclear Thermal Propulsion Technologies at the Center for Space Nuclear Research", in *AIAA Space 2012 Conference &*, Pasadena, California, USA, 2012.
- [11] F. Durham, "Nuclear Engine Definition Study Preliminary Report, Volume 1 - Engine Description", Los Alamos National Laboratory, Los Alamos, New Mexico, USA, 1972.
- [12] L. Snead, S. Zinkle, "Use of Beryllium and Beryllium Oxide in Space Reactors", in *Space Technology and Applications International Forum*, 2005.
- [13] J. Leppänen, "Serpent – a Continuous-energy Monte Carlo Reactor Physics Burnup Calculation Code", VTT Technical Research Centre of Finland, 2015.
- [14] J. Leppänen, "On the use of the Serpent Monte Carlo code for few-group cross section generation", *Annals of Nuclear Energy*, vol. 38, pp. 1399-1405, 2011.
- [15] D. Hetrick, "Dynamics of nuclear reactors", American Nuclear Society, 1993.

- [16] Nuclear Energy Agency, *Joint Evaluated Fission and Fusion (JEFF) Nuclear Data Library - JEFF 3.3*, 2017.
- [17] P. Venneri, et al., "A feasibility study on low-enriched uranium fuel for nuclear thermal rockets - I: Reactivity potential", *Progress in Nuclear Energy*, vol. 83, pp. 406-418, 2015.
- [18] P. Venneri, Y. Kim, "A feasibility study on low enriched uranium fuel for nuclear thermal rockets - II: Rocket and reactor performance", *Progress in Nuclear Energy*, vol. 87, pp. 156-167, 2016.
- [19] S.H. Nam, et al., "Preliminary conceptual design of a new moderated reactor utilizing an LEU fuel for space nuclear thermal propulsion", *Progress in nuclear energy*, vol. 91, pp. 183-207, 2016.
- [20] J. Stiglich, et al., "Processing and Testing of Ultrahigh Temperature Fiber-reinforced Ceramic and Metal Matrix Composites", in *AeroMat - ASM International*, Bellevue, Washington, USA, 2016.
- [21] F. Brown, "On the Use of Shannon Entropy of the Fission Distribution for Assessing Convergence of Monte Carlo Criticality Calculations", in *PHYSOR-2006, ANS Topical Meeting on Reactor Physics*, Vancouver, Canada, 2006.
- [22] B. Drake, S. Hoffman, D. Beaty, "Human Exploration of Mars, Design Reference Architecture 5.0", NASA Johnson Space Center, Houston, Texas, 2009.
- [23] H.C. Lee, et al., "A neutronic feasibility study on a small LEU fueled reactor for space applications", *Annals of Nuclear Energy*, vol. 77, pp. 35-46, 2015.
- [24] P. Venneri, Y. Kim, "Advancements in the Development of Low Enriched Uranium Nuclear Thermal Rockets", *Energy Procedia*, vol. 131, pp. 53-60, 2016.
- [25] J. King, M. El-Genk, "Submersion criticality safety of fast spectrum space reactor potential spectral shift absorbers", *Nuclear Engineering Design*, vol. 236, pp. 238-254, 2006.
- [26] J. King, M. El-Genk, "Submersion-Subcritical Safe Space (S4) Reactor", *Nuclear Engineering and Design*, vol. 236, pp. 1759-1777, 2006.
- [27] P. Venneri, et al., "An accident-tolerant control drum system for a small space reactor", *Annals of Nuclear Energy*, vol. 79, pp. 143-151, 2015.
- [28] H.M. Roder, et al., "Computer Programs for Thermodynamic and Transport Properties of Hydrogen (Tabcode-II)", Boulder, Colorado, USA: National Bureau of Standards, 1972.
- [29] F.P. Incropera, et al., "Fundamentals of Heat and Mass Transfer", Seventh Edition, Hoboken, New Jersey, USA: John Wiley & Sons, 2011.
- [30] J.A. Webb, et al., "Analytical determination of thermal conductivity of W-UO₂ and W-UN CERMET nuclear fuels", *Journal of Nuclear Materials*, vol. 427, pp. 87-94, 2012.
- [31] J.A. Webb, et al., "SPS Fabrication of Tungsten-Rhenium Alloys in Support on NTR Fuel Development", in *Proceedings of Nuclear and Emerging Technologies for Space 2011*, Albuquerque, New Mexico, USA, 2011.

- [32] M. S. Kazimi, N.E. Todreas, "Nuclear Systems I - Thermal Hydraulic Fundamentals", Taylor & Francis, 1993.
- [33] M. Turner, "Rocket and Spacecraft Propulsion, Chapter 7: Nuclear Propulsion", II edition, Springer, 2006.

List of figures

Fig. 1.1 - A common solid-core rocket engine [2].....	2
Fig. 1.2 - Schematic view of a rocket for NTP [6].....	7
Fig. 1.3 - Core poloidal section – NERVA derived reactor (Serpent input).....	9
Fig. 1.4 – Core poloidal section detail – NERVA derived reactor (Serpent input).	9
Fig. 1.5 - Axial reflector poloidal section – NERVA derived reactor (Serpent input).	10
Fig. 1.6 - Core axial section (Different colours on the axial direction refer to different fuel temperature, on the radial direction to different enrichments) – NERVA derived reactor (Serpent input).....	10
Fig. 1.7 - Coated-particle and composite fuel detail [8].	11
Fig. 1.8 - Core fuel element – NERVA derived reactor (Serpent input).	12
Fig. 1.9 - Neutron spectrum for moderated and unmoderated core – NERVA derived reactor.	13
Fig. 1.10 - Core moderating element and surfaces outer radii – NERVA derived reactor (Serpent input).....	14
Fig. 2.1 - Core temperature zones division – NERVA derived reactor (Serpent input).....	23
Fig. 2.2 - Shannon entropy vs. cycles number – NERVA derived reactor.....	25
Fig. 2.3 - $keff$ as a function of rotation angle ($\sigma=20$ pcm) – NERVA derived reactor.	26
Fig. 2.4 - $keff$ as a function of radial reflector thickness ($\sigma=20$ pcm) - NERVA derived reactor.....	29
Fig. 2.5 - $keff$ as a function of axial reflector thickness ($\sigma=20$ pcm) - NERVA derived reactor.	29
Fig. 2.6 - Neutron flux distribution (Serpent mesh detector) - NERVA derived reactor.	30
Fig. 2.7 - Fuel element power distribution. 15 cm axial reflector thickness (left), 5cm axial reflector thickness (right).	31
Fig. 2.8 - Neutron flux along the z-axis in a fuel element (Serpent cartesian detector) - NERVA derived reactor.....	31
Fig. 2.9 - $keff$ at different burnup steps - NERVA derived reactor.	34
Fig. 2.10 – Uranium-238 mass in the core at different burnup steps - NERVA derived reactor.	34
Fig. 2.11 - Uranium-235 mass in the core at different burnup steps - NERVA derived reactor.	35
Fig. 2.12 - $keff$ vs. Rhenium atomic fraction for natural and enriched tungsten ($\sigma=20$ pcm) – CERMET reactor.....	37
Fig. 2.13 - Neutron spectrum comparison between composite and CERMET fuel.	38
Fig. 2.14 - $keff$ as a function of radial reflector thickness ($\sigma=20$ pcm) – CERMET reactor.	40
Fig. 2.15 - $keff$ as a function of axial reflector thickness ($\sigma=20$ pcm) – CERMET reactor.	40
Fig. 2.16 - Neutron flux and power distribution at $z=0$ – CERMET reactor.	41
Fig. 2.17 - Fast neutron flux at $z=0$ – CERMET reactor.....	41

Fig. 2.18 - Thermal neutron flux at $z=0$ – CERMET reactor.	42
Fig. 2.19 - k_{eff} and F_{hc} for various reactor configurations obtained through the optimization procedure.	46
Fig. 3.1 - Thermal neutron flux and power distribution following an accidental scenario – CEREMET optimized configuration.	50
Fig. 3.2 - Effect of different SSA on reactor reactivity (normal operations) – CERMET optimized configuration.	52
Fig. 3.3 - Advanced tolerant control drum [27].	55
Fig. 3.4 - ATCD position for reactor operation and shutdown [26].	56
Fig. 3.5 - ATCD core. Absorber (yellow), moderator (green), fuel (pink). (Serpent input).....	56
Fig. 3.6 - Mesh detector for neutron flux. ATCD core. Dark zones are related to absorbers presence.	57
Fig. 4.1 – CERMET core fuel element section (Serpent input).	61
Fig. 4.2 - Fuel coolant channel model (not in scale).	62
Fig. 4.3 - Fuel and coolant temperature in the hot channel (cosine power profile) – ATCD reactor configuration.	68
Fig. 4.4 - Fuel and coolant temperature in the hot channel, orificed core (cosine power profile) – ATCD reactor configuration.	69
Fig. 4.5 - Fuel and coolant temperature in the hot channel, orificed core (real power profile) – ATCD reactor configuration.	70
Fig. 4.6 – Hot channel power profile per unit length – ATCD reactor configuration.....	71
Fig. 4.7 - Heat transfer coefficient along the hot channel – ATCD reactor configuration.	72
Fig. 4.8 - Fuel and coolant temperature in the average channel, orificed core (cosine power profile) – ATCD reactor configuration.	72
Fig. 4.9 - Thrust and specific impulse vs. propellant mass flow rate ($c_p = const = 16.5kJ/kg K$).	75

List of tables

Table 2.1 - Reference data for SNRE and C-LEU-NTR [18].	21
Table 2.2 - Mean temperature for different core axial zones.	22
Table 2.3 - Coolant density along channels [19].	22
Table 2.4 - k_{eff} for hot and cold reactor, NbC coating (50 inactive cycles, 75 active cycles, 100000 neutrons per cycle).	23
Table 2.5 - k_{eff} for hot and cold reactor, ZrC coating (50 inactive cycles, 75 active cycles, 100000 neutrons per cycle).	23
Table 2.6 - Reactor component mass.	27
Table 2.7 - Peaking factors for different configurations of radial (R) and axial (A) reflectors - NERVA derived reactor.	32
Table 2.8 - Results comparison of the reference and the current model.	36
Table 2.9 - CERMET reactor parameters.	39
Table 2.10 - Optimal configuration results – CERMET reactor.	47
Table 3.1 - k_{eff} following submersion accidents – CERMET optimized configuration.	51
Table 3.2 - Comparison between base configuration and optimized configuration with SSA sleeve.	53
Table 3.3 - Effect of seven $B4C$ control rods on core reactivity following submersion accidents – CERMET optimized configuration.	54
Table 3.4 - k_{eff} for ATCD core following a submersion accident.	57
Table 3.5 - Reactor data for the ATCD configuration.	59
Table 4.1 - Summary of ATCD reactor features.	63
Table 4.2 – Thermal-hydraulic results from 0-D analysis - ATCD reactor configuration.	65
Table 4.3 - Input data for hot channel analysis – ATCD reactor configuration.	67
Table 4.4 - Hot channel and average channel data after orificing – ATCD reactor configuration.	73
Table 4.5 – Comparison of reactor figures of merit from the propulsion viewpoint.	76
Table 4.6 - Thermal-hydraulics features and performances – ATCD reactor configuration.	78

Acknowledgments

I would like to offer my special thanks to Nicolò Abrate for its precious help during the early stages of my thesis, and to Professor Cammi from Politecnico di Milano for having followed me along this work even though we worked in different cities.

I would also like to thank all my friends that shared with me these years at university; it would not have been the same experience without them. I am particularly grateful to my friends from my hometown, Narni, for the time they have always found for me. To all of them I wish the best for their lives.

Finally, I wish to express my profound gratitude to my family, for its unconditional support and the encouragement throughout these years of study. This accomplishment would not have been possible without them. Thank you.